Interaction of Topoisomerase II-Targeted Anticancer Agents with the Doxorubicin
Cardioprotective Drug Dexrazoxane, and Synthesis of a Dexrazoxane Analog

By

Khanh Tuan Tran

A Thesis
Submitted to the Faculty of Graduate Studies
in Partial Fulfillment of the Requirements
for the Degree of

Master of Science

Faculty of Pharmacy
University of Manitoba
Winnipeg, Manitoba, Canada

© April, 1999

Canada

THE UNIVERSITY OF MANITOBA

FACULTY OF GRADUATE STUDIES
*****
COPYRIGHT PERMISSION PAGE

Interaction of Topoisomerase II-Targeted Anticancer Agents with the Doxorubicin
Cardioprotective Drug Dexrazoxane, and Synthesis of a Dexrazoxane Analog

A Thesis/Practicum submitted to the Faculty of Graduate Studies of The University

of Manitoba in partial fulfillment of the requirements of the degree

of

Master of Science

Khanh Tuan Tran ©1999

Abstract

The anthrapyrazoles losoxantrone and piroxantrone are topoisomerase II-targeted anticancer agents that were developed as alternatives to anthracycline anticancer drugs, such as doxorubicin to prevent cardiotoxicity. In this study the formation of the Fe^{3+} complexes of losoxantrone and piroxantrone, and the dissociation of the complexes in the presence of dexrazoxane (ICRF-187, Zinecard®, Cardioxane®), and its hydrolyzed form ADR-925 were investigated spectrophotometrically. Both losoxantrone and piroxantrone were shown to chelate to Fe^{3+}. These Fe^{3+}-drug complexes were shown to be dissociated in the presence of dexrazoxane and ADR-925. The Fe^{3+}-drug complex formation could be the cause of the observed cardiotoxic side effects induced by losoxantrone and piroxantrone in previous animal and clinical studies. The Fe^{3+}-drug dissociation could provide a way to minimize the cardiotoxicity when dexrazoxane and either losoxantrone or piroxantrone are used together. The antagonistic effects of dexrazoxane and topoisomerase II-targeted anticancer agents, such as m-amsacrine, etoposide, teniposide, losoxantrone, and piroxantrone were studied using Chinese hamster ovary cells. The above topoisomerase II-targeted anticancer agents were found to antagonize dexrazoxane at different concentrations. In order to improve the cardioprotective effect of dexrazoxane, an analog bisdioxopiperidine 1 was synthesized. The rate of the hydrolysis of compound 1 was found to be two times slower than that of dexrazoxane at 37 °C and pH 7.4. The hydrolyzed form of compound 1 was not a good Fe^{3+} chelator compared to the hydrolyzed form of dexrazoxane, ADR-925.

Acknowledgments

I would like to acknowledge Dr. B. B. Hasinoff, my graduate supervisor for all of his teaching, support, and guidance me throughout my projects. The financial support in the form of Post Graduate Scholarship Type A (PGS A) from the Natural Sciences and Engineering Research Council of Canada (NSERC), and the operational grant through Dr. Hasinoff from the Medical Research Council of Canada (MRC) are gratefully acknowledged. I would like to thank Drs. A. S. Abd-El-Aziz and K. J. Friesen, Mr. D. Latimer, and the Department of Chemistry at the University of Winnipeg for the support by granting me the full access to their NMR spectrometer. I would also like to express my gratitude to the thesis committee members, Drs. A. S. Abd-El-Aziz and J. F. Templeton for their suggestions and comments in the preparation of this thesis. Throughout my projects, I have learned a great deal from the helpful discussions and suggestions of Drs. J. F. Templeton, A. S. Grant, T. Li, J. L. Buss, L. G. Chee, and Mrs. H. Kozlowska. I would also like to thank the Faculty of Pharmacy at the University of Manitoba for allowing me to do my graduate studies in the faculty. Finally, I am grateful for the support and encouragement from my whole family, especially my parents, my aunt, and my two sisters throughout my many years at school.

Table of contents

List of figures

9

List of tables

1. Topoisomerase inhibitors as anticancer agents

1.1. Important roles of topoisomerases in cellular system

There are several types of topoisomerases present in prokaryotic and eukaryotic cells. Topoisomerase I and II are the two main types in eukaryotic cells, and DNA gyrase is the enzyme present in prokaryotic cells. These enzymes control the important steps in DNA replication and transcription, in the segregation of newly replicated chromosome pairs, in the condensation of chromosomes, and in DNA super coiling (Berger *et al.*, 1996; Redinbo *et al.*, 1998; Stewart *et al.*, 1998; Wang *et al.*, 1997). During DNA replication, the two strands of the twisted DNA are separated to serve as the two templates for two daughter DNA molecules. The torsional strain in the helical section of the DNA ahead of the replication fork would develop if this DNA section could not unwind rapidly enough (Alberts *et al.*, 1994; Lehninger *et al.*, 1993). Due to bulkiness of the whole DNA structure, and also the anchorage of the DNA in the cellular matrix, the unwinding process to remove the DNA torsional strain would require a lot of energy as shown in Figure 1.1. Alternatively, the cells remove the torsional strain with the use of topoisomerases without energy requirement as with topoisomerase I, and with a small amount of energy requirement through ATP hydrolysis as with topoisomerase II (Wang, 1985; Pommier, 1993; Pommier *et al.*, 1993; Nitiss, 1994a; Chen and Liu, 1994; Nitiss, 1994b; Wang *et al.*, 1997; Froelich-Ammon and Osheroff, 1995; Verweij, 1995). Topoisomerase I creates a transiently single stranded nick or breakage in the nucleic acid linkage of DNA, and passes the other intact strand through the breakage. After the passage of the intact strand through the transient breakage, the DNA breakage is resealed

without any energy requirement. Topoisomerase II can create transiently double stranded breakage, and pass the other intact double stranded circular daughter DNA through the breakage in the former DNA molecule with an energy requirement through the hydrolysis of ATP (Osheroff, 1989). The crystal structure of human topoisomerase I shows that the enzyme is monomeric, and in the closed clamp form with a cavity that can surround the B-form DNA to create a transiently single stranded break through the activation of the tyrosine residue at the active site (Redinbo *et al.*, 1998; Stewart *et al.*, 1998). A covalent transient linkage is formed between the tyrosine residue at the active site on the enzyme to the 3'-terminus of the DNA. This process creates a transient breakage on the phosphodiester bond on one strand of DNA (Madden *et al.*, 1995). After passing the other strand through the nick, the DNA breakage is religated. The whole process does not require any additional energy, since the energy in the phosphotyrosyl bond between the enzyme and DNA is retained, and is used in the resealing step (Osheroff, 1989; Alberts *et al.*, 1994). The structure and mechanism of the yeast topoisomerase II has been studied in detail (Berger *et al.*, 1996). These studies show that the eukaryotic topoisomerase II is dimeric, while the prokaryotic enzyme, which is also called DNA gyrase, is tetrameric. Topoisomerase II creates transiently double stranded breakage on one DNA duplex, and passes the other duplex through the opening, and then reseals the breakage (Wang *et al.*, 1997; Pommier, 1993; Pommier *et al.*, 1993). During this process, the enzyme binds covalently but transiently to the 5' end of the DNA at the two tyrosyl active sites on the enzymes, and creates a temporary opening. This allows the passage of the other DNA duplex through the breakage to separate the newly replicated

chromosome pairs. The binding process of topoisomerase II to DNA depends on ATP

binding and hydrolysis (Berger *et al.*, 1996).
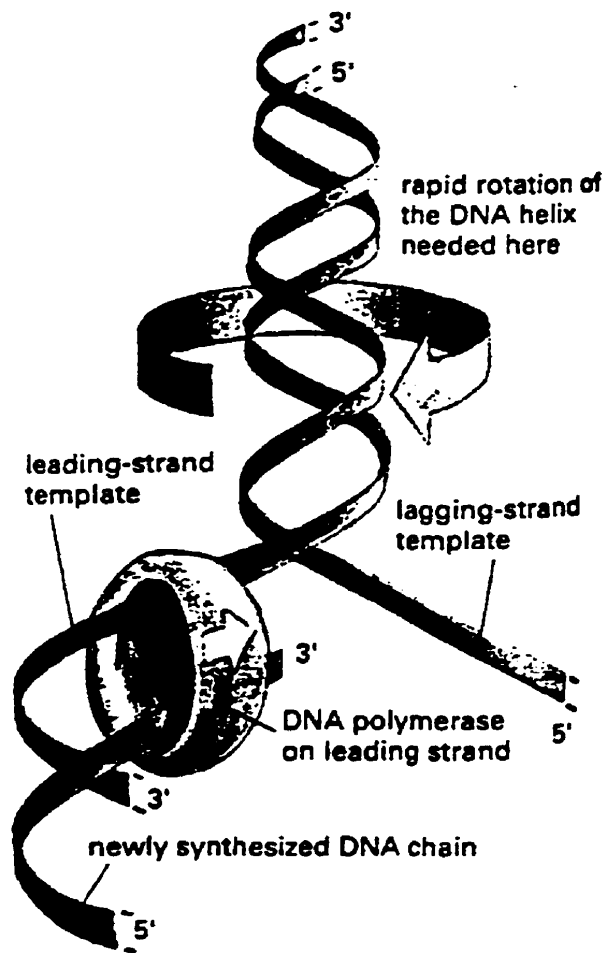
Figure 1.1. The "winding problem" during DNA replication. The figure was taken from Alberts *et al.*, 1994.

1.2. Stabilization of the topoisomerase-DNA complex by topoisomerase inhibitors and its application in chemotherapy

Because of the important roles of topoisomerases in controlling the topology of DNA structure in several processes, such as translation, transcription and mitosis, the stabilization of the enzyme-DNA complex by topoisomerase inhibitors may influence the control of the DNA topology. This strategy has been utilized quite extensively in inhibiting the growth of tumor cells (Wang, 1985; Pommier, 1993; Pommier *et al.*, 1993; Nitiss, 1994a; Chen and Liu, 1994; Nitiss, 1994b; Wang *et al.*, 1997; Froelich-Ammon and Osheroff, 1995). Due to the higher rate of proliferation in tumor cells, in which DNA and RNA are constantly synthesized, the levels of topoisomerase I and II are higher than that in normal cells. Thus, an active enzyme inhibitor would be more active in the tumor cells than in the healthy cells in the inhibition of the DNA and RNA syntheses, and would effectively inhibit the growth of the tumor cells (Froelich-Ammon and Osheroff, 1995). Several topoisomerase inhibitors have been used in the treatment of tumor cells by stabilizing the topoisomerase-DNA complex. In general, anticancer agents stabilize the topoisomerase-DNA complex in the form of a ternary complex of topoisomerase-DNA-anticancer agent, which leads to DNA damage and subsequent cell death as shown in Figure 1.2 (Froelich-Ammon and Osheroff, 1995). The effectiveness in topoisomerase inhibition is dependent on the cell cycle. Topoisomerase I level is constant throughout the cell cycle, and therefore, the enzyme inhibition is independent of the cell cycle (Macpherson *et al.*, 1997). In other studies, the enzyme inhibition by topoisomerase I inhibitor is cell cycle-dependent with the highest sensitivity in S-phase (Wang *et al.*,

1997). To date, camptothecin and its analogs are the most effective topoisomerase I inhibitors. Topotecan (Hycamtin™), a camptothecin analog has been approved for the treatment of metastatic carcinoma of the ovary in patients after having failure of initial or subsequent therapy (Healy *et al.*, 1998). The anticancer mechanism of topoisomerase inhibitors is proposed to be the collision of the replication fork with the stabilized complex of the topoisomerase I-DNA-drug as shown in Figure 1.3 (Froelich-Ammon and Osheroff, 1995; Pommier *et al.*, 1994; Hsiang *et al.*, 1989). The study in this work mainly concentrates on topoisomerase II inhibitors, which are classified into two main types, such as non-cleavable complex-forming (or catalytic) topoisomerase II inhibitors, and cleavable complex-forming topoisomerase II poisons (Hasinoff *et al.*, 1997).

Bisdioxopiperazines (Figure 1.4) and other agents, such as suramin, and merbarone are non-cleavable complex-forming topoisomerase II inhibitors (Fukuda *et al.*, 1992; Rajagopalan *et al.*, 1988; van-Reyk *et al.*, 1992; Muggia and Green, 1991; Hasinoff *et al.*, 1997). These agents inhibit the enzyme topoisomerases catalytically by possibly blocking the DNA entrance to the cavity of the enzyme. The enzyme inhibition by bisdioxopiperazines has been shown not to be significant for the application in chemotherapy; for example dexrazoxane (ICRF-187, Zinecard® or Cardioxane®), a bisdioxopiperazine, was first designed as an anticancer agent (Creighton, 1971). This compound has another application in chemotherapy as a cardioprotective agent, which is used in combination with doxorubicin to prevent oxygen-mediated free radical damage (Hasinoff *et al.*, 1998; Hasinoff, 1998; Synold *et al.*, 1998; Elihu *et al.*, 1998).

Another class of topoisomerase II inhibitors are the cleavable complex-forming topoisomerase II poisons. Some of them are anthracyclines (doxorubicin and daunorubicin), anthrapyrazoles (losoxantrone and piroxantrone), epipodophyllotoxins (etoposide and teniposide), and *m*-amsacrine (Figure 1.5) (Sengupta, 1995). These agents exert their cytotoxic effects by stabilizing the covalent cleavable complex of the topoisomerase II-DNA intermediate, and have been used in the treatment of a variety of tumors. Some of them have shown promise in chemotherapy; for example, doxorubicin (Adriamycin$^{®}$) has been approved for the treatment of a wide variety of tumors (Healy *et al.*, 1998). Besides stabilizing the cleavable complex of the drug-enzyme-DNA, another possible anticancer mechanism of anthracyclines is proposed to be the intercalation with DNA by stacking the planar portion of the molecule between the DNA base pairs (Sengupta, 1995).
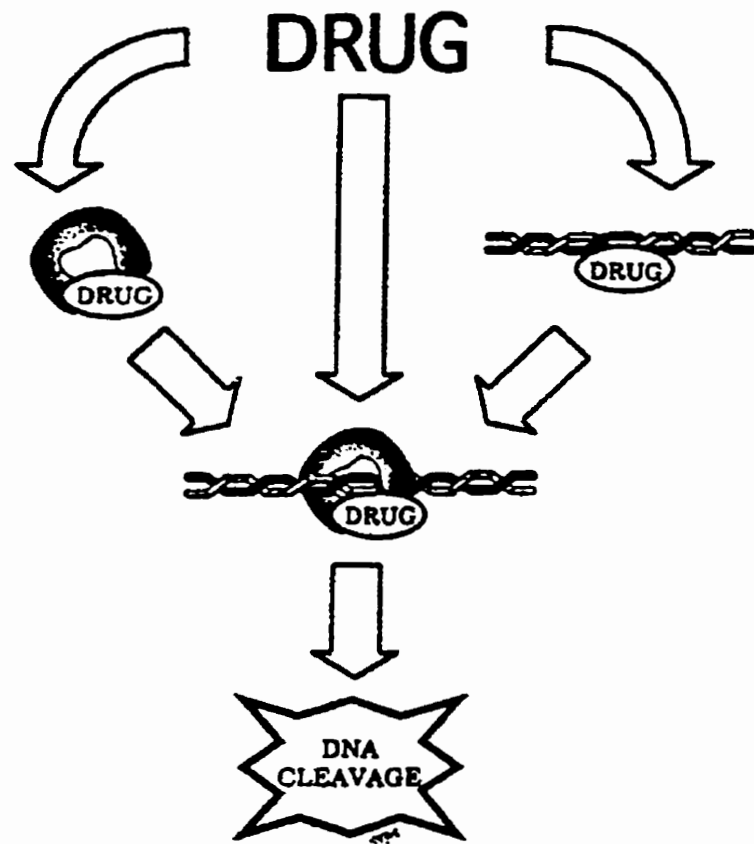
Figure 1.2. Formation of the topoisomerase-drug-DNA ternary complex. The figure was taken from Froelich-Ammon and Osheroff, 1995.
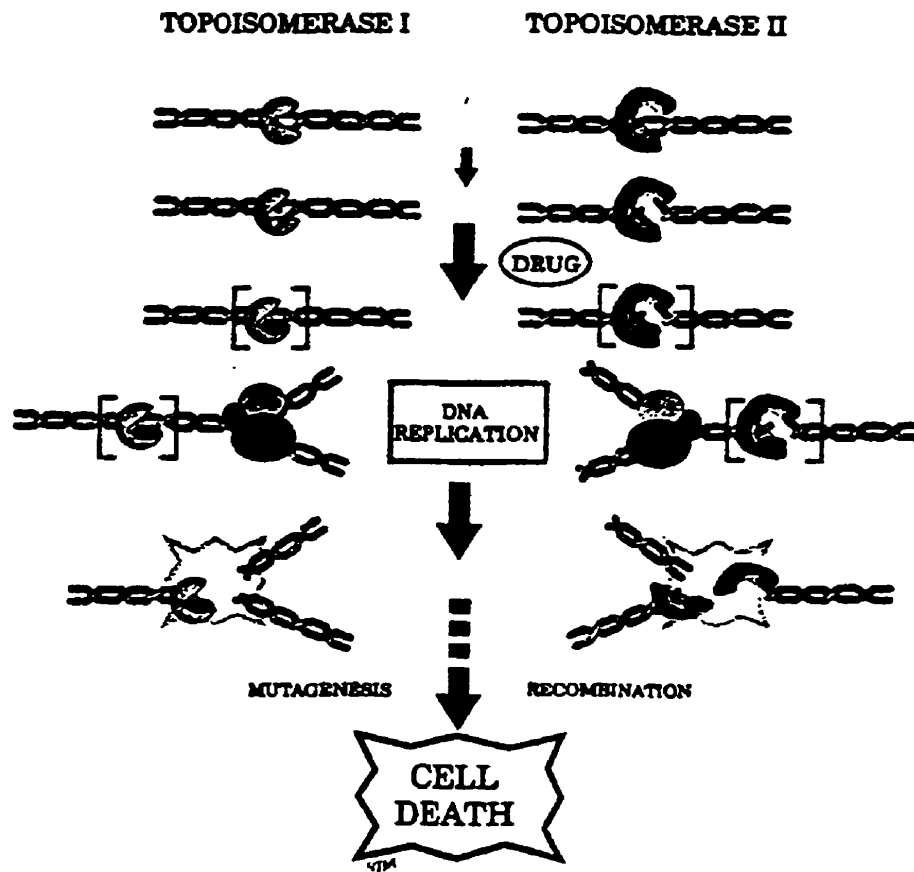
Figure 1.3. Cytotoxic effect induced by topoisomerase inhibitors. In the presence of topoisomerase inhibitors or drug, the ternary complexes of the enzyme-DNA-drug are stabilized, and lead to subsequent cell death. The figure was taken from Froelich-Ammon and Osheroff, 1995.
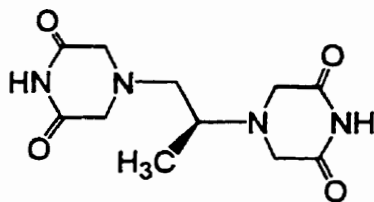
Dexraxozane (ICRF-187)
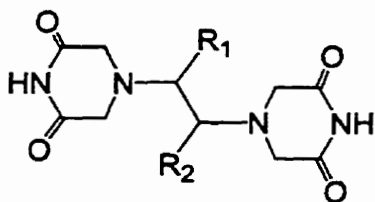
ICRF-154 $R_1 = R_2 = H$
ICRF-159 $R_1 = H$, $R_2 = CH_3$ (racemic)
ICRF-187 $R_1 = R_2 = CH_3$ ((S)-(+))
ICRF-186 $R_1 = R_2 = CH_3$ ((R)-(-))
ICRF-192 $R_1 = H$, $R_2 = C_2H_5$ (racemic)
ICRF-193 $R_1 = R_2 = CH_3$ (meso)
ICRF-201 $R_1 = R_2 = C_2H_5$ (meso)
ICRF-202 $R_1 = CH_3$, $R_2 = C_2H_5$ (erythro)
ICRF-215 $R_1 = CH_3$, $R_2 = C_3H_7$ (erythro)
ICRF-220 $R_1 = CH_3$, $R_2 = CH_2OCH_3$ (erythro)

Figure 1.4. Structures of several bisdioxopiperazines.

m-Amsacrine

Doxorubicin, R = CH$_2$OH
Daunorubicin, R = CH$_3$

Teniposide, R = (thiophene)
Etoposide, R = CH$_3$

Losoxantrone, R$_1$ = H
R$_2$ = CH$_2$CH$_2$NHCH$_2$CH$_2$OH
Piroxantrone, R$_1$ = OH,
R$_2$ = CH$_2$CH$_2$CH$_2$CH$_2$NH$_2$
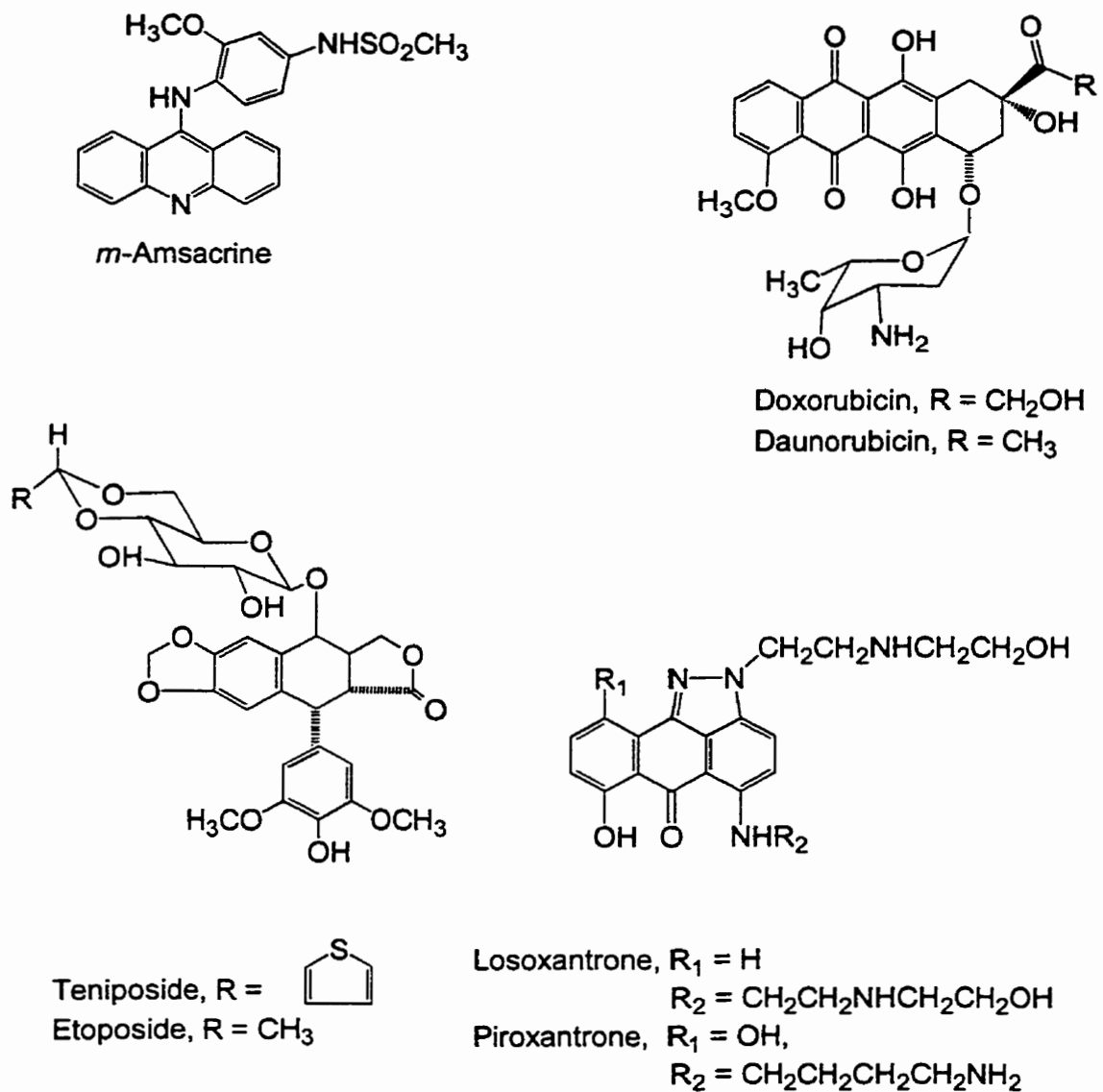
Figure 1.5. Structures of several anthracyclines (doxorubicin and daunorubicin), anthrapyrazoles (losoxantrone and piroxantrone), epipodophyllotoxins (etoposide and teniposide), and *m*-amsacrine.

1.3. Side effects of anthracycline anticancer agents

Among the cleavable complex-forming topoisomerase II inhibitors, doxorubicin, an anthracycline, has been shown to be the most potent anticancer agent in the treatment of a variety of tumors (Healy *et al.*, 1998). However, the use of doxorubicin is usually limited by the cumulative dose-dependent cardiotoxicity (Gianni *et al.*, 1983; Weiss, 1992). The mechanism of this side effect is not known well. Reactive cellular component damaging agents, such as hydroxyl and superoxide radicals are the products of the iron-dependent redox cycling by the Fenton reaction (Reaction 2.4). These reactive species initiate a variety of tissue damages, and the cardiac tissues are most affected (Hasinoff *et al.*, 1998; Hasinoff, 1998; Synold *et al.*, 1998; Elihu *et al.*, 1998). Various biological systems are also constantly producing hydrogen peroxide, superoxide and hydroxyl radicals. For example, superoxide from oxygen can be produced by the reaction of xanthine oxidase; reactive radical fatty acids, which damage cellular components can also be produced by the initiation of the lipid peroxidation chain reactions. Under normal conditions, various antioxidant enzymes, such as catalase, superoxide dismutase, and glutathione peroxidase can protect the cell by diminishing the radicals through a series of biological reactions (Nogrady, 1988). The protective mechanisms may be overwhelmed in patients being treated with doxorubicin. Thus, severe cellular damage due to the presence of reactive radicals may result in cardiac lesion, and lead to heart failure. The main mechanism of this cardiotoxic side effect is found to be the formation of free radicals, which are products of the redox reactions of the Fe^{3+}-anthracycline complexes as shown in the following reactions, where DOX is doxorubicin (Hasinoff *et al.*, 1998):

$$Fe^{3+}\text{-DOX} + e^- \rightarrow Fe^{2+}\text{-DOX} \qquad (2.1)$$

$$Fe^{2+}\text{-DOX} + O_2 \rightarrow Fe^{3+}\text{-DOX} + O_2^{\cdot-} \qquad (2.2)$$

$$2O_2^{\cdot-} + 2H^+ \rightarrow H_2O_2 + O_2 \qquad (2.3)$$

$$Fe^{2+}\text{-DOX} + H_2O_2 \rightarrow Fe^{3+}\text{-DOX} + OH^- + OH^{\cdot} \qquad (2.4)$$
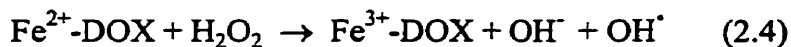
Despite the formation of the Fe^{3+}-doxorubicin complex, which leads to free radical-induced oxidative stress, doxorubicin can still be used for patients with pre-existing cardiac risk factors with the co-administration of dexrazoxane (ICRF-187, Zinecard®, Cardioxane®) (Hasinoff et al., 1998; Elihu et al., 1998). The chemistry and biochemistry of dexrazoxane have been reviewed (Hasinoff et al., 1998; Hasinoff, 1998). Upon hydrolysis, dexrazoxane (A) produces the one ring opened intermediates B and C forms, which lead to the production of ADR-925 (D) (Figure 1.6). The latter compound is structurally similar to ethylenediamine-N,N'-tetraacetic acid (EDTA). ADR-925 binds strongly to metal ions, such as Cu^{2+} and Fe^{3+} (Hasinoff, 1989a). The cardioprotective form of dexrazoxane is proposed to be its hydrolyzed form, ADR-925, which competitively dissociates the Fe^{3+}-drug complex. By lowering the level of the Fe^{3+}-drug complex, the production of free radicals can be lowered. This process leads to the reduction of the free radical-induced oxidative stress.
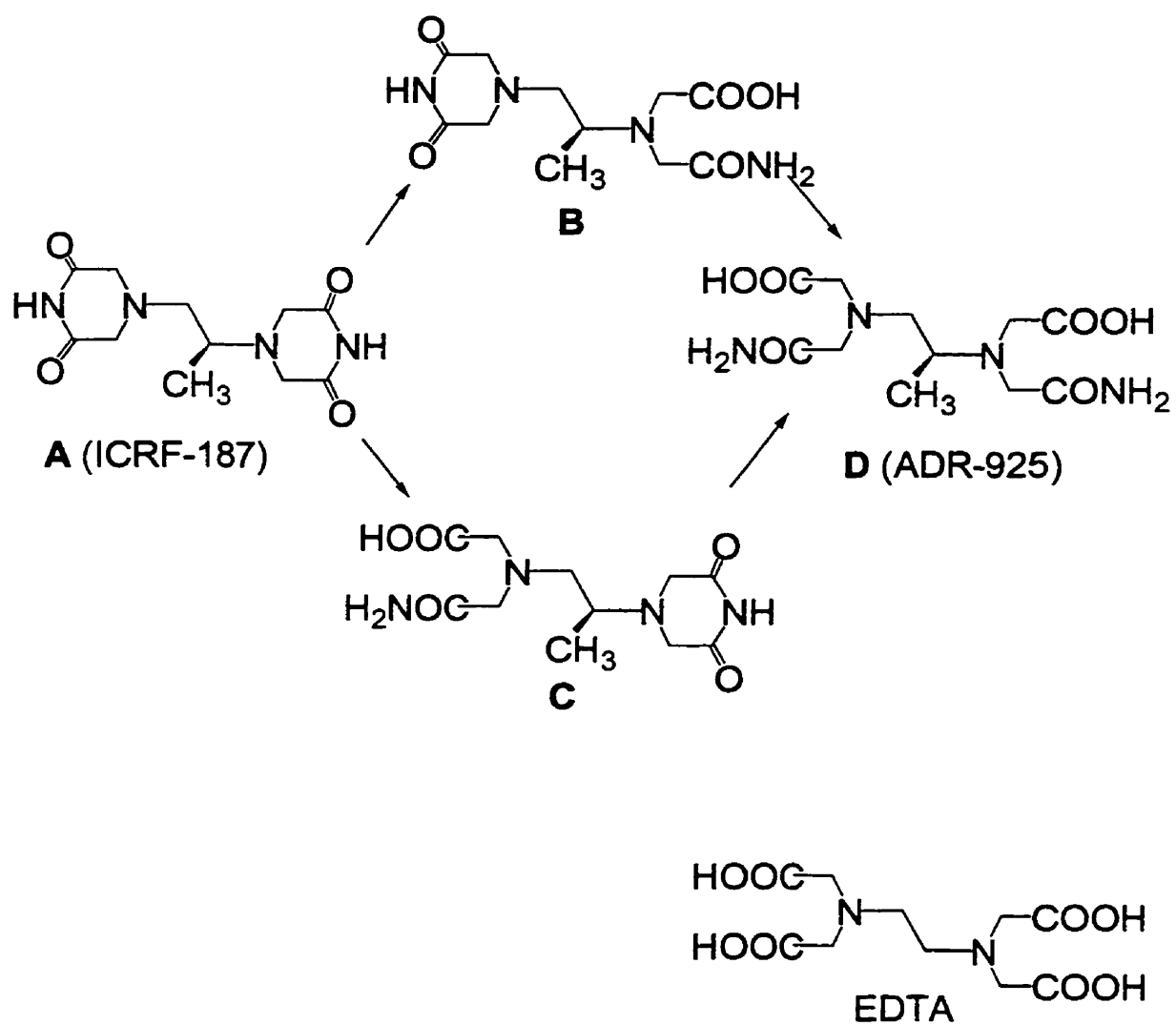
Figure 1.6. The hydrolysis of dexrazoxane (**A**) to **B**, **C**, and ADR-925 (**D**).

1.4. An overview of the projects
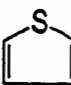
Because of the cardiotoxic side effect caused by doxorubicin, several analogs of doxorubicin have been developed as non-cardiotoxic anticancer agents, such as the anthrapyrazoles (Judson, 1991; Graham et al., 1989). However, the anthrapyrazoles, such as losoxantrone and piroxantrone still show a certain degree of cardiotoxicity (Sosman et al., 1995; Foster et al., 1992). These compounds are structurally similar to doxorubicin, and both contain quinone and hydroquinone moieties, which are good chelation sites for metal ions. These features may facilitate the formation of the metal ion-drug complexes, which undergo redox cycling, and produce reactive oxygen radicals. In this study, the formation of the Fe^{3+}-losoxantrone, and Fe^{3+}-piroxantrone complexes were investigated; and the dissociation of these complexes by the competitive metal ion chelator, ADR-925, which is the hydrolyzed form of the cardioprotective drug dexrazoxane, was also studied.

The cardioprotective drug dexrazoxane has been used successfully in the prevention of doxorubicin-induced cardiotoxicity, which may be caused by the metal ion complex formation of the antitumor anthracycline doxorubicin (Hasinoff et al., 1998). It is known that bisdioxopiperazines are catalytic topoisomerase II inhibitors, which bind to topoisomerase II, and prevent the enzyme from binding to DNA to control the DNA topology (Ishida et al., 1995; Kano et al., 1992; Snapka et al., 1996). Doxorubicin and other topoisomerase II inhibitors, such as m-amsacrine, etoposide, teniposide, losoxantrone, and piroxantrone are agents that stabilize the drug-DNA-enzyme cleavable complex. In order to reduce the cardiotoxic side effects, dexrazoxane, and other topoisomerase II inhibitors have been used together. This co-administration, however,

may lead to antagonistic effects, since both the agents target the same enzyme, topoisomerase II. In this study, the effects of *m*-amsacrine, etoposide, teniposide, losoxantrone, and piroxantrone combined with dexrazoxane on the growth of Chinese hamster ovary cells were investigated.

Although dexrazoxane has been found to be effective in the prevention of the cardiotoxic side effect produced by anthracycline doxorubicin (Hasinoff *et al.*, 1998), the cardioprotective effect of dexrazoxane would be improved if the transformation to its active hydrolyzed form ADR-925 were faster. Speeding the transformation to the active form would allow the reduction of the dexrazoxane dose, and would minimize its possible side effects, including myelosuppression, gastro-intestinal toxicity, and alopecia (Healy *et al.*, 1998). Thus, analogs of dexrazoxane with some structural modifications, which could shorten the time required for the hydrolysis to its active form as ADR-925 are desirable. In this study, an analog of dexrazoxane bisdioxopiperidine 1 (Figure 1.8) was synthesized, and the kinetics of the imide ring hydrolysis was investigated.
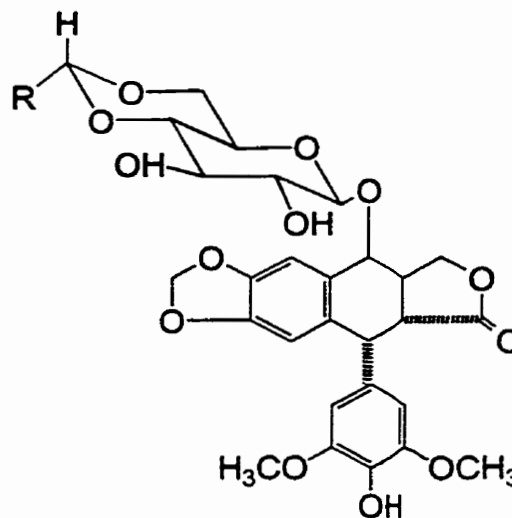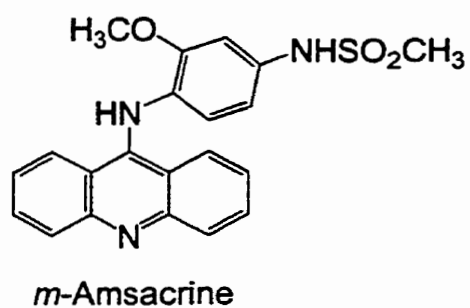
m-Amsacrine

Teniposide, R =
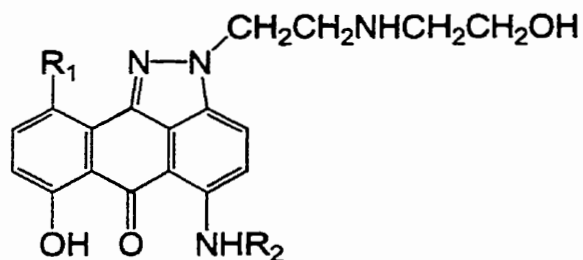
Etoposide, R = CH$_3$

Losoxantrone, R$_1$ = H

R$_2$ = CH$_2$CH$_2$NHCH$_2$CH$_2$OH

Piroxantrone, R$_1$ = OH,

R$_2$ = CH$_2$CH$_2$CH$_2$CH$_2$NH$_2$

Figure 1.7. Structures of *m*-amsacrine, etoposide, teniposide, losoxantrone, and piroxantrone.
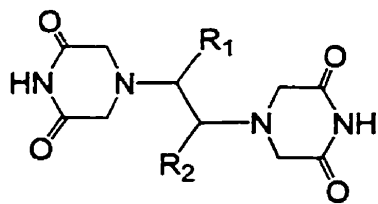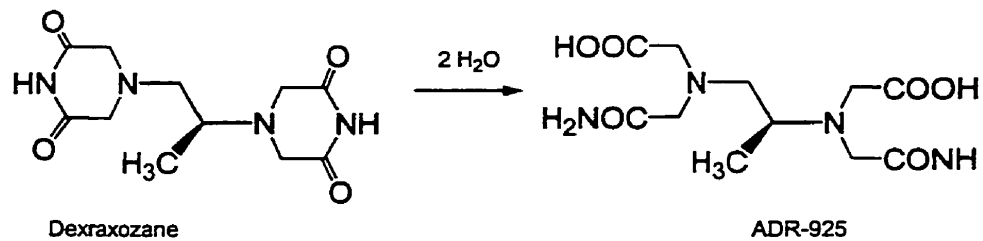
ICRF-154 R₁ = R₂ = H

ICRF-159 R₁ = H, R₂ = CH₃ (racemic)

ICRF-187 R₁ = R₂ = CH₃ ((S)-(+))

ICRF-186 R₁ = R₂ = CH₃ ((R)-(-))

ICRF-192 R₁ = H, R₂ = C₂H₅ (racemic)

ICRF-193 R₁ = R₂ = CH₃ (meso)

ICRF-201 R₁ = R₂ = C₂H₅ (meso)

ICRF-202 R₁ = CH₃, R₂ = C₂H₅ (erythro)

ICRF-215 R₁ = CH₃, R₂ = C₃H₇ (erythro)

ICRF-220 R₁ = CH₃, R₂ = CH₂OCH₃ (erythro)
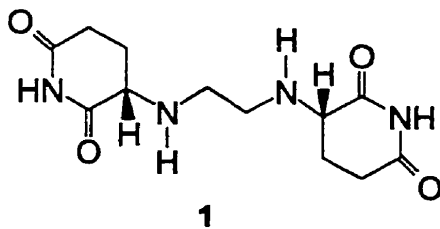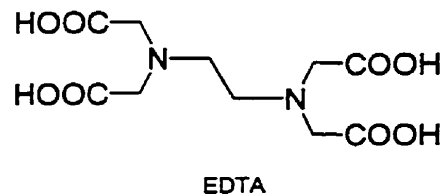
Figure 1.8. Structures of dexrazoxane, its analogs, ADR-925, EDTA, and the target compound bisdioxopiperidine **1**.

2. Formation of the Fe^{3+}-losoxantrone and Fe^{3+}-piroxantrone complexes

2.1. Introduction

2.1.1. The anticancer activity of losoxantrone and piroxantrone

Losoxantrone and piroxantrone are anthrapyrazoles, which were developed as alternatives to anthracyclines, such as doxorubicin (Judson, 1991; Graham et al., 1989). The antineoplastic activities of losoxantrone and piroxantrone were shown to be slightly different due to different models, on which the two drugs were tested (Herman et al., 1998). The antineoplastic spectrum of losoxantrone is generally broad, including carcinoma of the breast and the prostate, while that of piroxantrone is narrow, and limited against breast cancer (Herman et al., 1998). Cardiotoxicity results from the use of piroxantrone, which also has low efficacy for breast cancer (Ingle et al., 1994). Losoxantrone shows excellent activity against advanced breast cancer in phase II trials (Ogawa and Ariyoshi, 1993). It has a lower cardiotoxicity compared to doxorubicin, and is thought to induce cardiotoxicity by a free-radical-mediated mechanism (Ogawa and Ariyoshi, 1993; Graham et al., 1989). The dose limiting toxicities are neutropenia and leucopenia (Talbot et al., 1991). Other toxicities, such as nausea and vomiting mucositis, diarrhea, alopecia and skin discoloration, show at low levels (Foster et al., 1992). Losoxantrone was reported to induce cardiotoxicity in some cases (Walsh et al., 1995). Although losoxantrone and piroxantrone possess low cardiotoxicity, it is important to explain how the minimum cardiotoxicity of the two drugs could arise.

2.1.2. Cardiotoxic effect induced by doxorubicin, losoxantrone and piroxantrone

Losoxantrone and piroxantrone are two anthrapyrazole derivatives, which were developed as alternatives for doxorubicin, an anthracycline (Judson, 1991; Graham *et al.*, 1989). Similar to doxorubicin, losoxantrone and piroxantrone are inhibitors of topoisomerase II, an enzyme that is required for DNA replication and duplication (Leteurtre *et al.*, 1994). The inhibition of the enzyme leads to growth inhibition of tumor cells. However, the use of doxorubicin is limited by a cumulative dose-limiting cardiotoxic side effect (Gianni *et al.*, 1983; Weiss, 1992). Several studies on doxorubicin showed that the formation of the metal ion-anthracycline complex could lead to a serious cardiotoxic side effect (Leteurtre *et al.*, 1994; Hasinoff, 1998; Hasinoff *et al.*, 1998; Judson, 1991). The main mechanism of this cardiotoxic side effect may possibly be the formation of free radicals, which are the products of a series of redox reactions of the Fe^{3+}-anthracycline complex as shown in the following reactions, where DOX is doxorubicin:

$$Fe^{3+}\text{-DOX} + e^- \rightarrow Fe^{2+}\text{-DOX} \qquad (2.1)$$

$$Fe^{2+}\text{-DOX} + O_2 \rightarrow Fe^{3+}\text{-DOX} + O_2^{\cdot-} \qquad (2.2)$$

$$2O_2^{\cdot-} + 2H^+ \rightarrow H_2O_2 + O_2 \qquad (2.3)$$

$$Fe^{2+}\text{-DOX} + H_2O_2 \rightarrow Fe^{3+}\text{-DOX} + OH^- + OH^{\cdot} \qquad (2.4)$$
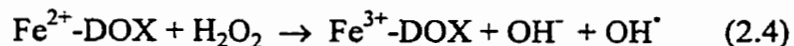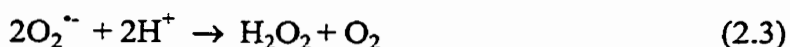
Fe^{3+}-doxorubicin can be reduced to Fe^{2+}-doxorubicin complex intra- or intermolecularly (Reaction 2.1). The latter complex then can undergo aerobic oxidation, and produce

reactive superoxide radicals (Reaction 2.2). These species can undergo further redox reaction to produce extremely reactive hydroxyl radicals (Reaction 2.4).

Losoxantrone and piroxantrone are structurally similar to doxorubicin (Figure 2.1). They all contain polycyclic aromatic fused rings, which are attached to electron rich atoms, such as nitrogen and oxygen. In addition, these compounds also possess hydroquinone-quinone functional groups. These groups are able to coordinate to metal ions, such as Cu^{2+} and Fe^{3+} (Herman et al., 1998; Hasinoff et al., 1998; Hasinoff, 1989a, 1998). The resulting complex could undergo subsequent redox reactions as that observed in the metal ion-doxorubicin complex, and produce reactive oxygen species, which damage a variety of tissues. It was found that doxorubicin can form a $Fe^{3+}(doxorubicin)_3$ complex under physiological conditions (Gianni et al., 1983; Myers et al., 1982; Gelvan and Samuni, 1988; May et al., 1980). This project investigates the formation of the Fe^{3+}-losoxantrone and Fe^{3+}-piroxantrone complexes, which could be the cause of the cardiotoxicity previously observed in animal and clinical trials of losoxantrone and piroxantrone (Ingle et al., 1994). The metal ion Fe^{3+} is biological relevant, and is of interest in this experiment. Fe^{2+}, a relatively abundant metal ion with free intracellular concentration of 80 μM is readily oxidized under aerobic condition to produce Fe^{3+} (Arslan et al., 1985). The results of these experiments together with the animal experimental results have been published (Herman et al., 1998).
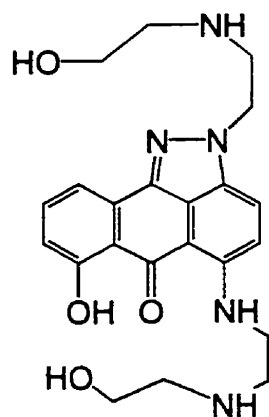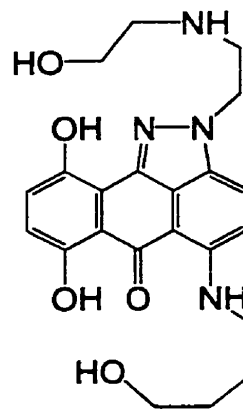
Losoxantrone (LXR)   Piroxantrone (PXR)
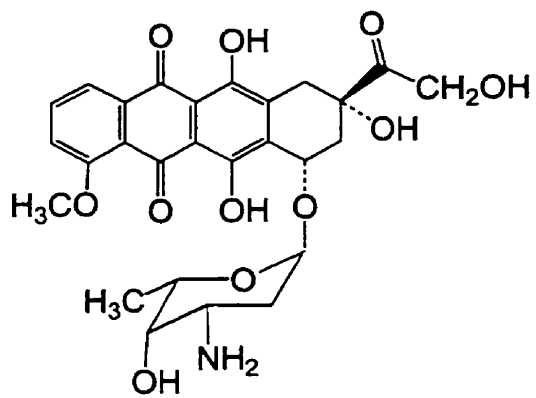
Doxorubicin (DOX)

Figure 2.1. Structures of doxorubicin, losoxantrone and piroxantrone.

2.2. Materials and methods

Losoxantrone and piroxantrone were gifts from Dr. E. H. Herman (FDA, Washington, DC). $FeCl_3 \cdot 6H_2O$ was from J. T. Baker Chemical Co. (Phillipsburg, NJ), and Tris·HCl (tris(hydroxymethyl)aminomethane·HCl) was from Sigma (cat. No. T-6666, St. Louis, MO). All other chemicals were obtained commercially at the highest grade available, and were used as received.

Losoxantrone and piroxantrone stock solutions (4 mM) were prepared in distilled water, and the solution concentrations were determined by weight using the microbalance (Micro Gram-Atic Balance, Fisher Scientific Company). The concentration of $FeCl_3 \cdot 6H_2O$ stock solution (10 mM) was determined spectrophotometrically by a previously reported method (Harris and Kratochvil, 1969). This solution was prepared in 2.0 mM HCl to prevent the formation of insoluble ferric hydroxides. Briefly, ferric chloride (10 mM) dissolved in 2 mM HCl was added to drug (4 mM). The solution turned a dark reddish-brown upon mixing, indicating complex formation. A small amount of the pre-formed Fe^{3+}-drug complex was added to a thermostatted (25 °C) 1 cm plastic spectrophotometer cell containing Tris/KCl (50 mM/150 mM, pH 7.2) buffer in a Cary 1 spectrophotometer (Varian, Mulgrave, Australia); the solution was allowed to equilibrate for about 10 min to allow the absorbance to stabilize. The formation of the Fe^{3+}-drug complex was examined by recording complete spectra (330 to 900 nm) at various Fe^{3+}:drug ratios, while the drug concentration was kept constant at 100 μM for losoxantrone, and 130 μM for piroxantrone. At high Fe^{3+}:drug ratios a dark red-brown precipitate was observed to form. The titration of losoxantrone by Fe^{3+} in aqueous buffer

was not highly reproducible, probably due to the formation of this precipitate. For this reason the losoxantrone titration was carried out in 80 % DMSO/20 % Tris/KCl (50 mM/150 mM, pH 7.2) (v/v) buffer. The absorbance changes for the titrations of losoxantrone and piroxantrone by Fe^{3+} were followed at 560 and 640 nm, respectively. At these wavelengths the extinction coefficients of the uncomplexed drugs were much lower than that of the Fe^{3+}-drug complexes, and this allowed a more accurate titration.

Molecular modeling of the Fe^{3+}-drug complexes was carried out using PCModel v. 5 (Serena Software, Bloomington, IN) on an IBM PC-compatible computer.

2.3. Formation of the Fe^{3+}-losoxantrone complex

As shown in Figure 2.2 significant spectral changes were observed as the ratios of the Fe^{3+}:losoxantrone increased, while the concentration of losoxantrone was maintained at 100 μM. For clarity only a few of the spectra at several Fe^{3+}:losoxantrone ratios are displayed in Figure 2.2. Isobestic points were observed at 460 and 510 nm. These are the points at which the spectral lines cross each other. This observation indicates the presence of only two species, the uncomplexed and complexed losoxantrone (Hasinoff, 1989a; Herman et al., 1998). The stoichiometry of the Fe^{3+}-losoxantrone complex was determined by measuring the absorbances at different Fe^{3+}:losoxantrone ratios. For the Fe^{3+}-losoxantrone complex, the absorbance was followed at 560 nm. This wavelength was chosen for an accurate stoichiometry determination because the absorbance due to losoxantrone alone (Fe^{3+}:losoxantrone ratio of zero) at this wavelength is very close to zero. The titration of the Fe^{3+}-losoxantrone complex is shown in Figure 2.3. The data points were simultaneously fit to two linear equations by a program (file name:

dogleg.fit) in SigmaPlot (Jandel Scientific, San Rafael, CA). From the titration curve in Figure 2.3, it was observed that the slope of the latter portion of the titration curve decreases at an Fe^{3+}:losoxantrone ratio above 0.8. This phenomenon indicates saturated binding of the drug to Fe^{3+}. An excess of Fe^{3+} did not result in the formation of more Fe^{3+}-drug complex, which absorbed at 560 nm. Also a small amount of dark precipitate was observed to form upon standing in the spectrophotometer cell at Fe^{3+}:ratio higher than 0.5. This precipitate may be either insoluble ferric hydroxide formed when uncomplexed Fe^{3+} was present in excess in solution, or possibly an insoluble polymeric Fe^{3+}-losoxantrone complex. This precipitate prevented accurate absorbance readings at high Fe^{3+}:losoxantrone ratios, and resulted in significant scatter in the upper region of the plot. Simultaneous least square fit the data to two linear line segments gives the Fe^{3+}:losoxantrone ratio at the intersection point of 0.72 ± 0.11 (± SEM). Thus, the losoxantrone:Fe^{3+} ratio of 1.39 ± 0.21 (± SEM) most closely corresponds to a 2:3 losoxantrone:Fe^{3+} complex of the molecular formula $(Fe^{3+})_2(losoxantrone)_3$. Within the error in the determination of the intersection point, 1:1 or 1:2 complexes of molecular formulas $Fe^{3+}(losoxantrone)$ or $Fe^{3+}(losoxantrone)_2$, are also likely. Computer modeling was utilized to propose the structure of the complex of the form $Fe^{3+}(losoxantrone)$ as shown in Figure 2.4.
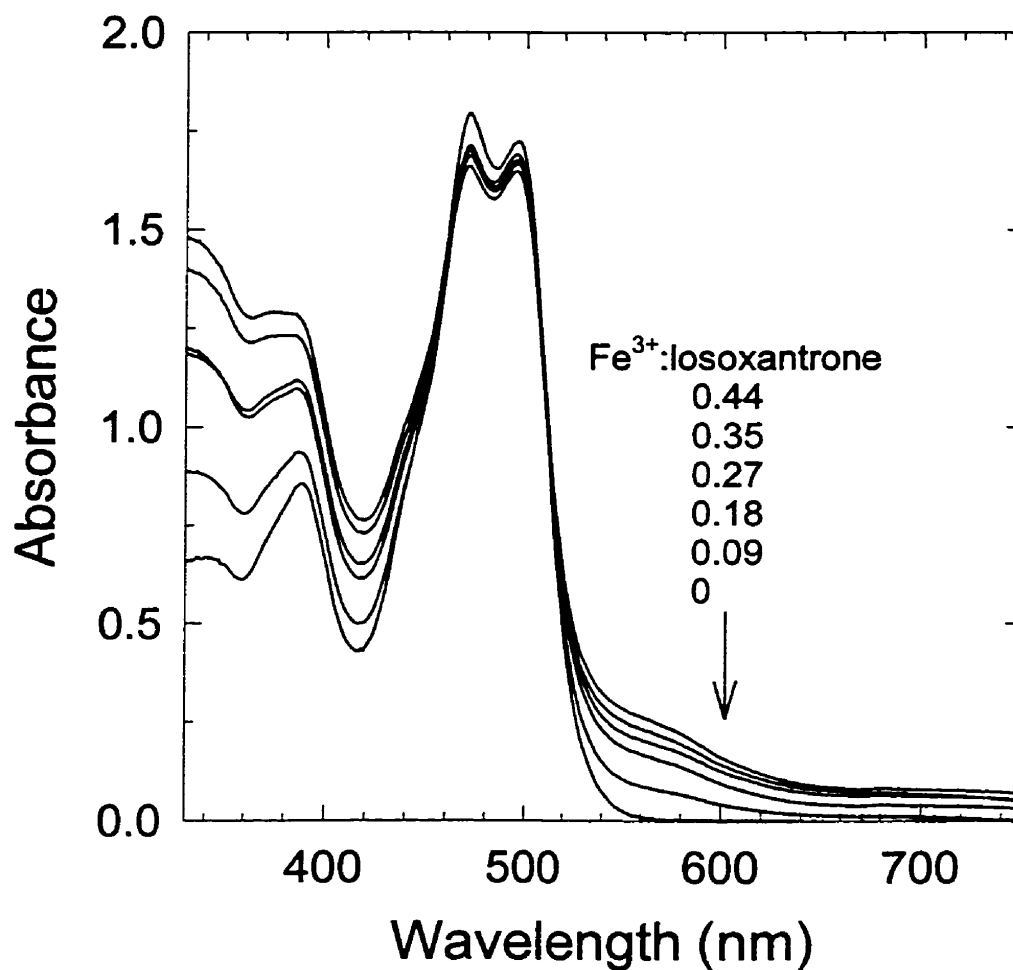
Figure 2.2. Spectra of pre-formed Fe^{3+}-losoxantrone complexes. The complexes at various Fe^{3+}:losoxantrone ratios were added to 80% DMSO/20% Tris/KCl (v/v) buffer at pH 7.2 and 25 °C. The concentration of losoxantrone was maintained constant at 100 μM, and the Fe^{3+} concentration was varied. The absorbance increased in the 550-750 nm region when the Fe^{3+}:losoxantrone ratios were increased as shown in the legend.
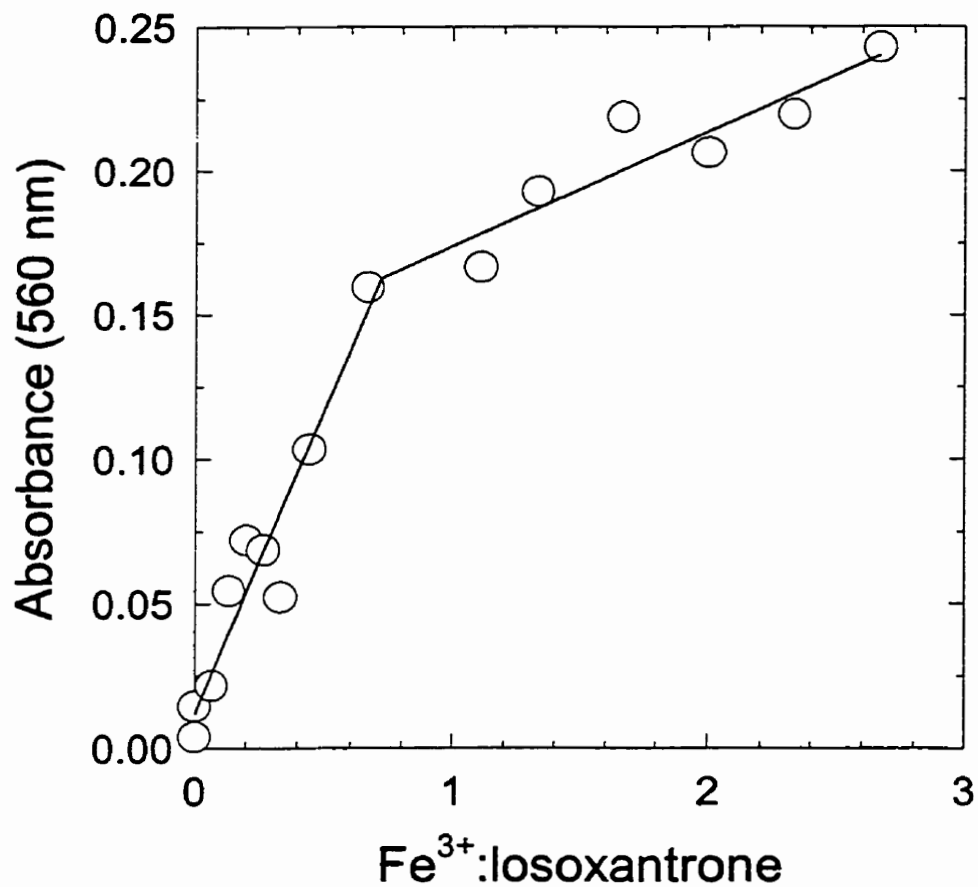
Figure 2.3. Spectrophotometric titration of losoxantrone with Fe^{3+}. The absorbance of the spectra of the pre-formed Fe^{3+}-losoxantrone complexes in Figure 2.2 was followed at the wavelength of 560 nm. The losoxantrone concentration was maintained constant at 100 μM. The complex was pre-formed at low pH and diluted into 80% DMSO/20% Tris/KCl (v/v) buffer (pH 7.2). The intersection of the least squares calculated two straight line segments occurs at a Fe^{3+}:losoxantrone ratio of 0.72 ± 0.11 (± SEM).
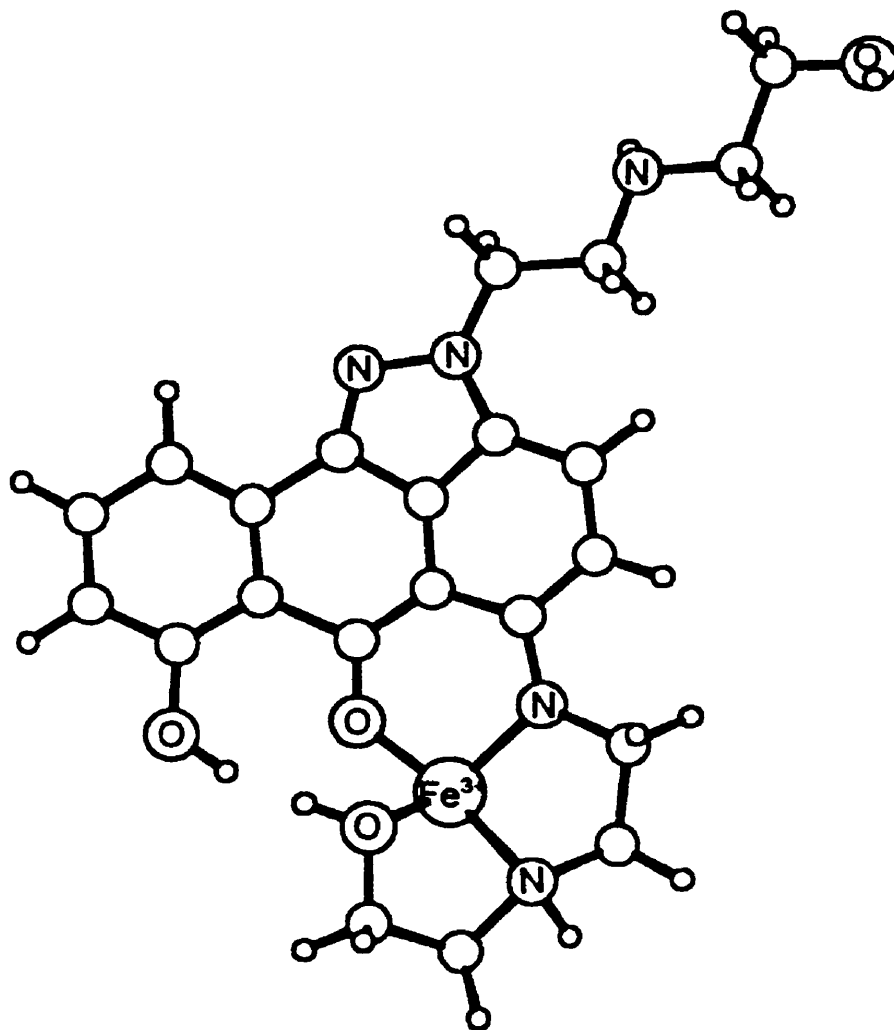
Figure 2.4. Proposed structure of Fe^{3+}(losoxantrone) using computer modeling with hetero atoms labeled only.

2.4. Formation of the Fe^{3+}-piroxantrone complex

The formation of the Fe^{3+}-piroxantrone complex (Figure 2.5) was indicated by spectral changes similar to those observed for the complex formation of losoxantrone (Figure 2.2). However, the spectral changes were more pronounced in this case. Isobestic points were observed at 540, 450, 420, and 390 nm. Again, this phenomenon indicates the presence of only two species in the solution, the complexed and uncomplexed piroxantrone. Figure 2.5 shows several spectra of the Fe^{3+}-piroxantrone complexes at different Fe^{3+}:piroxantrone ratios with a constant piroxantrone concentration of 130 μM. The stoichiometry of the Fe^{3+}-piroxantrone complex was characterized by following the absorbance changes at 640 nm. This wavelength was chosen as the absorbance of the uncomplexed piroxantrone is very close to zero. This allows a more accurate measurement of the absorbance due to the formation of the complex. The titration of the Fe^{3+}-piroxantrone complexes is shown in Figure 2.6. The data points were simultaneously fit to two linear equations by a program (file name: dogleg.fit) in SigmaPlot (Jandel Scientific, San Rafael, CA). The absorbance at 640 nm increases linearly with the Fe^{3+}:piroxantrone ratios up to 1.52. Above this ratio, the absorbance levels off and scatters. This observation indicates saturated binding of Fe^{3+} to piroxantrone. Also some brown precipitate formed in the complexed solution upon standing. This could be either insoluble ferric hydroxide formed when the uncomplexed Fe^{3+} was present in excess in solution, or possibly an insoluble polymeric Fe^{3+}-piroxantrone complex. Simultaneous least square fit of the data points into two linear line segments gives the Fe^{3+}:piroxantrone ratio at the intersection point of 1.52 ± 0.06 (±

SEM). This ratio corresponds most closely to a complex with a molecular formula of $(Fe^{3+})_3(piroxantrone)_2$. A 1:1 complex of the molecular formula of $(Fe^{3+})(piroxantrone)$ may also be possible with the uncertainties in determining the intersection point of the two linear line segments. Computer modeling was utilized to proposed the structure of the $(Fe^{3+})(piroxantrone)$ as shown in Figure 2.7.
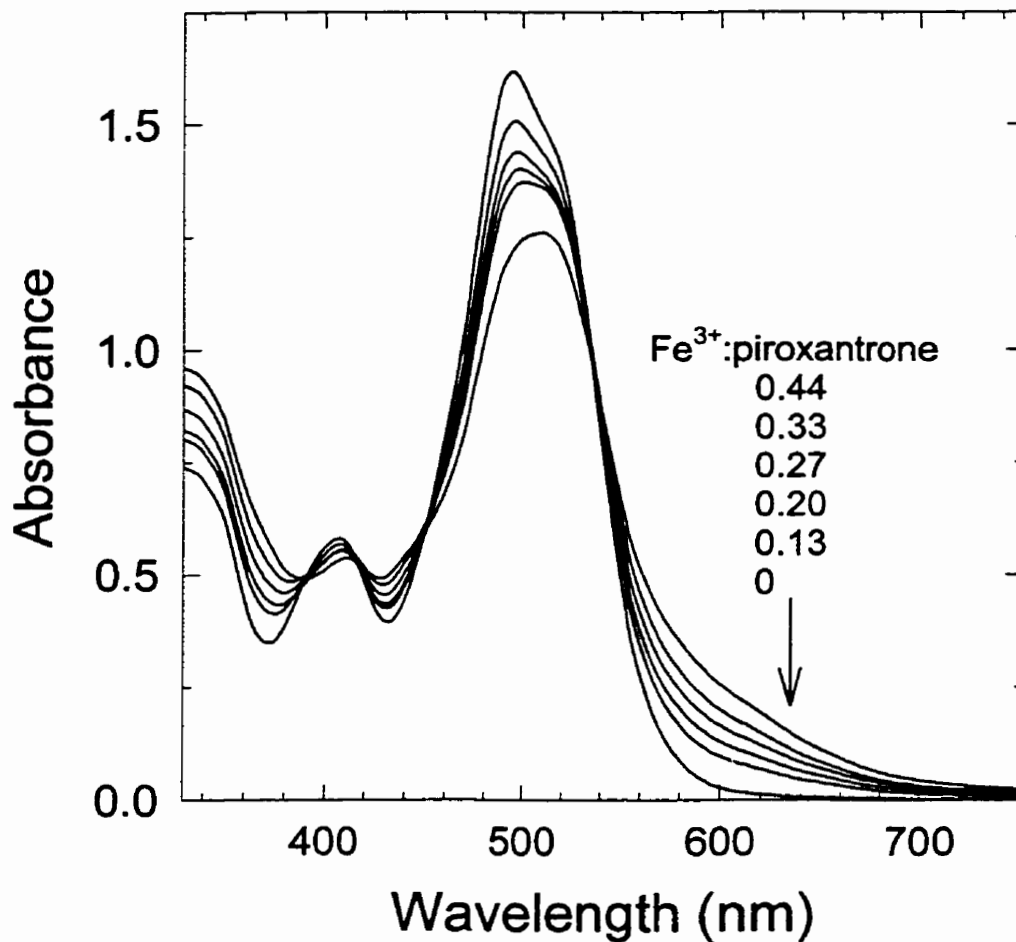
Figure 2.5. Spectra of pre-formed Fe^{3+}-piroxantrone complexes. The complexes at various Fe^{3+}:piroxantrone ratios were added to Tris/KCl buffer at pH 7.2 and 25 °C. The concentration of piroxantrone was maintained constant at 130 μM, and the Fe^{3+} concentration was varied. The absorbance increased in the 550-750 nm region when the Fe^{3+}:piroxantrone ratio was increased as shown in the legend.
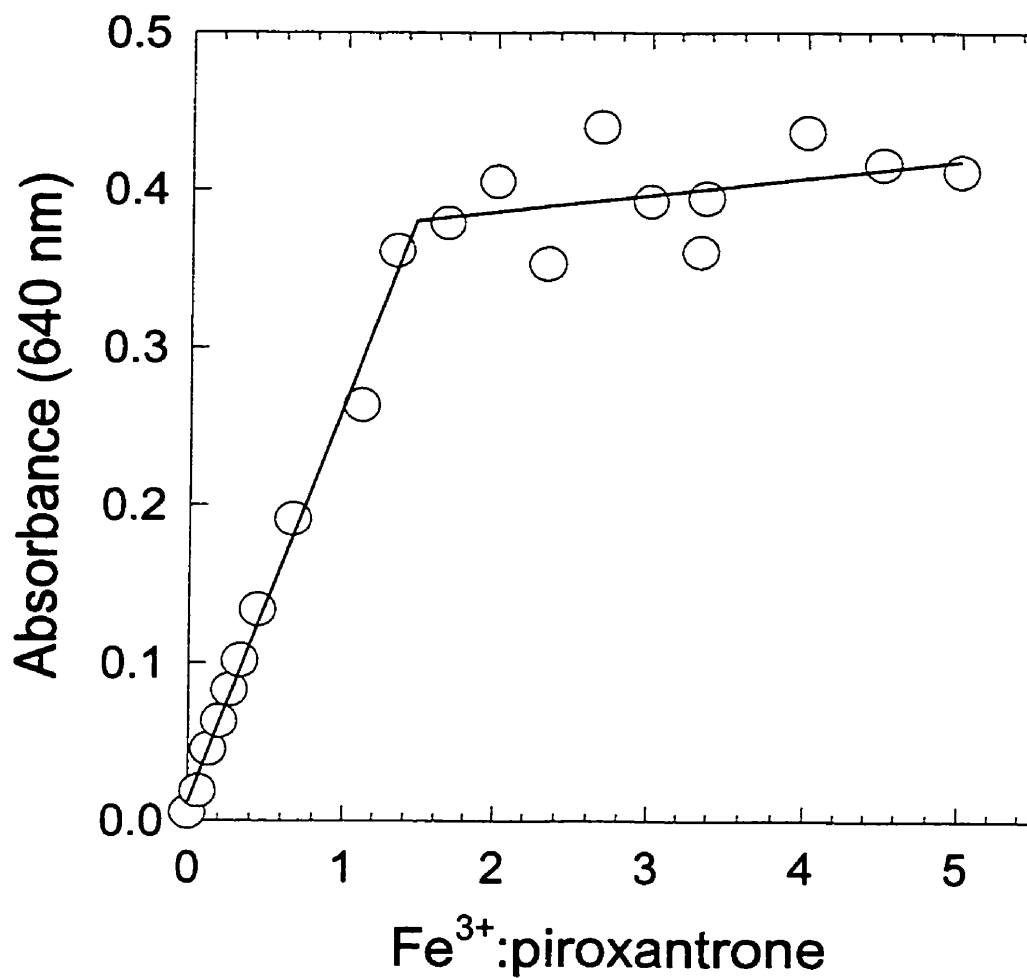
Figure 2.6. Spectrophotometric titration of piroxantrone with Fe^{3+}. The absorbance was followed at the wavelength of 640 nm. The piroxantrone concentration was maintained constant at 130 µM. The complex was pre-formed in Tris/KCl buffer at pH 7.2 and 25 °C. The intersection of the least squares calculated two straight line segments occurs at a Fe^{3+}:piroxantrone ratio of 1.52 ● 0.06 (± SEM).
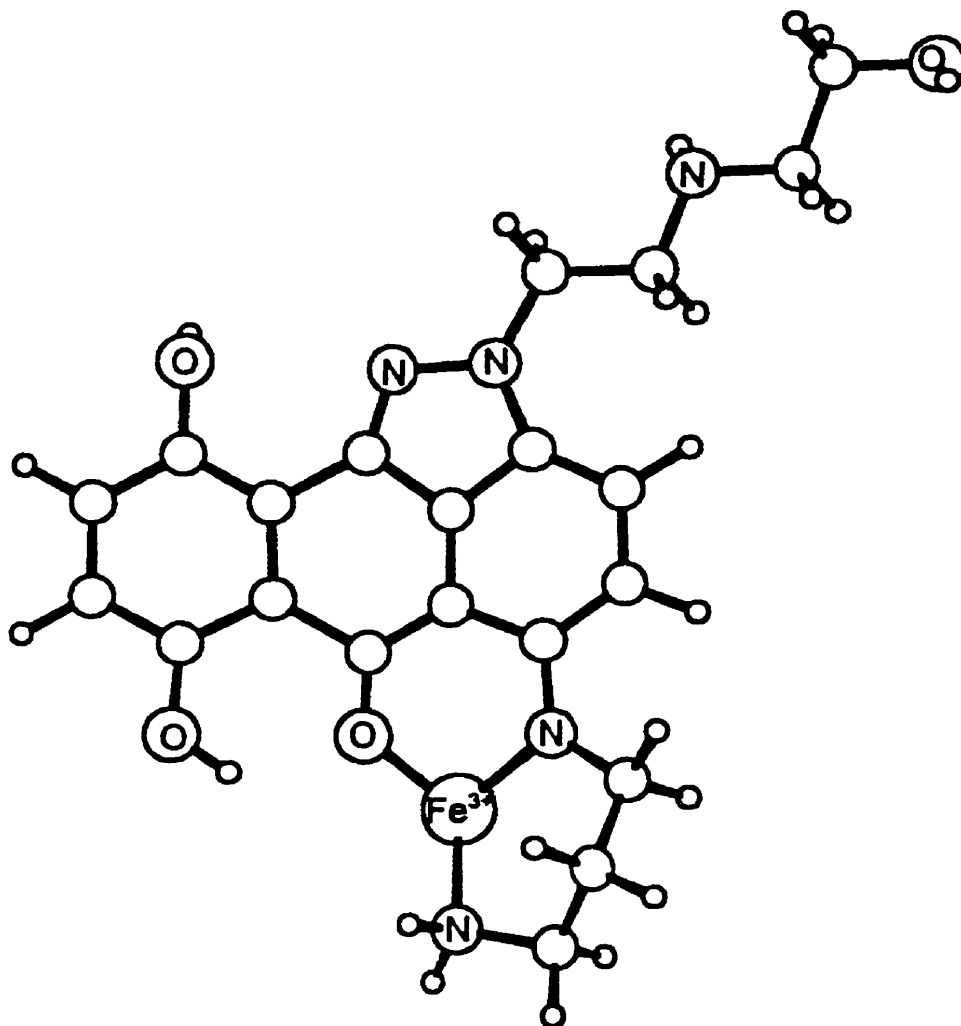
Figure 2.7. Proposed structure of Fe^{3+}(piroxantrone) using computer modeling with hetero atoms labeled only.

2.5. Implications for the Fe^{3+}-losoxantrone and Fe^{3+}-piroxantrone complex formation

The cardiotoxicity of doxorubicin is thought to be due to the production of reactive oxygen free radicals. Iron-based oxygen free radical-induced oxidative stress is normally observed in the heart muscle, which has a low level of antioxidant enzymes (Hasinoff et al., 1998; Hasinoff, 1998; Graham et al., 1989; Herman et al., 1997). The reactive free radicals are the products of a series of redox reactions (Reactions 2.1 to 2.4), in which metal ion such as Fe^{3+} is the main factor for the formation of free radicals. Upon complexation, Fe^{3+}-doxorubicin complex spontaneously autooxidizes producing hydrogen peroxide and hydroxyl radicals without the requirement of any enzyme (Zweier et al., 1986; Hasinoff, 1989b, 1990c). Doxorubicin can also undergo reduction to the corresponding semiquinone free radical by an enzyme, such as NADPH cytochrome P-450 (Bachur et al., 1979). The semiquinone radical then reacts with molecular oxygen under aerobic conditions to produce superoxide radical, and recycles the parent molecule. Superoxide undergoes rapid conversion to hydrogen peroxide, either spontaneously or via superoxide dismutase. Thus, doxorubicin involves quite a few possible reaction pathways producing reactive oxygen species, which result in oxidative stress (Gianni et al., 1983; Gutteridge, 1984; Myers et al., 1982; Gianni et al., 1985; Demant and Jensen, 1983; Malisza and Hasinoff, 1995b). Anthrapyrazoles, such as losoxantrone and piroxantrone were developed as alternatives to doxorubicin (Judson, 1991). The replacement of the hydroquinone-quinone moiety by the pyrazole ring is intended to reduce the formation of the metal ion-drug complexes, and thus reduce the production of

the reactive free radicals. The remaining anthracene moiety of losoxantrone and piroxantrone is very similar to that of doxorubicin.

In this experiment, spectrophotometric studies showed that both losoxantrone and piroxantrone were able to form complexes with Fe^{3+} under physiological pH, and the results have been published (Herman *et al.*, 1998). The molecular formulas are $(Fe^{3+})_2(losoxantrone)_3$, and $(Fe^{3+})_3(piroxantrone)_2$. Molecular modeling suggests that the ethylenediamine side chain, which is partly similar to ethylenediaminetetraacetic acid (EDTA) may be the good chelation sites for the metal ion. The Fe^{3+}:losoxantrone ratio (0.72 ± 0.11) from the titration (Figure 2.3) indicated that a complex of losoxantrone-Fe^{3+}-losoxantrone-Fe^{3+}-losoxantrone is also possible because the ethylenediamine attached to the pyrazole moiety could be a good chelation site as well. In addition, losoxantrone possesses a quinone-hydroquinone moiety, which also strongly chelates to metal ion. A similar argument could be applied to the Fe^{3+} complex of piroxantrone. A complex of Fe^{3+}-piroxantrone-Fe^{3+}-piroxantrone-Fe^{3+} could also be formed with Fe^{3+}:piroxantrone ratio of 1.52 ● 0.06 (Figure 2.6). In summary, losoxantrone and piroxantrone have several metal ion chelation sites. These chelation sites could result in a few number of Fe^{3+}-drug complexes, which were not understood.

Both losoxantrone and piroxantrone form Fe^{2+} complexes in the presence of ferrous ion; and the resulting ferrous ion-drug complexes could be aerobically oxidized to ferric complexes (Frank and Novak, 1986). Thus, the formation of the Fe^{3+}-losoxantrone and Fe^{3+}-piroxantrone complexes found in this experiment is consistent with previously related work (Frank and Novak, 1986). The metal ion complex formation of these two

drugs may be the cause of the observed dose-limiting toxicity in previous studies. These Fe^{3+}-losoxantrone and Fe^{3+}-piroxantrone complexes could undergo subsequent redox reactions (Reaction 2.1 to 2.4) as shown with the Fe^{3+}-doxorubicin complex, and induce oxidative damage leading to cardiotoxicity (Judson, 1991; Walsh *et al.*, 1995).

3.   Interaction of the cardioprotective drug dexrazoxane (ICRF-187, Zinecard®, Cardioxane®) and its hydrolysis product ADR-925 with the pre-formed Fe^{3+}-losoxantrone and Fe^{3+}-piroxantrone complexes

3.1. Introduction

According to the study in Chapter 2, both losoxantrone and piroxantrone were able to form complexes with Fe^{3+} ion in Tris/KCl buffer at pH 7.2. These metal ion-drug complexes may be responsible for the production of reactive oxygen species, which cause cardiotoxicity. The results in Chapter 2 have been published in combination with the animal studies of losoxantrone and piroxantrone in a comparison of the chronic toxicities of losoxantrone, piroxantrone, and doxorubicin (Herman et al., 1998). This study showed that the Fe^{3+}-drug complexes may cause oxidative damage to various tissues.

Despite the formation of Fe^{3+}-doxorubicin complex, which is thought to be the cause of the oxidative damage to various tissues, doxorubicin is still widely used as an anticancer agent for the treatment of a variety of tumors (Healy et al., 1998). The cause of doxorubicin-induced oxidative damage is reduced by other protective agents, such as deferoxamine, and dexrazoxane (Elihu et al., 1998). Dexrazoxane strongly reduces the cardiotoxicity of doxorubicin; several recent review articles have been published on this subject (Hasinoff et al., 1998; Hasinoff, 1998). It has been shown that dexrazoxane can prevent oxidative damage upon hydrolysis under physiological conditions to its active form ADR-925, which is structurally similar to EDTA, a metal ion chelator (Figure 3.1) (Hasinoff, 1989a; Hasinoff et al., 1998; Hasinoff, 1998; Synold et al., 1998). The hydrolyzed form ADR-925 competitively removes Fe^{3+} from the pre-formed Fe^{3+}-

doxorubicin complex, or coordinate with the free Fe^{3+} (Hasinoff, 1989a). Another study also shows that dexrazoxane interacts directly with the Fe^{3+}-doxorubicin complex to form a ternary complex of Fe^{3+}-doxorubicin-dexrazoxane (Sobol *et al.*, 1992). These results suggest that by either competitively dissociating the pre-formed Fe^{3+}-doxorubicin, or coordinating with the free Fe^{3+}, or interacting directly with the Fe^{3+}-doxorubicin to form a ternary complex, the ability to produce free radicals by the Fe^{3+}-doxorubicin is reduced. The reduction in free radical production should lead to less oxidative damage to various tissues.

In this study, the reactions of the pre-formed Fe^{3+}-losoxantrone, and Fe^{3+}-piroxantrone with dexrazoxane, ADR-925, and EDTA were investigated. It was hypothesized that by dissociating the metal ion-drug complex, the production of reactive oxygen species might be minimized, and thereby could reduce the oxidative damage in various tissues. These experiments may provide useful information on the concentration, or time of the administration for the combination of losoxantrone or piroxantrone with dexrazoxane in future studies using animal models.
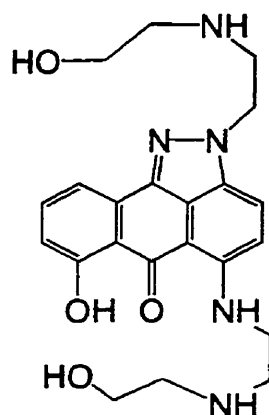
Losoxantrone (LXR)
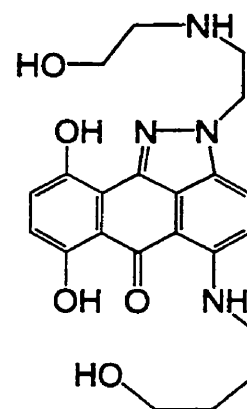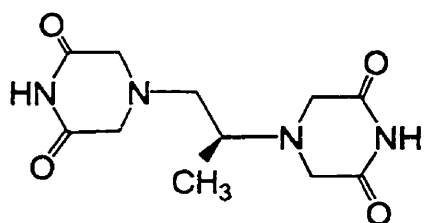
Piroxantrone (PXR)

Dexrazoxane
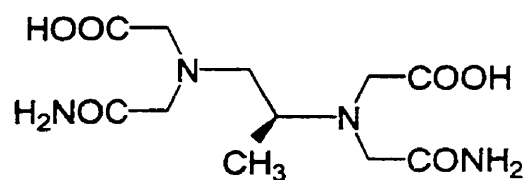
ADR-925
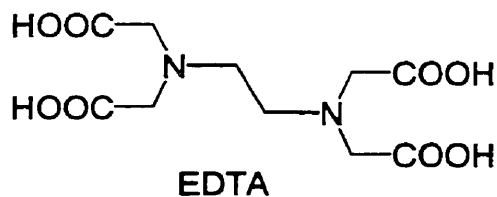
EDTA

Figure 3.1. Structures of losoxantrone, piroxantrone, dexrazoxane, ADR-925, and EDTA.

3.2. Materials and methods

Losoxantrone and piroxantrone were gifts from Dr. E. H. Herman (FDA, Washington, DC). $FeCl_3 \cdot 6H_2O$ was from J. T. Baker Chemical Co. (Phillipsburg, NJ). Tris·HCl (tris(hydroxymethyl)aminomethane·HCl) was from Sigma (cat. No. T-6666, St. Louis, MO). Dexrazoxane and ADR-925 were gifts from Pharmacia & Upjohn (Columbus, OH). EDTA was from Aldrich Chemical Company, Inc. (cat. No. 31,888-4, Milwaukee, MI). All other chemicals were obtained commercially at the highest grade available, and were used as received.

The Fe^{3+}-losoxantrone and Fe^{3+}-piroxantrone complexes were prepared at fixed concentrations of Fe^{3+} at 135 μM, and of losoxantrone or piroxantrone at 68 μM under slightly acidic conditions to prevent the formation of insoluble ferric hydroxides. Ferric chloride (10 mM) dissolved in 1 mM HCl was added to drug (4 mM). The solution turned to dark reddish-brown upon mixing, which indicates complex formation. A small amount of the pre-formed Fe^{3+}-drug complex was added to a thermostatted (25 °C) 1 cm plastic cell containing Tris/KCl (50 mM/150 mM, pH 7.2) buffer in a Cary 1 spectrophotometer, and the solution was allowed to equilibrate for about 1 min to allow the absorbance to stabilize. The absorbance of the Fe^{3+}-drug complex solutions was followed with time at 560 nm for the Fe^{3+}-losoxantrone complex, and 640 nm for the Fe^{3+}-piroxantrone complex. These two wavelengths were chosen for the spectrophotometric titrations of the Fe^{3+}-losoxantrone and Fe^{3+}-piroxantrone complexes as described in Sections 2.3 and 2.4. One min after starting the absorbance reading, various concentrations of the chelators, such as EDTA, dexrazoxane and its hydrolyzed

form ADR-925 were added. The Cary kinetics software (Varian, Mulgrave, Australia) was used to determine the first-order rate constants for the dissociation of the Fe^{3+}-drug complexes.

3.3. Reaction of the Fe^{3+}-losoxantrone complex in the presence of various chelators

The absorbance-time traces of the Fe^{3+}-losoxantrone complex in the presence of EDTA, dexrazoxane, and ADR-925 are shown in Figure 3.2. A fast initial drop in the absorbance at 560 nm is observed in each trace. Also, the absorbance drops faster as the concentration of the chelators increases. It should be noted that at 560 nm the absorbance due to the presence of free losoxantrone is very close to zero as shown in Chapter 2, and at this wavelength the absorbance due to the presence of EDTA, dexrazoxane, and ADR-925 alone is close to zero. Thus, the drop in the absorbance at 560 nm of the Fe^{3+}-losoxantrone complex indicates the dissociation of the pre-formed Fe^{3+}-losoxantrone complex. These absorbance-time traces were fit by non-linear least square analysis, which gives the observed pseudo-first order rate constants, k_{obs} as shown in the following Equation 3.1

$$A = (Amp) \cdot e^{-k_{obs} \cdot t} + A_{\infty} \qquad (3.1)$$

in which A and A_{∞} are the absorbances at time t and infinity, respectively, and k_{obs} is the pseudo-first-order rate constant, and Amp is the amplitude of the absorbance change. The values of k_{obs} were determined by fitting the absorbance-time traces after adding the chelators to the Fe^{3+}-losoxantrone complex solution. During this short period of time the absorbance at 560 nm dropped significantly, and also the absorbance of the control trace

without any chelator gradually decreased with time (Figure 3.2). These observations indicated the instability of the Fe^{3+}-losoxantrone complex. The values of k_{obs} were plotted against the concentrations of the chelators (Figure 3.3), and fit to a linear equation (Equation 5.2):

$$k_{obs} = k_2 \cdot [chelator] \qquad (5.2)$$

in which k_2 is a second order rate constant, describing the dependence of the Fe^{3+}-losoxantrone complex dissociation on the concentration of the chelators. The slope of the line gives the value of k_2, which is a good estimation of the second-order rate constant. The slopes were found to be 116 ± 10.8 $M^{-1} \cdot min^{-1}$ with dexrazoxane, and 4.8 ± 3.1 $M^{-1} \cdot min^{-1}$ with ADR-925. The values of k_{obs} were not very reliable due to the fast drop in the absorbance within the first few minutes of the reaction of the Fe^{3+}-losoxantrone complex in the presence of ADR-925. Only the last part of the absorbance-time traces were utilized in the kinetic fittings. For this reason the second-order rate constant k_2 for the reaction of the Fe^{3+}-losoxantrone complex with ADR-925 was found to be smaller than that with dexrazoxane, but the absorbance at 560 nm dropped further in the presence of ADR-925 compared to that in the presence of dexrazoxane (Figure 3.2). Thus, the percentage of the Fe^{3+}-losoxantrone complex dissociation was used to compare the effect of the Fe^{3+} removal in the presence dexrazoxane and ADR-925 (Table 2.1). The absorbances at 560 nm and at 50 min were used in the comparison, in which 100 % Fe^{3+} removal was assigned when the absorbance dropped to zero, and 0 % Fe^{3+} removal was assigned for the absorbance of the control trace at 50 min.

Table 3.1. Fe^{3+}-losoxantrone complex dissociation in the presence of various chelators. The values of k_{obs} and % dissociation at time 50 min were obtained from Figure 3.2, and 100 % Fe^{3+} removal was assigned when the absorbance at 560 nm dropped to zero, and 0 % Fe^{3+} removal was assigned for the absorbance of the control trace.

Chelator	Concentration (μM)	% dissociation	k_{obs} (min^{-1})
control	0	0	0.077
EDTA	100	62.4	0.090
ADR-925	100	46.7	0.084
ADR-925	200	49.3	0.081
ADR-925	500	49.6	0.082
ADR-925	700	58.6	0.083
ADR-925	1000	58.6	0.085
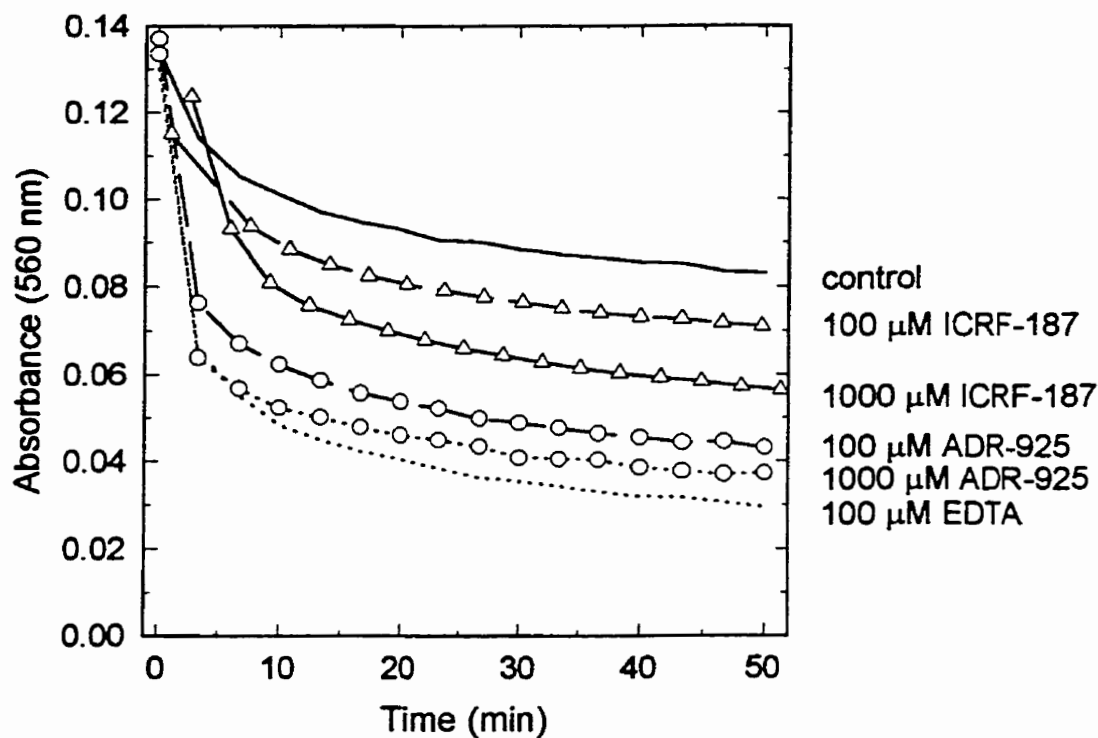
Figure 3.2. Absorbance-time traces of Fe^{3+}-losoxantrone at 560 nm upon the addition of various chelators. The Fe^{3+}-losoxantrone complexes reacted with different chelators under physiological conditions (Tris/KCl buffer, pH 7.2, 25 °C). The Fe^{3+}-losoxantrone complex was formed at 68 μM Fe^{3+} and 135 μM losoxantrone. There was no chelator added for the control trace. Various concentrations of chelators were used for the other traces as shown in the legend, and were added 1 min after starting the recording of the absorbance.
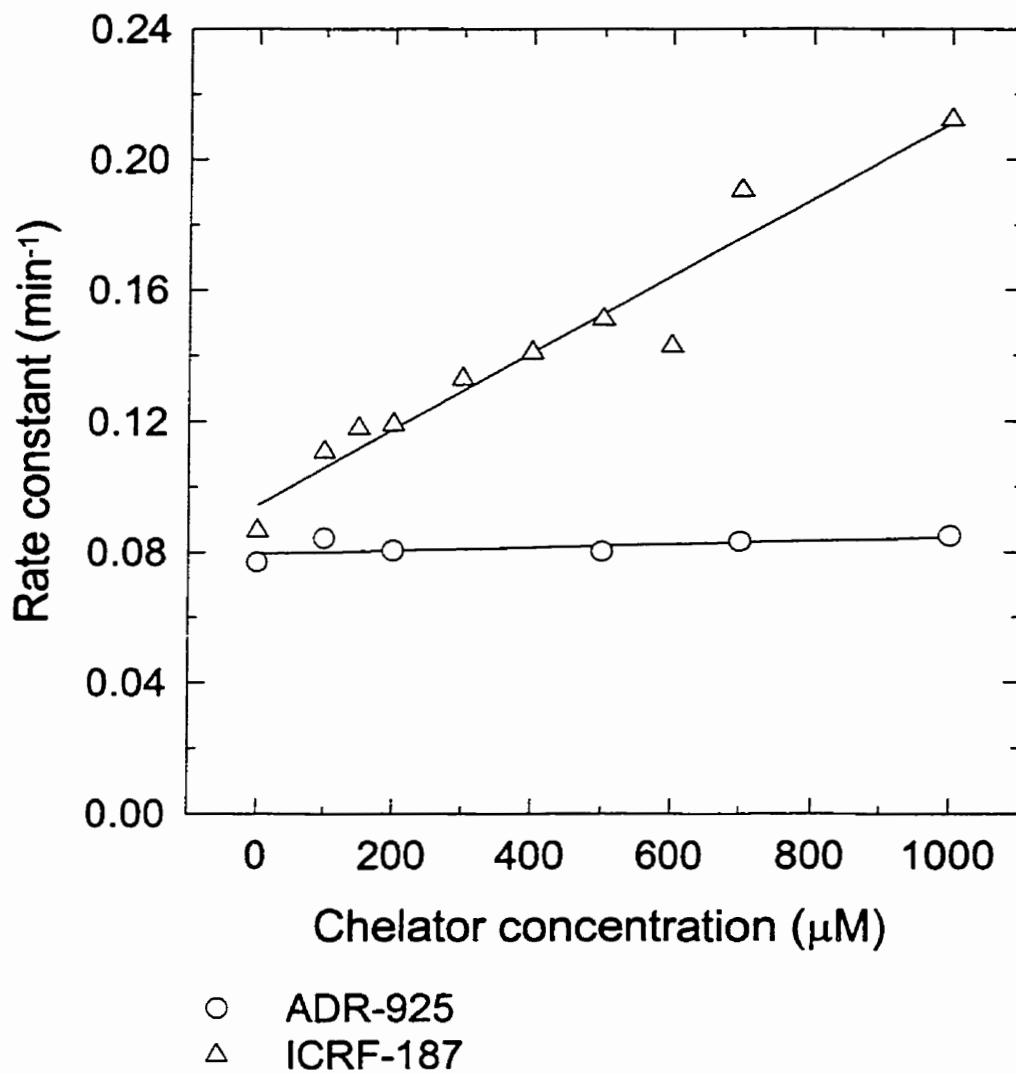
Figure 3.3. Plots of pseudo-first-order rate constants, k_{obs}, for the reaction of Fe^{3+}-losoxantrone complex in the presence of various concentrations of dexrazoxane, and ADR-925 measured at 560 nm as shown in the legend. The slopes of the fit lines are 116 $\pm$ 10.8 $M^{-1} \cdot min^{-1}$ for dexrazoxane and 4.8 $\pm$ 3.1 $M^{-1} \cdot min^{-1}$ for ADR-925.

3.4. Reaction of the Fe^{3+}-piroxantrone complex in the presence of various chelators

The absorbance-time traces of the Fe^{3+}-piroxantrone complex in the presence of various chelator concentrations are shown in Figure 3.4. For the reactions with ADR-925, a fairly fast drop of the absorbance at 640 nm was observed. This observation indicates the dissociation of the Fe^{3+}-piroxantrone complex because both the chelators and the dissociated piroxantrone (or free piroxantrone) do not significantly absorb at this wavelength. The data treatment was similar to that for the Fe^{3+}-losoxantrone complex (Section 3.3). The absorbance-time traces were fit to a non-linear least square using Equation 3.1. The obtained values of k_{obs} were then fit to Equation 3.2. A good linear relationship was observed over a wide range of ADR-925 concentrations as shown in Figure 3.5. The slope of the best fit line (481 $\bullet$ 30 $M^{-1} \cdot min^{-1}$) gives the second order rate constant. The reaction of the Fe^{3+}-piroxantrone complex in the presence of various dexrazoxane concentrations showed no decrease in the absorbance at 640 nm (Figure 3.4). This indicates that there was no significant Fe^{3+}-piroxantrone complex dissociation in the presence of dexrazoxane. Over longer periods of time of up to 15 h, the absorbance increased due to the formation of visible precipitates.
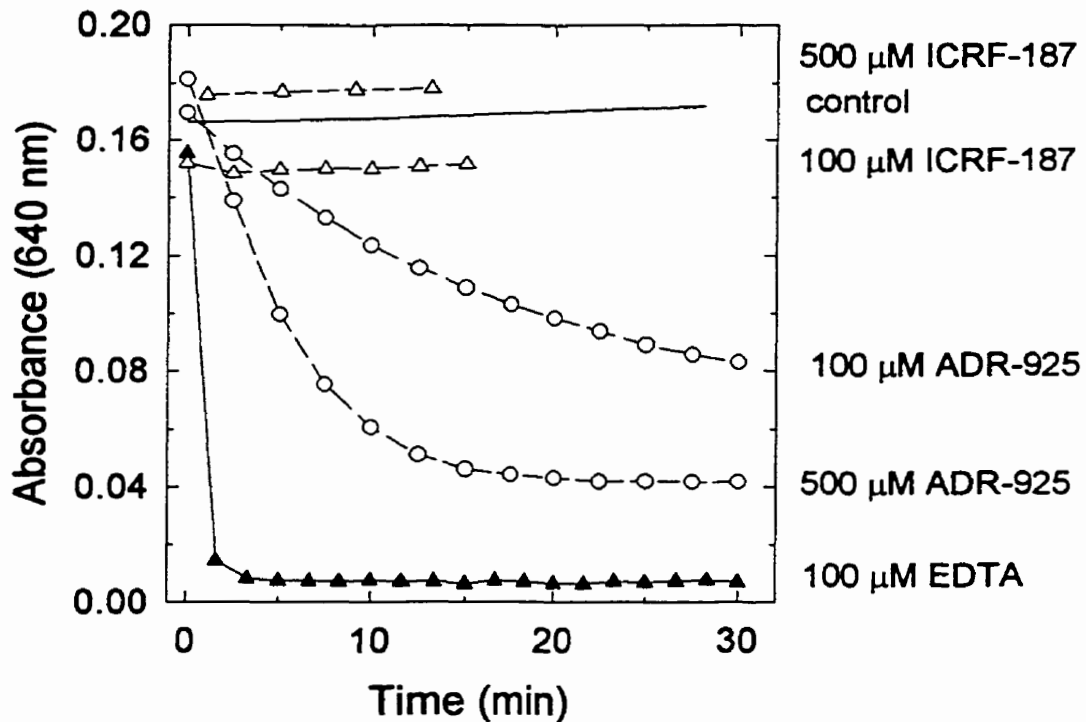
Figure 3.4. Absorbance-time traces of Fe^{3+}-piroxantrone at 640 nm upon the addition of various chelators. The Fe^{3+}-piroxantrone complex reacted with different chelators under physiological conditions (Tris/KCl buffer, pH 7.2, 25 °C). The Fe^{3+}-piroxantrone complex was formed at 68 μM Fe^{3+}, 135 μM piroxantrone. There was no chelator added for the control trace. Various concentrations of chelators were used for the other traces as shown in the legend, and were added 1 min after starting the recording of the absorbance.
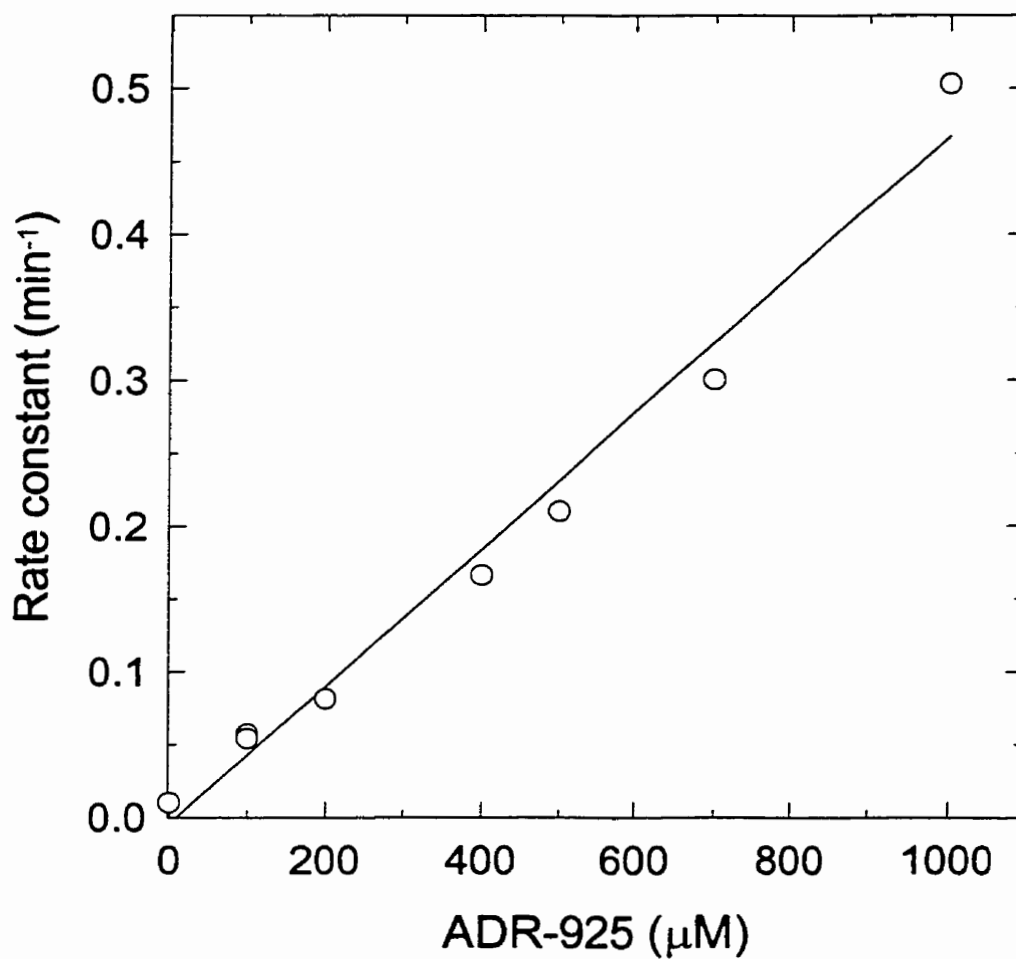
Figure 3.5. Plot of pseudo-first-order rate constants, k_{obs}, for the reaction of Fe^{3+}-piroxantrone complex in the presence of various concentrations of ADR-925 measured at 640 nm as shown in the legend. The slope of the fit line is 481 ± 30 $M^{-1} \cdot min^{-1}$ for ADR-925.

3.5. Implications for the Fe^{3+}-losoxantrone and Fe^{3+}-piroxantrone complex dissociation in the presence of the cardioprotective drug dexrazoxane and its hydrolyzed form ADR-925

Previous studies have shown that dexrazoxane is effective in preventing NADPH-dependent doxorubicin semiquinone formation (Malisza and Hasinoff, 1996b), and the loss of the cytochrome c oxidase, and NADH cytochrome c reductase activity on submitochrondrial particles (Hasinoff, 1989a). Dexrazoxane exerts its cardioprotective activity through its hydrolyzed form, ADR-925, which is structurally similar to EDTA. However, there is evidence that Fe^{3+}-ADR-925 could also produce hydroxyl radicals in a NADPH-cytochrome-P-450 reductase system at a very low level (Hasinoff, 1995; Malisza and Hasinoff, 1996a). Upon chelating to either free or doxorubicin-bound metal ions, such as Fe^{3+} or Cu^{2+}, ADR-925 was found to be effective in preventing the loss of cytochrome c oxidase activity (Hasinoff, 1989a). This study investigated the Fe^{3+} removal from the pre-formed Fe^{3+}-losoxantrone, and Fe^{3+}-piroxantrone complexes in the presence of both dexrazoxane and ADR-925. The results in these studies showed spectrophotometrically that Fe^{3+}-losoxantrone and Fe^{3+}-piroxantrone complexes could be dissociated at different degrees.

The reactions of the Fe^{3+}-losoxantrone complex with dexrazoxane at various concentrations were monitored spectrophotometrically. It was found that the Fe^{3+} removal from the metal ion-drug complexes increased linearly with dexrazoxane concentrations (Figure 3.3). Dexrazoxane can hydrolyze with half times of 0.4 min and 170 min in the presence of unbound Fe^{2+} and Fe^{3+}, respectively (Buss and Hasinoff,

1995). The absorbance at 560 nm in Figure 3.2 showed a fast initial drop in the first 10

min after the addition of dexrazoxane. During this first short period of time, there might

be a small fraction of dexrazoxane that hydrolyzed to ADR-925, which quickly removed

Fe^{3+} from the Fe^{3+}-losoxantrone complex. Thus, this observation indicated that

losoxantrone loosely bound to Fe^{3+} to form a weak complex. Consistently, the formation

of the Fe^{3+}-losoxantrone complex in Section 2.3 was performed in 80 % DMSO/20 %

Tris/KCl (50 mM/150 mM, pH 7.2) (v/v) buffer, instead of Tris/KCl buffer due to the

instability of the Fe^{3+}-losoxantrone complex formation. For the reaction of Fe^{3+}-

losoxantrone with ADR-925, the absorbance dropped significantly in less than 30 sec

right after the addition of ADR-925. Kinetically, the k_{obs} increased linearly with the

chelator concentrations over a wide range (100 to 1000 μM). However, the slope of the

best fit line is not large because the Fe^{3+} removal has been completed in the first few

seconds of the reaction of the Fe^{3+}-losoxantrone complex with ADR-925. The values of

k_{obs} were obtained from the first-order kinetic fittings of only the last part of the traces.

This resulted in equally small values of k_{obs} at various concentrations of ADR-925. In the

presence of EDTA, a very strong metal ion chelator, the Fe^{3+} removal was not complete

as shown in Figure 3.2. The observation that the absorbances did not go down to zero,

indicates both dexrazoxane and ADR-925 could remove quickly, but not completely, all

of the bound Fe^{3+} from the pre-formed Fe^{3+}-losoxantrone complex. Mixed complexes,

such as dexrazoxane-Fe^{3+}-losoxantrone, and (ADR-925)-Fe^{3+}-losoxantrone might also be

formed. Previously, it was proposed that mixed-ligand complex of Fe^{3+}-doxorubicin with

other chelators might be less active in the stimulation of hydroxyl radical production (Hasinoff, 1990b).

The reactions of the pre-formed Fe^{3+}-piroxantrone complex with dexrazoxane and ADR-925 were also investigated spectrophotometrically. The absorbance-time traces of the Fe^{3+}-drug complex in the presence of various dexrazoxane concentrations showed that there was no Fe^{3+} removal. Indeed, over a period of 15 h the absorbance started to increase due to the formation of visible precipitates. This result indicates that unlike Fe^{3+}-losoxantrone complex, the Fe^{3+}-piroxantrone complex is more stable. A small fraction of ADR-925 present in dexrazoxane might be not enough to remove the Fe^{3+} from the complex. The reaction of the Fe^{3+}-piroxantrone complex with ADR-925 was more kinetically favorable. The degree of Fe^{3+} removal increased with the chelator concentrations. This observation indicates that the metal ion removal from the Fe^{3+}-piroxantrone complex in the presence of ADR-925 is slow enough to follow spectrophotometrically as shown in Figure 3.4. Unlike Fe^{3+}-losoxantrone complex, the Fe^{3+}-piroxantrone complex was dissociated almost completely at 100 μM EDTA (Figure 3.4). The Fe^{3+} removal proceeded quickly but not completely for the Fe^{3+}-losoxantrone complex, while a slower but more complete Fe^{3+} removal proceeded for the Fe^{3+}-piroxantrone complex reactions.

A comparison of the cytotoxicities of losoxantrone and piroxantrone showed that the cardiac lesions induced by losoxantrone were significantly more severe than those induced by piroxantrone, and that the cardiac lesions might be the result of the chelation of the drugs to Fe^{3+} (Herman *et al.*, 1998). The results in this study have shown that the

Fe^{3+}-losoxantrone and Fe^{3+}-piroxantrone complexes could be dissociated by ADR-925, the hydrolyzed form of dexrazoxane. This observation might be useful in a future study, in which the combination of the drug treatment of losoxantrone or piroxantrone with dexrazoxane (the cell membrane permeable form) might lower the level of the Fe^{3+}-drug complexes, which might be responsible for the cardiac lesions. These results suggest that dexrazoxane may be clinically useful in reducing losoxantrone and piroxantrone cardiotoxicity.

4. Effects on the growth inhibition of Chinese hamster ovary cells induced by *m*-amsacrine, etoposide, teniposide, losoxantrone, and piroxantrone combined with dexrazoxane

4.1. DNA-topoisomerase II interaction

Topoisomerases I and II are the two major types of the enzymes in all eukaryotic cells. These enzymes are essential for normal functioning of the cells in several important cellular processes, such as in the relaxation of the torsional strain of duplex DNA during DNA replication and transcription, separating two newly formed circular DNA molecules, and so on (Redinbo *et al.*, 1998; Stewart *et al.*, 1998; Berger *et al.*, 1996). General descriptions on the important roles and mechanisms of topoisomerases were described in Chapter 1. In this study the combined effects of two different topoisomerase II inhibitors, such as non-cleavable complex-forming topoisomerase II inhibitors (or catalytic inhibitors), and cleavable complex-forming topoisomerase II poisons were investigated. The crystal structure of the yeast topoisomerase II shows that the enzyme has a clamp form, which can open and wrap around DNA to form a cleavable complex of topoisomerase II-DNA for the transient cleavage reaction (Berger *et al.*, 1996). Some topoisomerase II-targeted drugs can interact with the cleavable complex of topoisomerase II-DNA to form a ternary drug-DNA-topoisomerase II complex (Froelich-Ammon and Osheroff, 1995; Hasinoff *et al.*, 1997; Wang *et al.*, 1997). The formation and stabilization of the ternary complex by the topoisomerase II-targeted drug can convert this ternary complex into a cellular poison, and thereby inhibit DNA replication and transcription. Since rapidly growing cells, such as tumor cells have a high level of

topoisomerase II, stabilization of the cleavable complex by topoisomerase II inhibitor is utilized to inhibit the growth of tumors. In this study, the interactions between the two types of topoisomerase II inhibitors, non-cleavable complex-forming topoisomerase II inhibitors, such as dexrazoxane (Figure 4.1), and cleavable complex-forming topoisomerase II poisons, such as *m*-amsacrine, etoposide, teniposide, losoxantrone, and piroxantrone (Figure 4.2) were investigated using Chinese hamster ovary cells.

m-Amsacrine is a member of the antitumor class of 9-anilinoacridines (Figure 4.2). Several antineoplastic mechanisms have been proposed for this agent (Sengupta, 1995). The planar portion of the molecule is important for stacking with the base pairs in DNA. Besides being a DNA intercalating agent, *m*-amsacrine has been considered to be a topoisomerase II inhibitor. The main cytotoxic effect of *m*-amsacrine is the formation of a ternary complex of DNA, topoisomerase II, and *m*-amsacrine (Corbett and Osheroff, 1993).

Etoposide and teniposide are epipodophyllotoxins, which are extracted from the dried roots of *Podophyllum peltatum* (Figure 4.2). Etoposide and teniposide inhibit topoisomerase II by stabilizing the enzyme-DNA cleavable complex (Hasinoff *et al.*, 1997; Sengupta, 1995). These two compounds are also shown to cause fragmentation of DNA, inhibit DNA topoisomerase II activity, and produce topoisomerase II-DNA cross-links (Wang *et al.*, 1997).

Losoxantrone and piroxantrone are two anthrapyrazoles that are structurally similar to doxorubicin (Figure 4.2). The planar aromatic fused rings with several attached functional groups carrying positive charges are essential for intercalating with

DNA, and affecting the DNA topology (Wang *et al.*, 1997). Several studies on losoxantrone and piroxantrone show that these compounds could also directly inhibit the activity of topoisomerase II by stabilizing cleavable complex formation (Judson, 1991; Leteurtre *et al.*, 1994).

Several bisdioxopiperazines, such as ICRF-154, ICRF-159, dexrazoxane, and ICRF-193 (Figure 4.1) also target topoisomerase II; and in the presence of ATP, ICRF-193 converts the enzyme to a form incapable of binding circular DNA (Kano *et al.*, 1992; Snapka *et al.*, 1996; Ishida *et al.*, 1995). Since *m*-amsacrine, etoposide, teniposide, losoxantrone and piroxantrone (Figure 4.2) are cytotoxic by the stabilization of the topoisomerase II-DNA cleavable complex, it is important to understand the interaction of these drugs in combination with dexrazoxane on the growth of Chinese hamster ovary cells.

ICRF-154 $R_1 = R_2 = H$
ICRF-159 $R_1 = H$, $R_2 = CH_3$ (racemic)
ICRF-187 $R_1 = R_2 = CH_3$ $((S)-(+))$
ICRF-186 $R_1 = R_2 = CH_3$ $((R)-(-))$
ICRF-192 $R_1 = H$, $R_2 = C_2H_5$ (racemic)
ICRF-193 $R_1 = R_2 = CH_3$ (meso)
ICRF-201 $R_1 = R_2 = C_2H_5$ (meso)
ICRF-202 $R_1 = CH_3$, $R_2 = C_2H_5$ (erythro)
ICRF-215 $R_1 = CH_3$, $R_2 = C_3H_7$ (erythro)
ICRF-220 $R_1 = CH_3$, $R_2 = CH_2OCH_3$ (erythro)
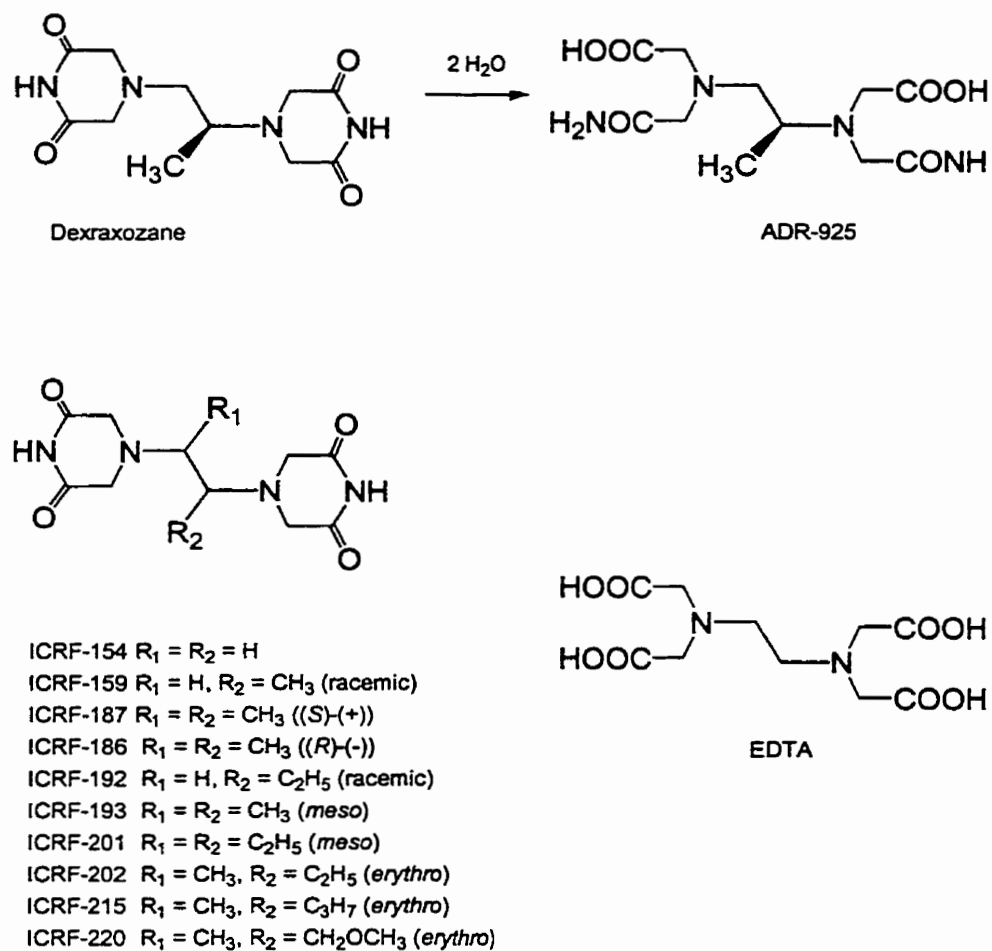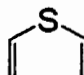
Figure 4.1. Structures of several bisdioxopiperazines, ADR-925, and EDTA.
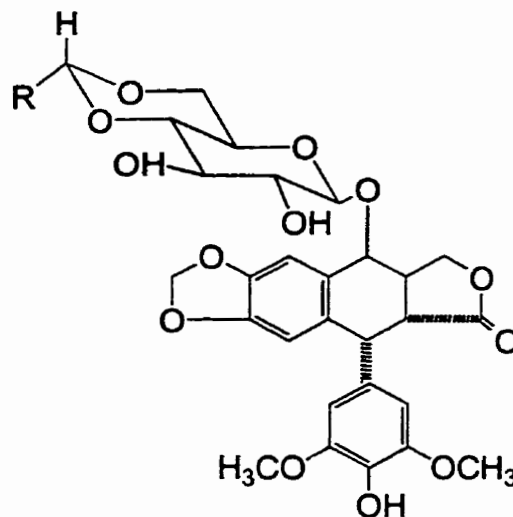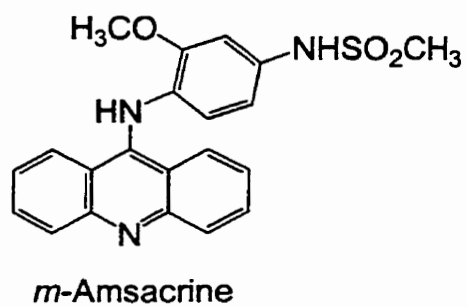
m-Amsacrine

Teniposide, R =
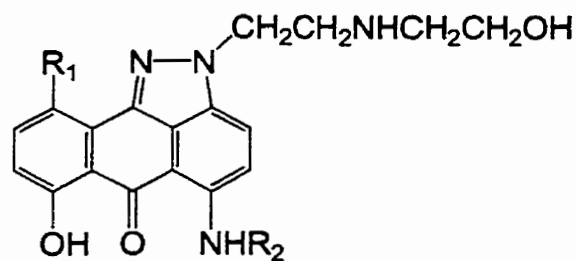
Etoposide, R = CH$_3$

Losoxantrone, R$_1$ = H

    R$_2$ = CH$_2$CH$_2$NHCH$_2$CH$_2$OH

Piroxantrone, R$_1$ = OH,

    R$_2$ = CH$_2$CH$_2$CH$_2$CH$_2$NH$_2$

Figure 4.2. Structures of *m*-amsacrine, etoposide, teniposide, losoxantrone, and piroxantrone.

4.2. Materials and methods

4.2.1. Materials

Dexrazoxane was a gift from Pharmacia & Upjohn (Columbus, OH). Teniposide was a gift from Bristol-Myers Squibb (Saint-Laurent, Québec). Losoxantrone and piroxantrone were gifts from Dr. E. H. Herman (FDA, Washington, DC). m-Amsacrine and other chemicals were from Sigma Chemical Co. (St. Louis, Mo). Chinese hamster ovary (CHO) cells (type AA8; ATCC CRL-1859) were obtained from American Type Culture Collection (Rockville, MD). The cells were grown in α-MEM (alpha-minimum essential medium) (cat. No. 12000-022 Gibco BRL, Burlington). Fetal Bovine Serum (cat. No. 26140-087), penicillin-streptomycin (cat. No. 15140-122), and trypsin, 0.25% (w/v) with 1 mM Na$_4$EDTA (cat. No. 25200-072) were obtained from Gibco BRL, Life Technbologies Inc. (Burlington, Ontario). Dulbecco's phosphate buffered saline (cell culture, cat. No. D-5652), and MTT (3-(4,5-dimethylthiazol-2-yl)-2,5-diphenyltetrazolium bromide) were from Sigma Chemical Co. (St. Louis, Mo).

4.2.2. Cell culture and cytotoxicity assay

4.2.2.1. Culturing the cells

Chinese hamster ovary cells were cultured in a 25 cm^2 T-flask (cat. No. 25100-25, Corning Inc., New York) in α-MEM containing 20 mM HEPES, 100 units/mL penicillin G, 100 μg/mL streptomycin, 10% (v/v) fetal bovine serum. The cells solution was incubated in an incubator at an atmosphere of 5% CO$_2$ and 95% air (v/v) at 37 °C and pH 7.4. The cell culture medium was prepared by the dissolving one pack (10.0 g) of α-MEM, 4.76 g of HEPES, and 2.2 g of NaHCO$_3$ in 700 mL of double distilled water. The

pH of the solution was brought up to 7.2 at room temperature with 1.0 M NaOH. Penicillin with streptomycin (10 mL) was added to the solution, and followed by the addition of another 200 mL double distilled water to make up to a total volume of 900 mL. The solution was then sterile filtered through a 0.2 μm Nalgene bottle top filter (Nalgene Company, Rochester, New York). The solution was stored in a refrigerator for up to one month. Before use, the medium solution was added under sterile condition with fetal bovine serum with a final concentration of 10% (v/v) in the laminar flow hood (Enviro Safety Cabinet, model ESC, Albuquerque, New Mexico).

4.2.2.2. Harvesting and seeding the cells

Cells in exponential growth at the pre-confluent stage were harvested. The culture medium was decanted in the laminar flow hood, and followed by washing with 10 mL of Dulbecco's phosphate buffered saline. One mL of 0.25 % (w/v) trypsin with 1 mM EDTA was added, and left for 4 min to detach the cells from the bottom of the T-flask. After 4 min the cells detached, and 9 mL of cell culture medium was added. The solution was then transferred to a 10 mL sterile centrifuge tube, and centrifuged at 5000 rpm for 6 min. The supernatant was decanted, and the cell pellet was resuspended in 10 mL fresh cell culture medium. The cell density and the total number of cells were determined by counting on a hemocytometer. The cells were then seeded on a 96-well, sterile tissue culture plate (flat bottom with lid, cat. No. 831835, Sarstedt Inc., Newton, NC) with 100 μL cell culture medium per well, and with a density of 2000 cells/well, and allowed to attach for 24 h in the incubator before the addition of the drugs.

4.2.2.3. Drugging the cells

Losoxantrone, piroxantrone, and dexrazoxane were dissolved in the cell culture medium, and filtered through a 0.2 μm sterile cellulose acetate syringe filter (25 mm, cat. No. 831826001, Sarstedt Inc., Newton, NC). *m*-Amsacrine, etoposide, and teniposide were dissolved in DMSO where the final DMSO concentration in the cell culture medium was 0.5 % (v/v). In each multi-well plate, a DMSO control was included to ensure that DMSO itself did not significantly affect the cell growth. The amount of inhibition due to DMSO alone at 0.5 % (v/v) was less than 10 % growth inhibition.

For single drugging, after 24 h incubating the seeded cells, the drug solution was added to each well at an appropriate concentration. For drugs that are soluble in DMSO, each concentration was prepared from separate stock solutions, such that only 1 μL of the DMSO (0.5 % v/v) drug solution was added to each well. Before the addition of the drug, cell culture medium was added to each well, so that the final volume of each well was at 200 μL including the volume of the drug added. Six replicates were performed at each drug concentration. For drugs that are soluble in the cell culture medium, the drug concentrations were prepared from a common stock solution, such that the volume of the stock solution required, which were added to each well did not exceed 40 μL. Before the addition of the drug solution, cell culture medium was added to each well so that the final volume of each well was at 200 μL including the volume of the drug added. Six replicates were performed at each drug concentration.

For double drugging, the preparation of the drug solution was similar to that for single drugging. After administering the first drug (dexrazoxane in these experiments),

the cells was kept in the incubator for 1 h. The second drug solution (*m*-amsacrine, etoposide, teniposide, losoxantrone, or piroxantrone) was then delivered to the cells at the appropriate concentration. The volumes of the drug solutions were added so that the final volume of each well was at 200 μL.

4.2.2.4. Determination of the growth inhibition using MTT assay

The tetrazolium salt MTT (3-(4,5-dimethylthiazol-2-yl)-2,5-diphenyltetrazolium bromide) solution was prepared by dissolving 0.25 g of MTT in 50 mL of the Dulbecco's phosphate buffered saline and 50 mL of distilled water. The MTT solution is light sensitive, and was kept in dark in a refrigerator.

After drugging, the cells were incubated with drugs continuously for another 48 h. The MTT solution (20 μL) was then added to each well to determine the cell survival at each drug concentration. The yellow tetrazolium salt MTT is converted into water-insoluble blue formazan crystals by the mitochondrial dehydrogenase of viable cells during the period of 4 h of incubation. The cell culture medium was removed by aspiration, and 100 μL of DMSO was added to dissolve the crystals. A plate reader (Molecular Devices, Menlo Park, CA) was used to measure absorbance at 550 nm in the wells. The absorbance was corrected by subtracting the absorbance at 650 nm from the absorbance at 550 nm to minimize non-specific, scattered light.

4.2.2.5. Dose-response curve to determine the growth inhibition of the cells

The absorbance-drug concentration data were fit to non-linear, least-squares with a three- or four-parameter logistic equation (Equation 4.1) using SigmaPlot (Jandel Scientific, San Rafael, CA)

$$A_{550/650} = ((a-d)/(1+(D/IC_{50})^b)) + d \qquad (4.1)$$

where $A_{550/650}$ is the absorbance at 550 nm minus the absorbance at 650 nm, D is the drug concentration, IC_{50} is the median inhibitory concentration, b is a Hill-type exponential factor, a is the estimated maximal absorbance, and d is the estimated minimum absorbance at the highest drug concentration. When the minimum absorbance at the highest drug concentration is close to zero, d is set equal to zero, and the data was fit to the three-parameter logistic equation.

4.2.2.6. Design of the experiment for the combination of dexrazoxane with other topoisomerase II inhibitors, such as *m*-amsacrine, etoposide, teniposide, losoxantrone, and piroxantrone

Each of the above drugs was administered to Chinese hamster ovary cells over wide concentration ranges of up to 500 μM for dexrazoxane, and at various concentrations of the other topoisomerase II-targeted drugs. The IC_{50} of each drug was determined through the dose-response curve as described in Section 4.2.2.5. Incubating the cells for 48 h in the presence of dexrazoxane alone up to 500 μM resulted around 30% cell kill at the highest dexrazoxane concentration. A good linear correlation between the logarithm of the absorbance at 550 nm with the concentration of dexrazoxane was observed. This observation was utilized to design the slope comparison experiment. Fixed doses of the other drugs were used in combination with the wide concentration range of dexrazoxane to study the combined effect of the two drugs. The fixed doses of the other drugs were chosen so that these concentrations covered most of the steep section of its dose-response curve. In other word, these concentrations bracketed the IC_{50} of the

second drug. Briefly, dexrazoxane (with a concentration range of 0 - 500 μM) was added

to the cells for 1 h before a second drug was delivered at various concentrations, which

bracketed the IC_{50} of the second drug. The IC_{50} value of the second drug was pre-

determined in the absence of dexrazoxane. After 48 h of incubation, MTT was added for

4 h, and the MTT assay was performed as described in Section 4.2.2.4.

4.2.2.7. Analyzing the antagonistic effect using slope comparison method

The combined effect of two drugs may be analyzed by several methods, such as

Loewe isobole, envelop of additivity, combination index, response surface, or slope

comparison methods (Kozlowska, 1998). In this study the slope comparison method was

used to analyze the antagonistic effects of m-amsacrine, etoposide, teniposide,

losoxantrone, and piroxantrone in the presence of dexrazoxane. Due to the nature of the

dose response curve of the cell growth inhibition of dexrazoxane alone, or dexrazoxane in

the presence of the above topoisomerase II-targeted agents, the dose response curve was

fit to a linear least square equation. This dose response curve can also be referred to a

dose response line because it actually is a straight line rather than a curve. Dexrazoxane

alone caused about 30 % cell kill, and the linear least square fit gave a negative slope,

while the linear least square fit of the dose response line of dexrazoxane in the presence

of a second topoisomerase II-targeted agent gave a less negative or positive slope. The

two agents antagonize each other when the slopes of the linear least square fit of the dose

response lines of dexrazoxane alone, and dexrazoxane in the presence of a second agent

are significantly different, which are compared by a t-test statistical evaluation. In this

experiment, this slope comparison method was used to study the antagonistic effects of

dexrazoxane and other topoisomerase II-targeted anticancer agents, such as m-amsacrine, etoposide, teniposide, losoxantrone, and piroxantrone.

Exposing Chinese hamster ovary cells continuously for 48 h to dexrazoxane resulted in a low cell kill over a wide concentration range (0 - 500 μM of dexrazoxane). The maximum cytotoxicity was observed around 30 % at the highest drug concentration. The logarithm of the absorbances from the MTT assay were then plotted against the logarithm of the drug concentrations, and these data points were then fit to a linear least square equation. When a fixed dose of a second drug was used in combination with various dexrazoxane concentrations, the second drug at the fixed dose affected the y-intercept and the slope of the dexrazoxane dose-response line. The interaction of dexrazoxane with other drugs were defined by the changes in the slope and y-intercept of the dexrazoxane dose-response lines in the presence of fixed doses of the second drug. In the following experiments, the dose-response line of dexrazoxane alone was compared with those of dexrazoxane in the presence of fixed doses of m-amsacrine, etoposide, teniposide, losoxantrone, and piroxantrone. A student's t-test was used to evaluate changes in the slopes of the dose-response lines. A transform program in SigmaPlot (comp2reg.xfm, Jandel Scientific, San Rafael, CA) was used for the comparison of the slope b of a linear least square fit of the form $logA = a + b \cdot logD$, where A is the absorbance from the MTT assay, and D is the dexrazoxane drug concentration. The slopes of the dose-response lines of dexrazoxane alone, and of dexrazoxane in the presence of the second drug were considered to be significantly different when $P < 0.05$.

4.3. Effects of *m*-amsacrine, etoposide, teniposide, losoxantrone, and piroxantrone combined with dexrazoxane on Chinese hamster ovary cell growth

4.3.1. Effect of *m*-amsacrine combined with dexrazoxane on Chinese hamster ovary cell growth

The effect of *m*-amsacrine on Chinese hamster ovary cell growth over a 48 h continuous exposure gave a median inhibitory concentration, IC_{50} of 5.8 ± 0.5 µM (Figure 4.4). Dexrazoxane did not cause a high degree of growth inhibition on the cells when it was delivered to the cells for 48 h as shown in Figure 4.3. These results were utilized to design the next experiment, in which dexrazoxane with the concentration range of 1 - 500 µM was pre-incubated for 1 h, and *m*-amsacrine was added at fixed concentrations of 1, 2, 3, 5, 6, 7.5, and 10 µM. These concentrations were chosen so that they bracketed the IC_{50} value of *m*-amsacrine alone in the growth inhibition of the cells. The effects of dexrazoxane alone, and in combination with *m*-amsacrine on the cell growth were analyzed by MTT assay in Figure 4.5. The slopes of the lines were compared by a *t*-test. The parameters and the results of the *t*-test are shown in Table 4.1. The slopes of the lines were also plotted against the *m*-amsacrine concentrations in Figure 4.6. The slopes increased from negative to positive values with the increase in the concentration of *m*-amsacrine, and it decreased at 10 µM *m*-amsacrine.

Figure 4.3. Growth inhibition of Chinese hamster ovary cells by dexrazoxane. The cells were incubated with the drug for 48 h, and then assayed with MTT. Each data point is the average of six replicates with the errors shown as standard deviations. The data points were fit to a linear least square equation. The lowest data point is a control without drug.

Figure 4.4. Growth inhibition of Chinese hamster ovary cells by *m*-amsacrine. The cells were incubated with the drug for 48 h and then assayed with MTT. Each data point is the average of six replicates with the errors shown as standard deviations. The solid line is a non-linear least square best fit to the logistic Equation 4.1. An IC_{50} value of 5.8 ± 0.5 μM was calculated for *m*-amsacrine. The lowest data point is a control without any drug and without DMSO, and the next data point is a control with 0.5 % (v/v) DMSO.

Figure 4.5. Combined effect of *m*-amsacrine and dexrazoxane on the growth inhibition of Chinese hamster ovary cells. The cells were incubated for 48 h with dexrazoxane alone, and dexrazoxane with fixed doses of *m*-amsacrine, and then assayed with MTT. Each data point is the average of six replicates with the errors shown as standard deviations. The data points were fit to a linear least square equation to obtain the slope and intercept values. The lowest concentrations are the controls without drug and without DMSO. The concentrations next to the lowest ones are other controls with 0.5 % (v/v) DMSO. The next concentrations are the controls with *m*-amsacrine in DMSO.

Figure 4.6. Slope comparison of the combined effect of *m*-amsacrine and dexrazoxane on the growth inhibition of Chinese hamster ovary cells. The slopes were obtained from the linear least square fit in Figure 4.5.

Table 4.1. *t*-Test for the comparison of the slopes obtained from the combined effects of *m*-amsacrine and dexrazoxane on the growth inhibition of Chinese hamster ovary cells in Figure 4.5.

Parameters	Concentrations of *m*-amsacrine (µM)							
	0	1	2	3	5	6	7.5	10
a ± SEM	-0.246 ± 0.007	-0.367 ± 0.011	-0.380 ± 0.025	-0.443 ± 0.018	-0.585 ± 0.018	-0.788 ± 0.021	-1.245 ± 0.031	-1.413 ± 0.014
b ± SEM	-0.078 ± 0.004	-0.032 ± 0.007	-0.046 ± 0.015	-0.022 ± 0.011	-0.004 ± 0.011	0.002 ± 0.012	0.038 ± 0.018	-0.007 ± 0.008
Tb		-5.784	-2.073	-4.862	-6.346	-6.064	-6.228	-7.626
Vb		12	12	12	12	12	12	12
P		<0.001	<0.05	<0.001	<0.001	<0.001	<0.001	<0.001

t-Test parameters:
a: y-intercept
b: slope
Tb: *t* value for slope comparison
Vb: degree of freedom for slope comparison
P: statistical significance

4.3.2. Effect of etoposide combined with dexrazoxane on Chinese hamster ovary cell growth

Continuous exposure of Chinese hamster ovary cells to etoposide for 48 h gave a median inhibitory concentration, IC_{50} of 24.0 ± 2.9 µM (Figure 4.7). Five different concentrations of etoposide at 20, 50, 100, 200, and 500 µM were used in combination with dexrazoxane in the range of 1 - 500 µM, which was pre-incubated for 1 h before the administration of etoposide at the above chosen concentrations. The growth inhibition of the cells were analyzed by the MTT assay as shown in Figure 4.8. The slopes of the fit lines were compared by a t-test. The parameters and the test results were presented in Table 4.2. The slopes of the dose response lines were plotted against the etoposide concentrations in Figure 4.9. It was observed that the slopes increased from negative to positive values as the concentration of etoposide increased. However at very high etoposide concentrations, the slopes began to decrease.

Figure 4.7. Growth inhibition of Chinese hamster ovary cells by etoposide. The cells were incubated with the drug for 48 h, and then assayed with MTT. Each data point is the average of six replicates with the errors shown as standard deviations. The solid line is a non-linear least square best fit to the logistic Equation 4.1. An IC_{50} value of 24.0 ± 2.9 μM was calculated for etoposide. The lowest data point is a control without any drug or DMSO, and the next data point is a control with 0.5 % (v/v) DMSO only.

Figure 4.8. Combined effect of etoposide and dexrazoxane on the inhibition of growth of Chinese hamster ovary cells. The cells were incubated for 48 h with dexrazoxane alone, and dexrazoxane with fixed doses of etoposide, and then assayed with MTT. Each data point is the average of six replicates with the errors shown as standard deviations. The data points were fit to a linear least square equation to obtain the slope and intercept values. The lowest concentrations are the controls without drug and without DMSO. The concentrations next to the lowest ones are other controls with etoposide and 0.5 % (v/v) DMSO.

Figure 4.9. Slope comparison of the combined effect of etoposide and dexrazoxane on the growth inhibition of Chinese hamster ovary cells. The slopes were obtained from the linear least square fit in Figure 4.8.

Table 4.2. *t*-Test for comparison of the slopes obtained from the combined effect of etoposide and dexrazoxane on the inhibition of growth of Chinese hamster ovary cells in Figure 4.8.

Parameters	Concentrations of etoposide (μM)					
	0	20	50	100	200	500
a ± SEM	-0.095 ± 0.013	-0.239 ± 0.027	-0.430 ± 0.039	-0.764 ± 0.036	-1.051 ± 0.026	-1.170 ± 0.018
b ● SEM	-0.089 ± 0.007	-0.010 ± 0.015	0.057 ± 0.021	0.164 ± 0.019	0.200 ± 0.014	0.051 ± 0.009
Tb		-4.917	-6.606	-12.34	-18.47	-12.04
Vb		14	14	14	14	14
P		<0.001	<0.001	<0.001	<0.001	<0.001

t-Test parameters:
a: y-intercept
b: slope
Tb: *t* value for slope comparison
Vb: degree of freedom for slope comparison
P: statistical significance

4.3.3. Effect of teniposide combined with dexrazoxane on Chinese hamster ovary cell growth

Continuous exposure of Chinese hamster ovary cells to teniposide for 48 h gave a median inhibitory concentration, IC_{50} of 2.2 ● 0.1 µM (Figure 4.10). Seven concentrations of teniposide of 0.1, 1, 1.5, 2, 3, 5, and 10 µM were used in combination with dexrazoxane in the range of 1- 500 µM. The cells were pre-incubated for 1 h with dexrazoxane before the addition of teniposide at the above chosen concentrations. The growth inhibition of the cells were measured by the MTT assay as shown in Figure 4.11. The data points were fit to a linear least square equation, and the slopes of the lines were compared by a t-test. The t-test parameters and the results are listed in Table 4.3. The slopes of the lines were plotted against the teniposide concentrations in Figure 4.12. It was observed that the slopes of the fit lines increased from negative to positive values as the teniposide concentration increased. However, the slope leveled off at high teniposide concentration.
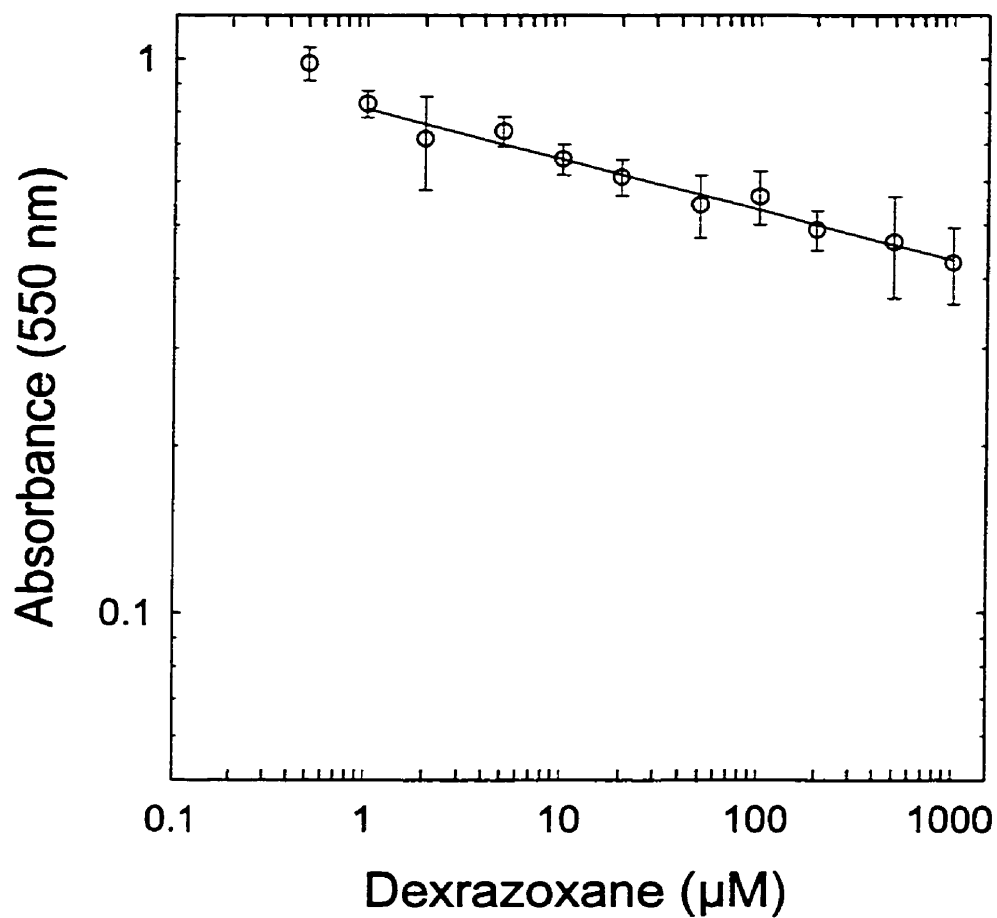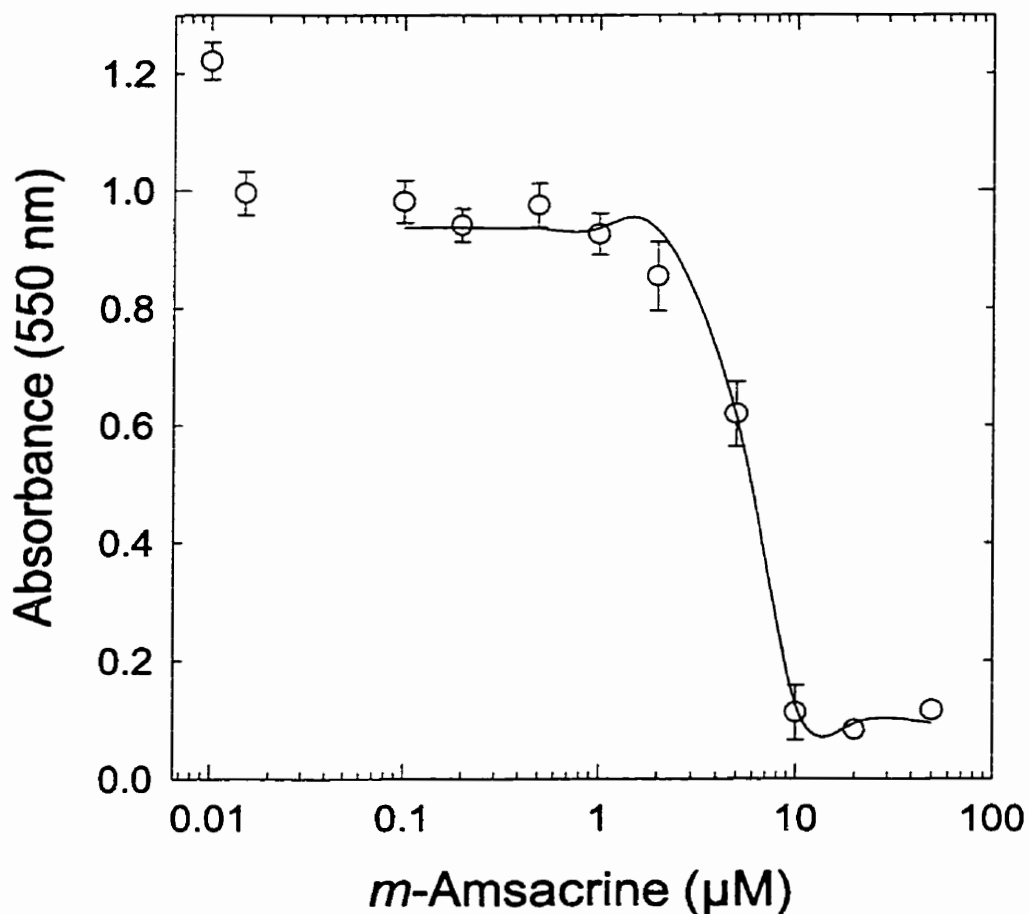
Figure 4.10. Growth inhibition of Chinese hamster ovary cells by teniposide. The cells were incubated with the drug for 48 h, and then assayed with MTT. Each data point is the average of six replicates with the errors shown as standard deviations. The solid line is a non-linear least square best fit to the logistic Equation 4.1. An IC_{50} value of 2.2 ± 0.1 μM was calculated for teniposide. The lowest data point is a control without drug and without DMSO, and the next data point is a control with 0.5 % (v/v) DMSO.
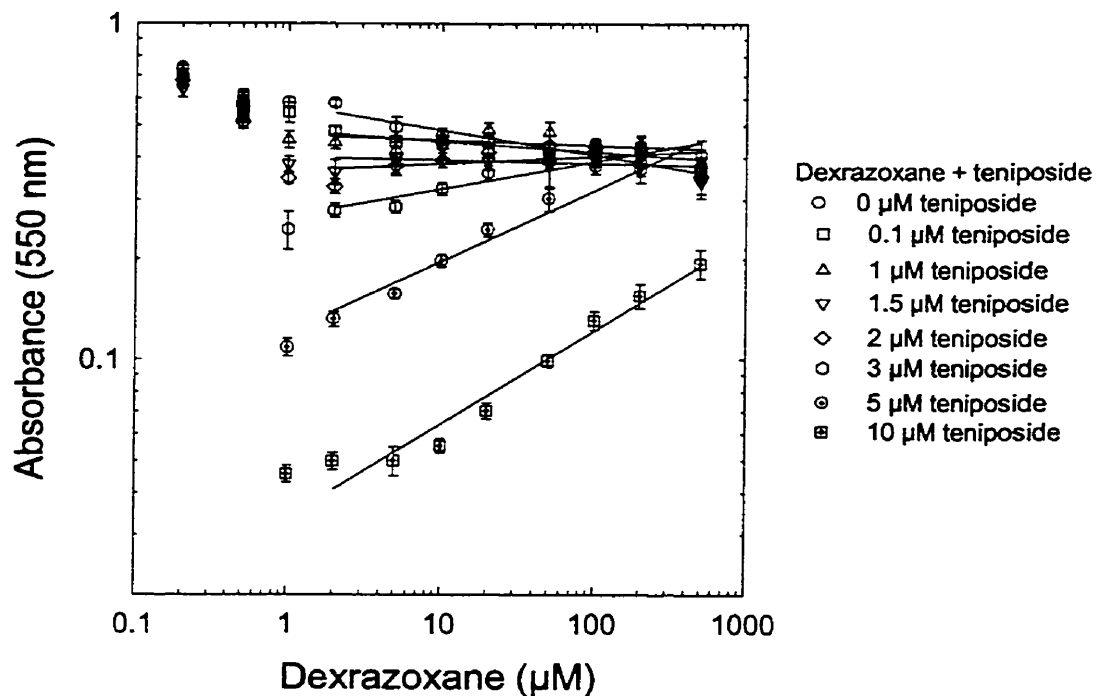
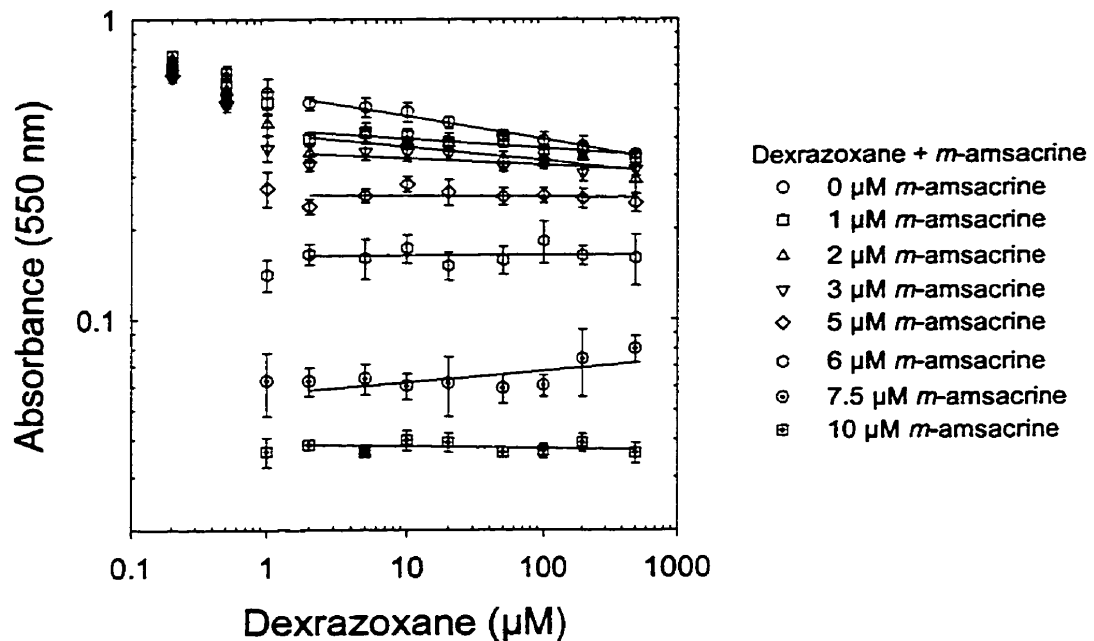**Figure 4.11.** Combined effect of teniposide and dexrazoxane on the inhibition of growth of Chinese hamster ovary cells. The cells were incubated for 48 h with dexrazoxane alone, and dexrazoxane with fixed doses of teniposide, and then assayed with MTT. Each data point is the average of six replicates with the errors shown as standard deviations. The data points were fit to a linear least square equation to obtain the slope and intercept values. The lowest concentrations are the controls without drug and without DMSO. The concentrations next to the lowest ones are other controls with 0.5 % (v/v) DMSO. The next concentrations are the controls with teniposide in DMSO.
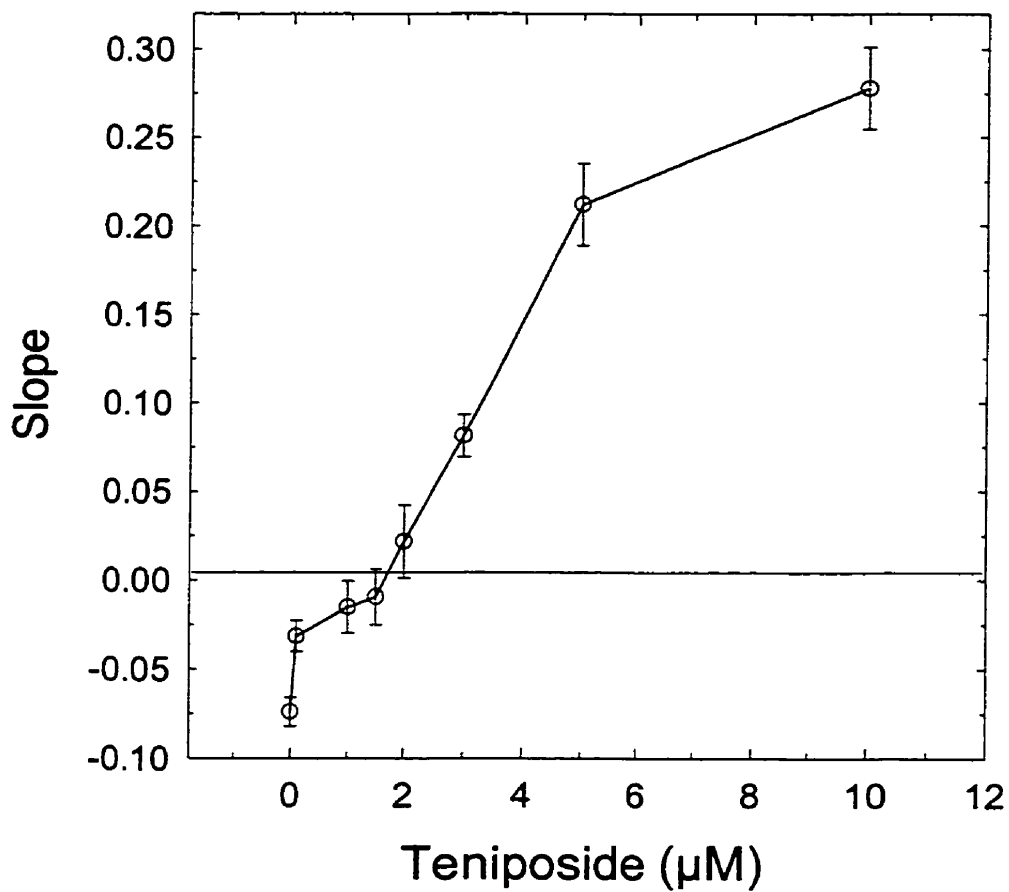
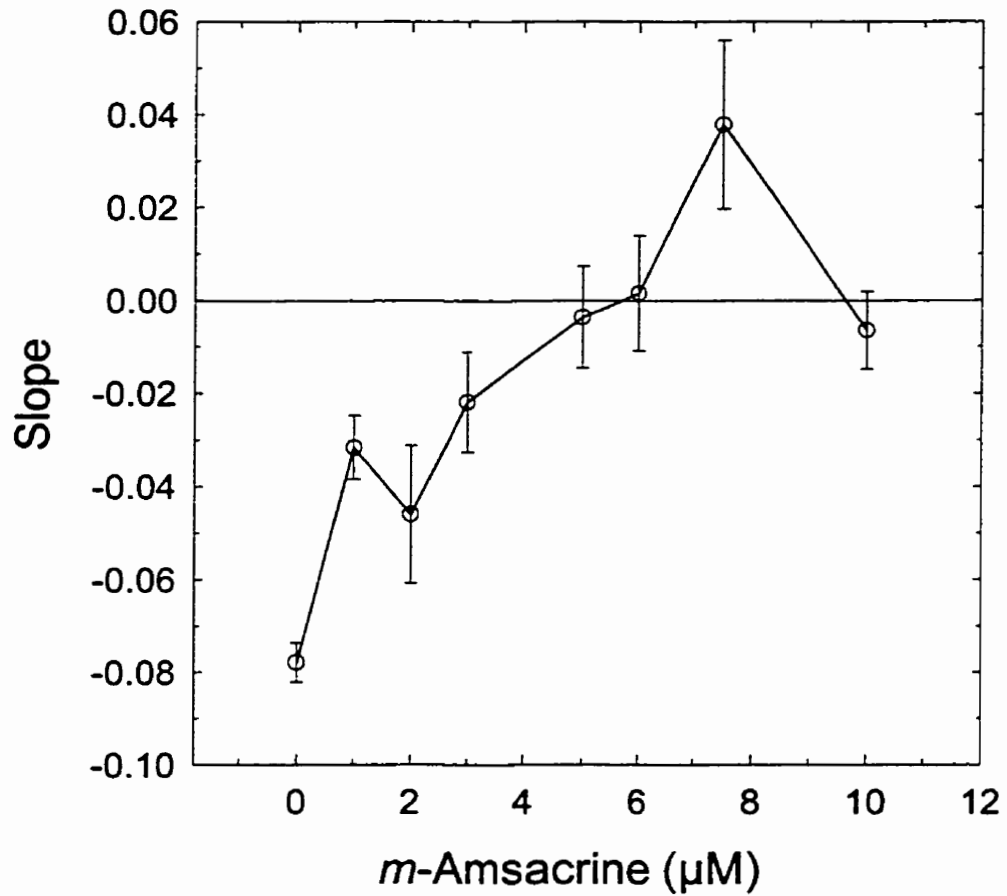**Figure 4.12.** Slope comparison of the combined effect of teniposide and dexrazoxane on the growth inhibition of Chinese hamster ovary cells. The slopes were obtained from the linear least square fit in Figure 4.11

Table 4.3. *t*-Test for comparison of the slopes obtained from the combined effect of teniposide and dexrazoxane on the inhibition of growth of Chinese hamster ovary cells in Figure 4.11.

Parameters	Concentrations of teniposide (μM)							
	0	0.1	1	1.5	2	3	5	10
a ± SEM	-0.242 ± 0.014	-0.319 ± 0.015	-0.331 ± 0.025	-0.396 ± 0.026	-0.437 ± 0.035	-0.571 ± 0.020	-0.918 ± 0.039	-1.470 ± 0.039
b ± SEM	-0.074 ± 0.008	-0.031 ± 0.009	-0.015 ± 0.015	-0.009 ± 0.016	0.022 ± 0.021	0.081 ± 0.012	0.212 ± 0.023	0.278 ± 0.023
Tb		-3.587	-3.536	-3.689	-4.337	-10.82	-11.61	-14.32
Vb		12	12	12	12	12	12	12
P		<0.005	<0.005	<0.005	<0.001	<0.001	<0.001	<0.001

t-Test parameters:
a: y-intercept
b: slope
Tb: *t* value for slope comparison
Vb: degree of freedom for slope comparison
P: statistical significance

4.3.4. Effect of losoxantrone combined with dexrazoxane on Chinese hamster ovary cell growth

Continuous exposure of Chinese hamster ovary cells to losoxantrone for 48 h gave a median inhibitory concentration, IC_{50} of 5.1 ± 1.0 (Figure 4.13). The two data points at the second and third lowest concentrations of losoxantrone were not used to fit the dose response curve due to a possible biphasic curve with minor and major IC_{50} values. Seven concentrations of losoxantrone of 0.2, 1, 2, 5, 10, 20, and 50 μM were used in combination with dexrazoxane in the range of 1 - 500 μM, which were pre-incubated for 1 h before the addition of losoxantrone at the above chosen concentrations. The growth inhibition of the cells were determined by the MTT assay as shown in Figure 4.14. The data points were fit to a linear least square equation, and the slopes were compared by a t-test. The test parameters and the results were listed in Table 4.4. The slopes of the lines were plotted against the losoxantrone concentrations in Figure 4.15. It was found that the slopes increased from negative to positive values as the losoxantrone concentration increased. However, at high losoxantrone concentration the slope started to decrease.
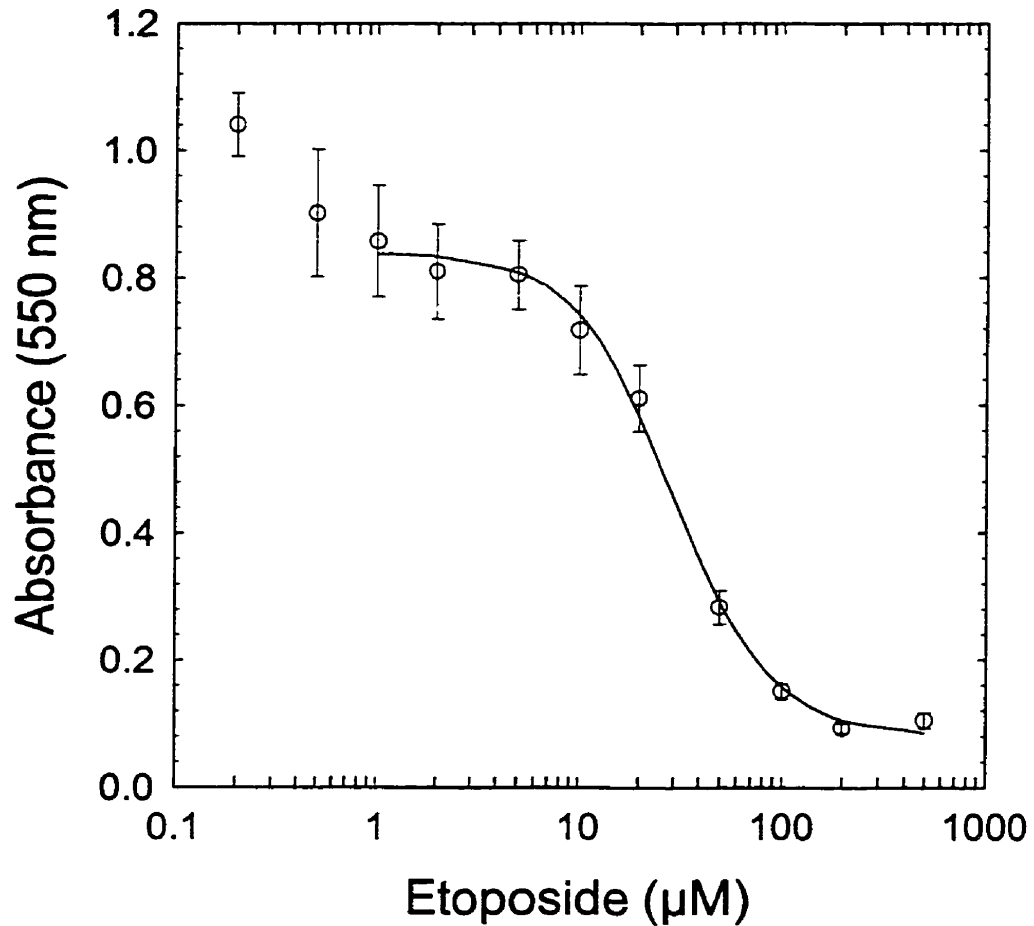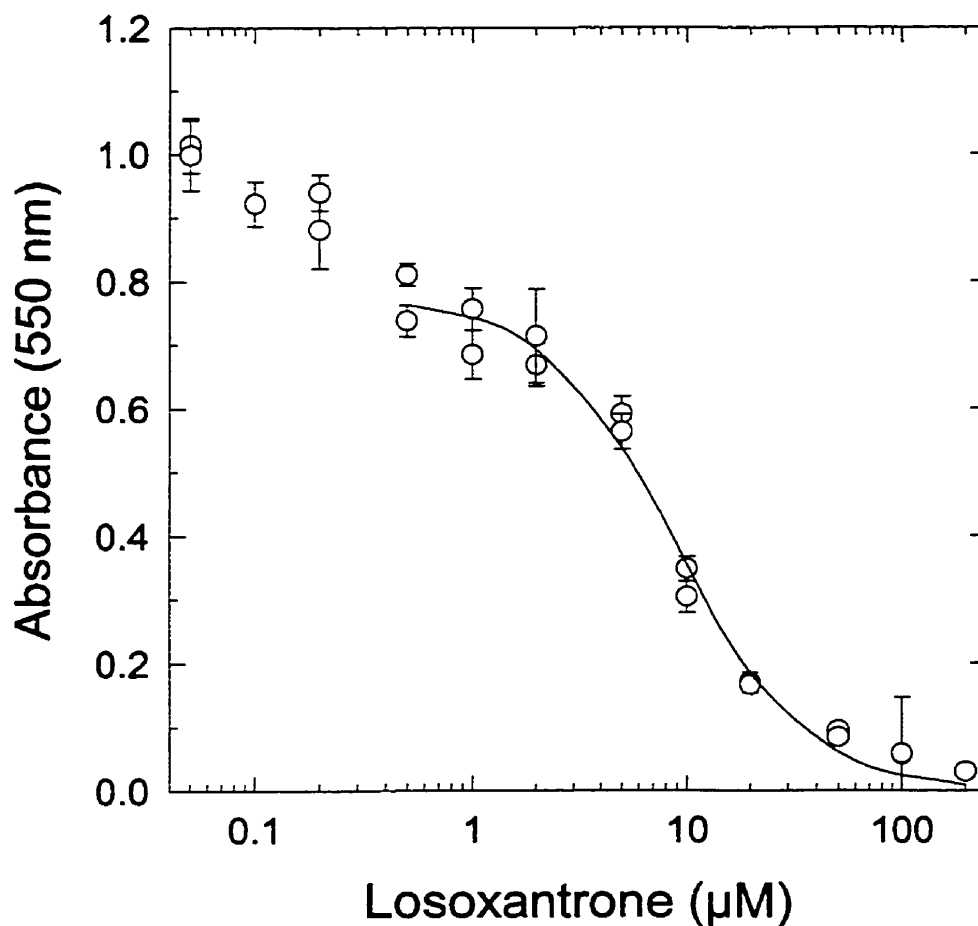
Figure 4.13. Growth inhibition of Chinese hamster ovary cells by losoxantrone. The cells were incubated with the drug for 48 h and then assayed with MTT. Each data point is the average of six replicates with the errors shown as standard deviations. The solid line is a non-linear least square best fit to the logistic Equation 4.1. An IC_{50} value of 5.1 ± 1.0 µM was calculated for losoxantrone. The lowest data point is a control without drug. The next two data points were not used in the non-linear least square fit due to a possible biphasic dose response curve.
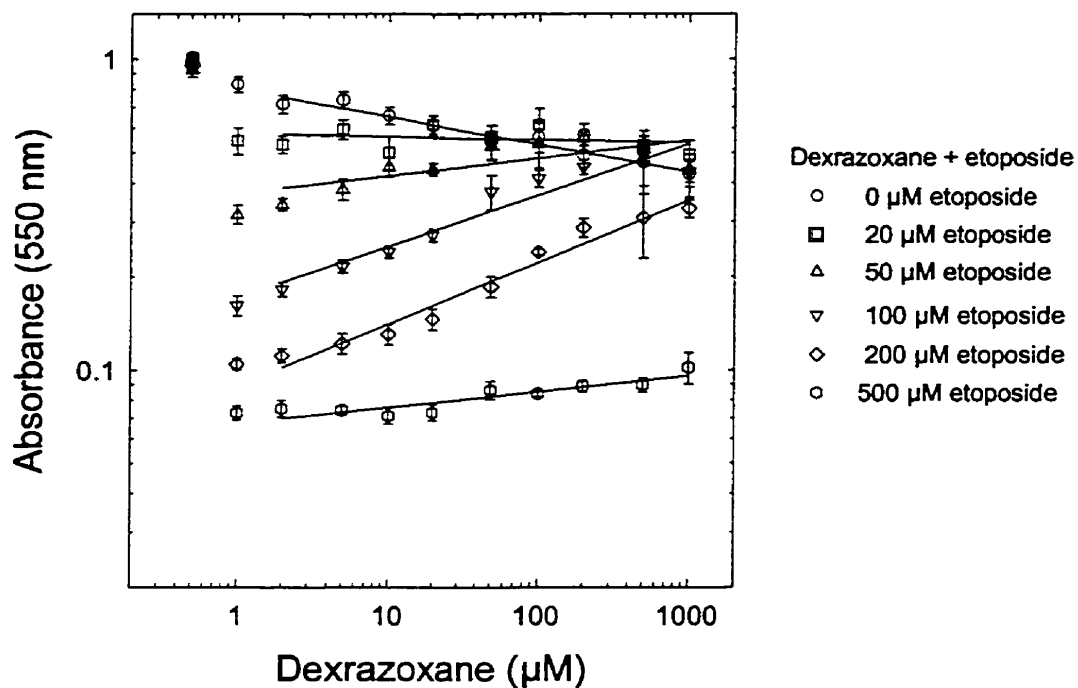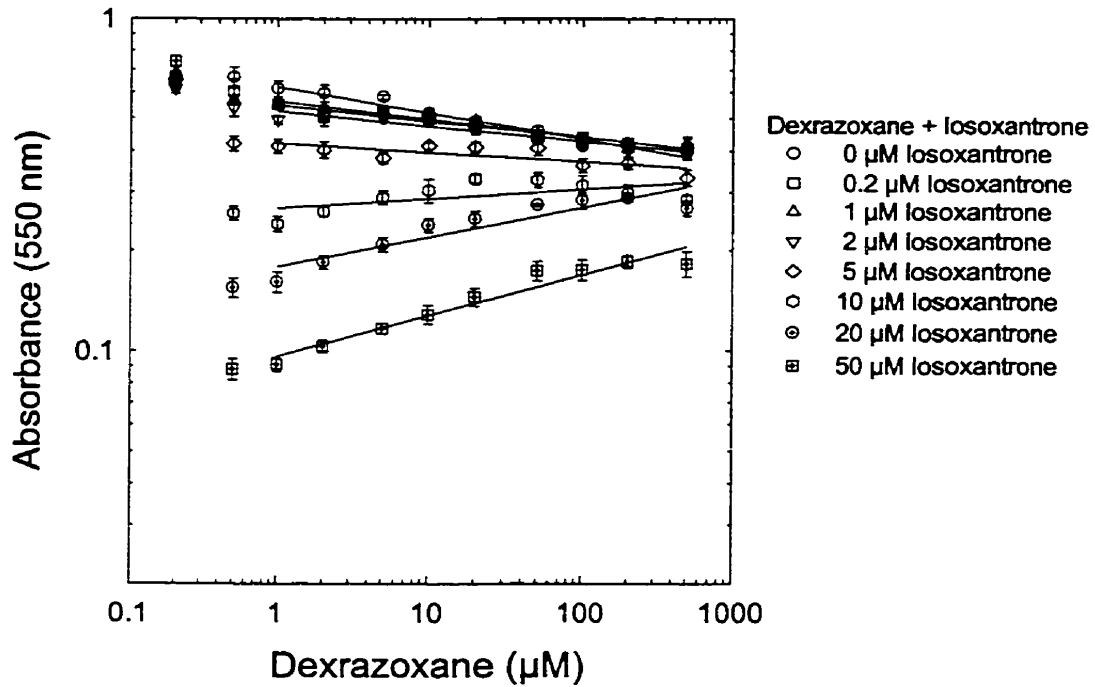
Figure 4.14. Combined effect of losoxantrone and dexrazoxane on the growth inhibition of Chinese hamster ovary cells. The cells were incubated for 48 h with dexrazoxane alone, and dexrazoxane with fixed doses of losoxantrone, and then assayed with MTT. Each data point is the average of six replicates with the errors shown as standard deviations. The data points were fit to a linear least square equation to obtain the slope and intercept values. The lowest concentrations are the controls without drug. The concentrations next to the lowest ones are other controls with losoxantrone in cell culture medium only.
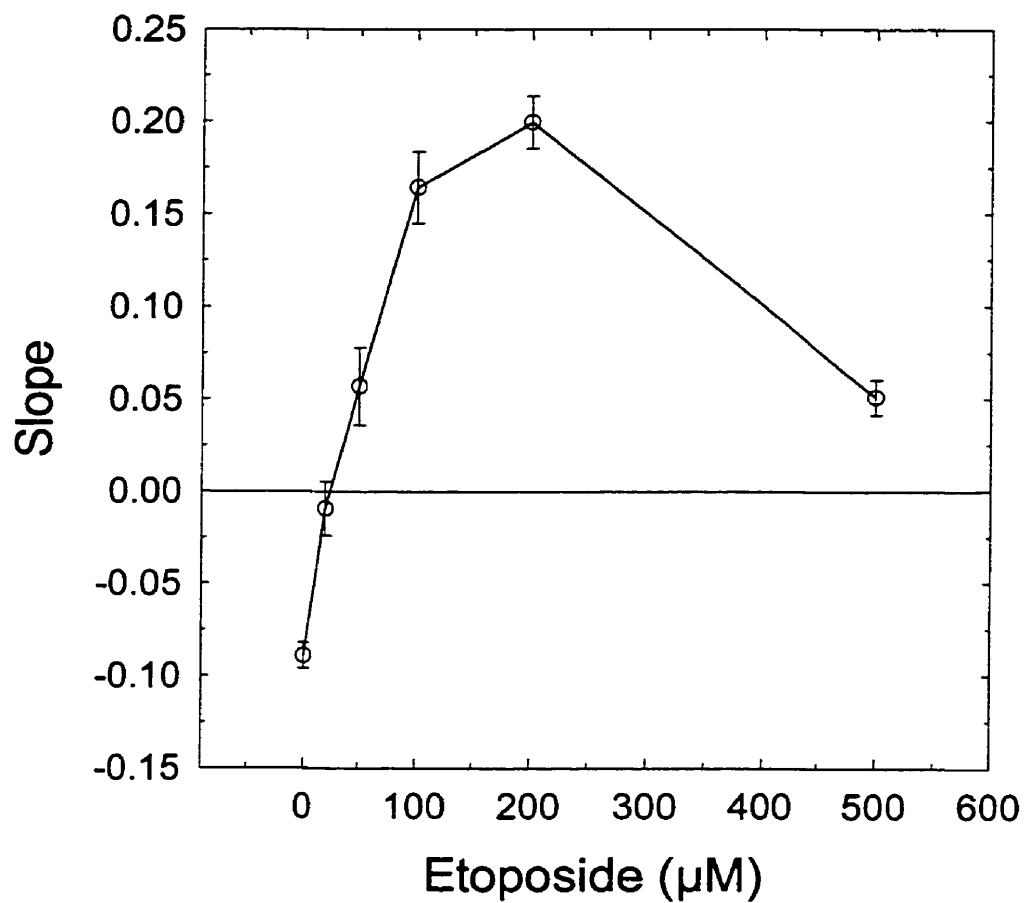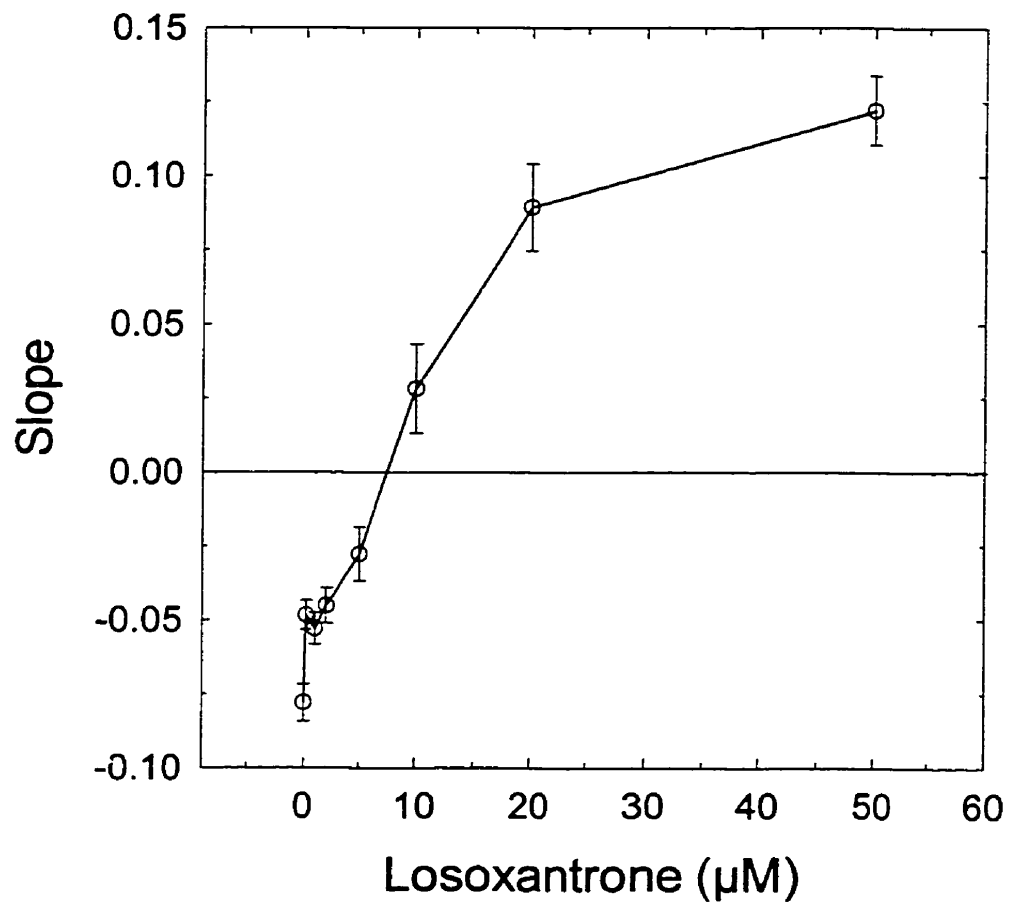
Figure 4.15. Slope comparison of the combined effect of losoxantrone and dexrazoxane on the growth inhibition of Chinese hamster ovary cells. The slopes were obtained from the linear least square fit in Figure 4.14.

Table 4.4. t-Test for comparison of the slopes obtained from of the combined effect of losoxantrone and dexrazoxane on the growth inhibition of Chinese hamster ovary cells in Figure 4.14.

Parameters	Concentrations of losoxantrone (μM)							
	0	0.2	1	2	5	10	20	50
a $\pm$ SEM	-0.206 $\pm$ 0.010	-0.260 $\pm$ 0.008	-0.250 $\pm$ 0.009	-0.279 $\bullet$ 0.010	-0.374 $\pm$ 0.015	-0.569 $\pm$ 0.024	-0.746 $\pm$ 0.023	-1.016 $\bullet$ 0.018
b $\pm$ SEM	-0.078 $\pm$ 0.006	-0.048 $\pm$ 0.005	-0.053 $\pm$ 0.005	-0.045 $\pm$ 0.006	-0.028 $\pm$ 0.009	0.028 $\pm$ 0.015	0.089 $\pm$ 0.015	0.122 $\pm$ 0.012
Tb		-3.726	-3.035	-3.783	-4.530	-6.499	-10.44	-15.19
Vb		14	14	14	14	14	14	14
P		<0.005	<0.01	<0.005	<0.001	<0.001	<0.001	<0.001

t-Test parameters:
a: y-intercept
b: slope
Tb: t value for slope comparison
Vb: degree of freedom for slope comparison
P: statistical significance

4.3.5.   Effect of piroxantrone combined with dexrazoxane on Chinese hamster ovary cell growth

Continuous exposure of Chinese hamster ovary cells to piroxantrone for 48 h gave a median inhibitory concentration, IC_{50} of 7.0 ± 0.5 μM (Figure 4.16). Due to visible staining of the wells by piroxantrone, the absorbance did not go down to zero even at a very high piroxantrone concentration. The two data points at the second and third lowest concentrations of piroxantrone were not used to fit the dose response curve due to a possible biphasic curve with minor and major IC_{50} values. Seven concentrations of piroxantrone of 0.2, 0.5, 3, 5, 7, 10, and 20 μM were used in combination with dexrazoxane in the range of 1 - 500 μM, which were pre-incubated for 1 h before the addition of piroxantrone at the above chosen concentrations. The growth inhibition of the cells were determined by the MTT assay as shown in Figure 4.17. The data points were fit to a linear least square equation, and the slopes were compared by a t-test. The test parameters and the results were listed in Table 4.5. The slopes of the fit lines were plotted against the piroxantrone concentrations (Figure 4.18). It was found that the slopes increased from more negative to less negative values as the piroxantrone concentrations increased.
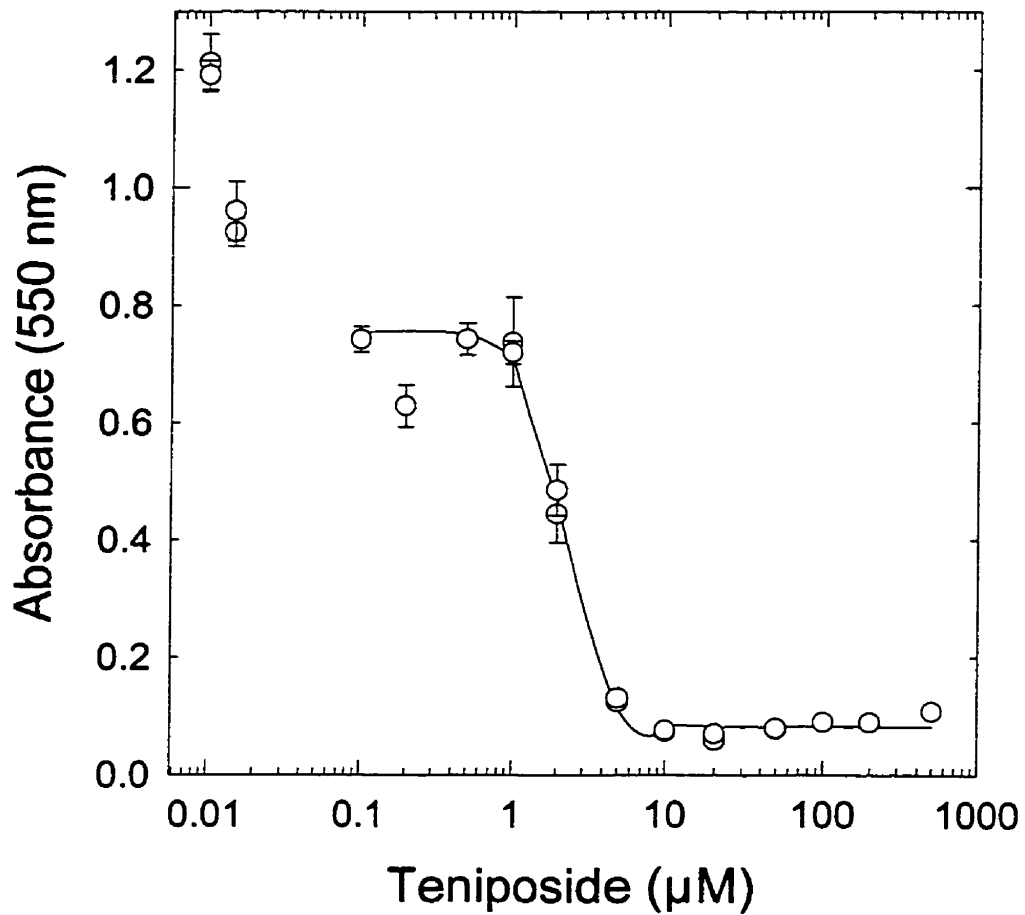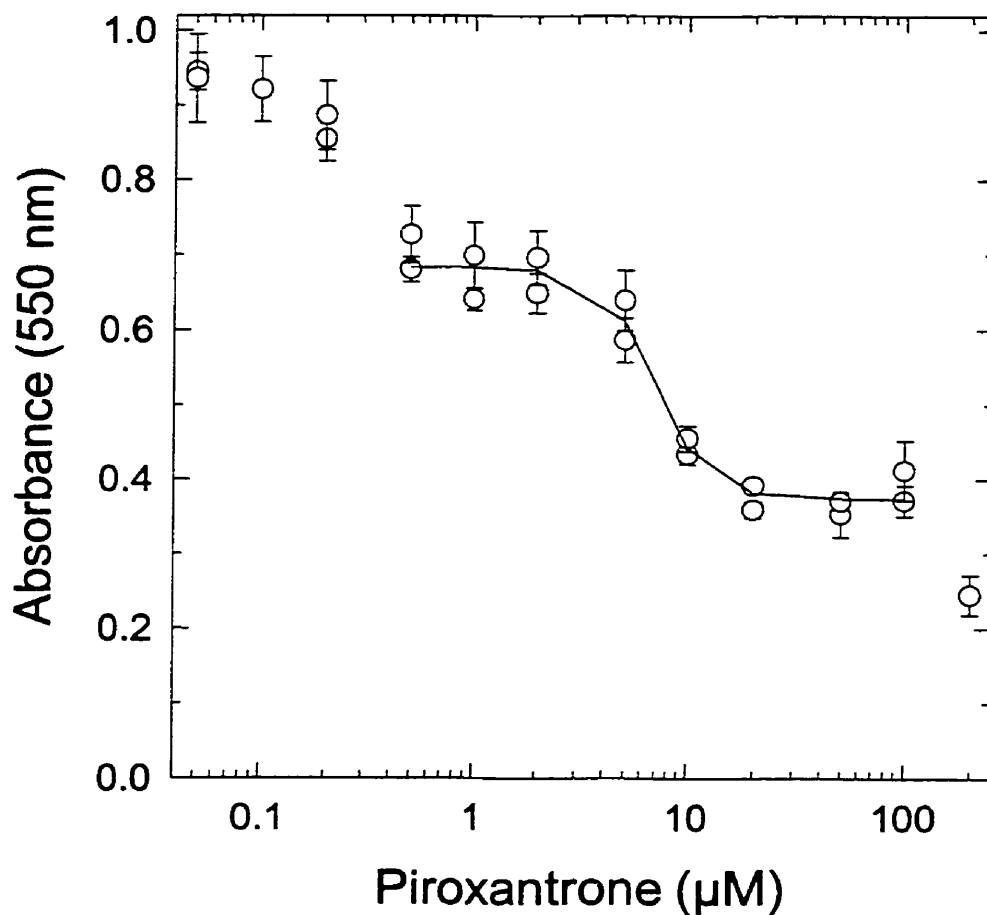
Figure 4.16. Growth inhibition of Chinese hamster ovary cells by piroxantrone. The cells were incubated with the drug for 48 h, and then assayed with MTT. Each data point is the average of six replicates with the errors shown as standard deviations. The solid line is a non-linear least square best fit to the logistic Equation 4.1. An IC_{50} value of 7.0 ± 0.5 μM was calculated for piroxantrone. The lowest data point is a control without drug. The next two data points were not used in the non-linear least square fit due to a possible biphasic dose response curve.
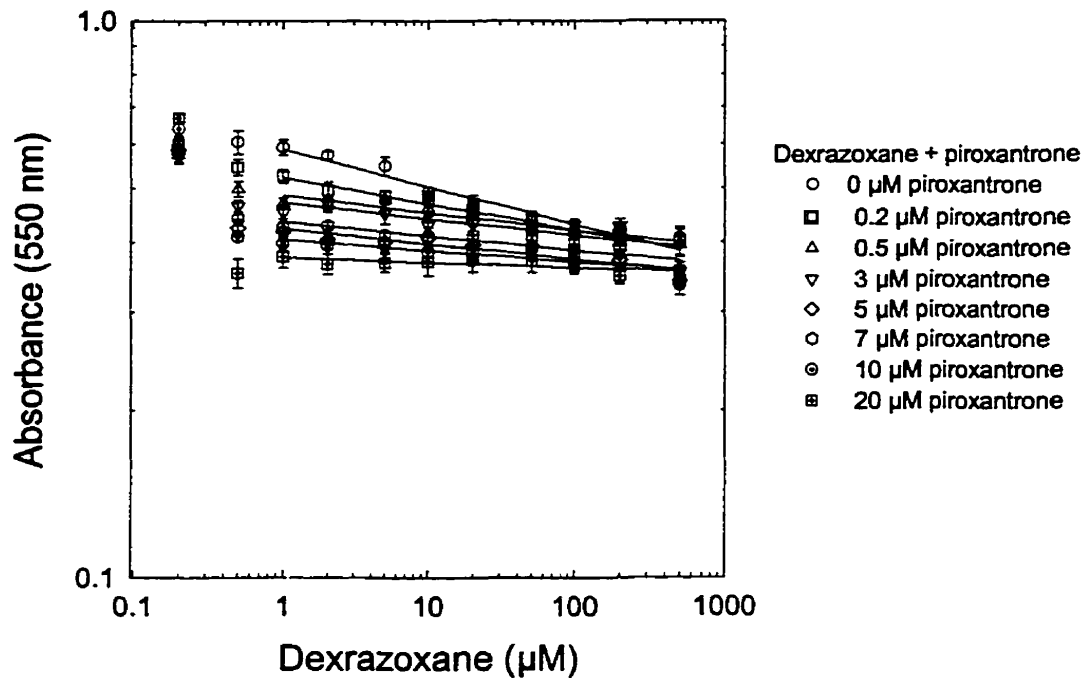
Figure 4.17. Combined effect of piroxantrone and dexrazoxane on the growth inhibition of Chinese hamster ovary cells. The cells were incubated for 48 h with dexrazoxane alone, and dexrazoxane with fixed doses of piroxantrone, and then assayed with MTT. Each data point is the average of six replicates with the errors shown as standard deviations. The data points were fit to a linear least square equation to obtain the slope and intercept values. The lowest concentrations are the controls without drug. The concentrations next to the lowest ones are other controls with piroxantrone in cell culture medium only.
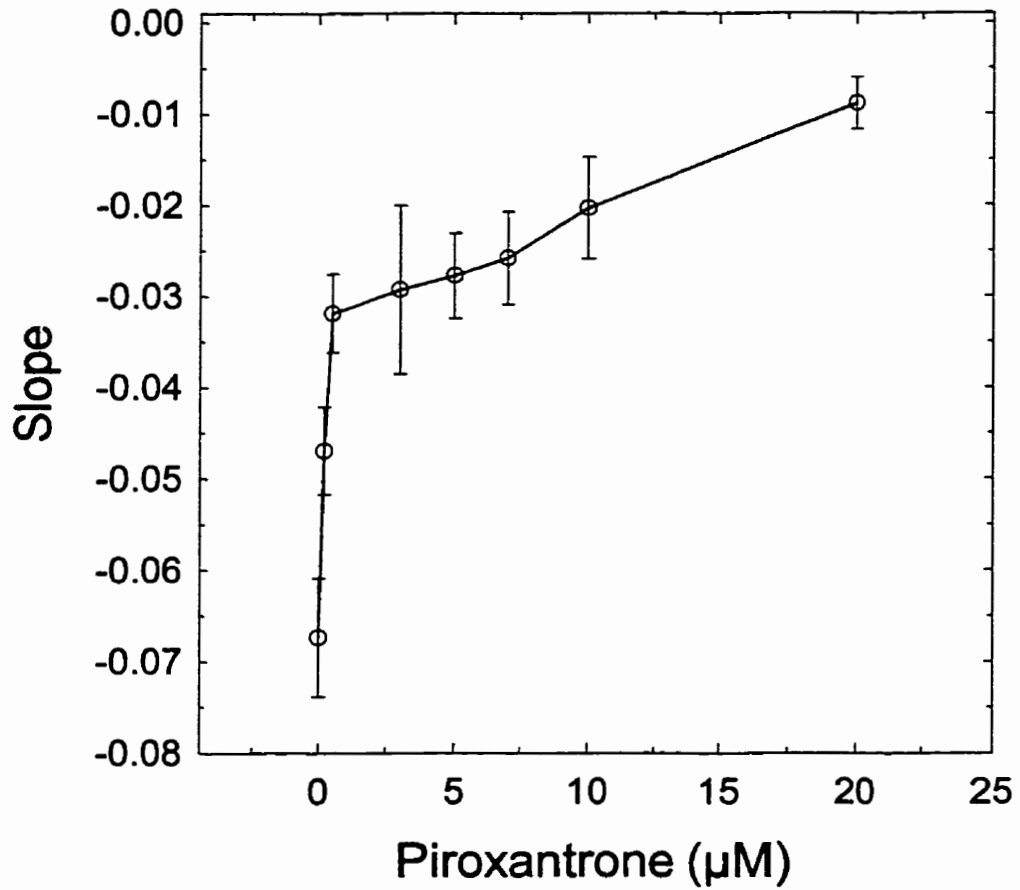
Figure 4.18. Slope comparison of the combined effect of piroxantrone and dexrazoxane on the growth inhibition of Chinese hamster ovary cells. The slopes were obtained from the linear least square fit in Figure 4.17.

Table 4.5. *t*-Test for comparison of the slopes obtained from the combined effect of piroxantrone and dexrazoxane on the growth inhibition of Chinese hamster ovary cells in Figure 4.17.

Parameters	Concentrations of piroxantrone (μM)							
	0	0.2	0.5	3	5	7	10	20
a ± SEM	-0.231 ± 0.010	-0.282 ± 0.008	-0.313 ± 0.007	-0.327 ± 0.015	-0.373 ± 0.007	-0.361 ± 0.008	-0.392 ± 0.009	-0.426 ± 0.004
b ± SEM	-0.067 ± 0.006	-0.047 ± 0.005	-0.032 ± 0.004	-0.029 ± 0.009	-0.028 ± 0.005	-0.026 ± 0.005	-0.020 ± 0.006	-0.009 ± 0.002
Tb		-2.532	-4.558	-3.366	-4.957	-5.047	-5.496	-8.278
Vb		14	14	14	14	14	14	14
P		<0.05	<0.001	<0.005	<0.001	<0.001	<0.001	<0.001

t-Test parameters:
a: y-intercept
b: slope
Tb: *t* value for slope comparison
Vb: degree of freedom for slope comparison
P: statistical significance

4.4. Implications for the effects of *m*-amsacrine, etoposide, teniposide, losoxantrone, and piroxantrone combined with dexrazoxane on Chinese hamster ovary cell growth

The effect on Chinese hamster ovary cell growth inhibition of *m*-amsacrine combined with dexrazoxane is shown in Figure 4.5. The slopes of the dose response lines increased from negative to positive values with the *m*-amsacrine concentrations (Figure 4.6). Dexrazoxane, a bisdioxopiperazine inhibits topoisomerase II by preventing the binding of the enzyme to DNA (Hasinoff *et al.*, 1997; Kano *et al.*, 1992; Snapka *et al.*, 1996; Ishida *et al.*, 1995). When the cells were pre-incubated with dexrazoxane for 1 h, the topoisomerase II inside the cells was inhibited by dexrazoxane. Under these conditions, when *m*-amsacrine was administered to the cells 1 h later, there would be little free topoisomerase II for the latter drug to inhibit. Thus, the dose response lines leveled off (Figure 4.5). At certain concentrations of *m*-amsacrine the absorbance at 550 nm did not only level off but also increased gradually. This observation indicates that dexrazoxane antagonized *m*-amsacrine because both of them target the same enzyme, topoisomerase II. At *m*-amsacrine concentration of 10 μM, which is too high compared to the IC_{50} value of 5.8 μM, the slope of the linear least square dose response line decreased. At this high *m*-amsacrine concentration, dexrazoxane probably could not compete for the enzyme, and thus, the inhibitory effect of *m*-amsacrine became dominant, and high cell kill was observed.

The effect of dexrazoxane and etoposide on Chinese hamster ovary cells were studied based on the combined influence of the two compounds on the cell growth

(Figure 4.8). Statistical evaluation of the slopes of the linear least square dose response lines in the presence of dexrazoxane alone, and dexrazoxane with etoposide were found to be significantly different with $P<0.001$ (Table 4.2). Comparison of the slopes of the linear least square dose response lines showed that the slopes of the lines increased from negative to positive values as the etoposide concentration increased up to 200 μM. This concentration was much higher than the IC_{50} value of 24.0 μM, which was pre-determined on the same Chinese hamster ovary cell line (Figure 4.7). The dose response line of dexrazoxane alone, and that of dexrazoxane plus etoposide intersected at certain etoposide concentrations (Figure 4.8). This observation indicated that dexrazoxane strongly antagonized etoposide. The slope comparison of the fit dose response line of dexrazoxane by itself, and dexrazoxane with etoposide were significantly different with $P<0.001$. However, antagonism was not observed at very high etoposide concentration of 500 μM. Pre-incubation for 1 h with dexrazoxane may be long enough for the drug to get inside the cells, and inhibit topoisomerase II. As etoposide was administered to the cells, most of the targeted topoisomerase II was already inhibited by the dexrazoxane antagonist. There was no further cytotoxic effect observed as etoposide concentration increased. At high concentration of 500 μM etoposide, the effect produced by etoposide became dominant, and resulted in a high cell kill. Thus, antagonism was not observed at this high etoposide concentration.

The effect of teniposide on the 1 h pre-incubated cells with dexrazoxane were also studied by the MTT assay. The slopes of the linear least square dose response lines were found to be significantly different with $P<0.005$ or smaller (Table 4.3). The slopes

increased from negative to positive values as the teniposide concentration increased up to 10 μM; and the absorbance at 550 nm increased gradually, and intersected the fit line of the dose response curve of dexrazoxane alone (Figure 4.11). This observation indicated that dexrazoxane strongly antagonized teniposide. Up to 5 μM teniposide, the antagonism was observed as the dexrazoxane concentration increased. At 10 μM teniposide, the cell survival slightly increased. These results showed that a pre-incubation for 1 h with dexrazoxane could be long enough to inhibit the targeted topoisomerase II of the cells. When teniposide was delivered to the cells, the enzymes were already inhibited. There was no further cell kill due to the presence of teniposide. All of these observations indicate strong antagonism of dexrazoxane in the presence of teniposide.

The effect of losoxantrone on the 1 h pre-incubated cells with dexrazoxane were studied using the slope comparison method. The slopes of the linear least square dose response lines of dexrazoxane by itself, and with losoxantrone were compared. They were found to be significantly different with $P<0.01$ or smaller (Table 4.4). The slopes increased from negative to positive values. This observation indicated that dexrazoxane antagonized losoxantrone. The fit dose response lines in the presence of dexrazoxane and losoxantrone showed a certain degree of antagonism (Figure 4.14). At high concentration of dexrazoxane, most of the cells were recovered from the cytotoxic effect induced by losoxantrone. With 1 h of pre-incubation with dexrazoxane, most of the topoisomerase II were inhibited. When losoxantrone was administered to the cells, the targeted topoisomerase II would be already inhibited. Antagonism was observed when

dexrazoxane and losoxantrone were used together with 1 h pre-incubation of the cells with dexrazoxane.

The effect of piroxantrone on the 1 h pre-incubated cells with dexrazoxane were also examined by the comparison of the linear least square dose response lines in the presence of dexrazoxane by itself, and dexrazoxane with piroxantrone. The slopes were found to be significantly different with $P<0.05$ or smaller (Table 4.5). These slopes increased from more negative to less negative values (Figure 4.18). This observation indicated a weak antagonistic interaction between dexrazoxane and piroxantrone. Piroxantrone at high concentration did not kill all of the cells, the minimum absorbance went down to only 30 % of the total absorbance (Figure 4.16). The absorbance at 550 nm did not drop down significantly even at high piroxantrone concentration probably due to the visible staining of the wells by piroxantrone. Thus, the degree of antagonism was not very clear for the combination of dexrazoxane with piroxantrone.

4.5. Conclusions

The combined effects of dexrazoxane with *m*-amsacrine, etoposide, teniposide, losoxantrone, and piroxantrone were all found to be antagonistic based on the slope comparison method. Dexrazoxane is a catalytic topoisomerase II inhibitor, which does not cause any change in DNA topology. Dexrazoxane has been approved as a cardioprotective agent, which can be used in combination with doxorubicin, a topoisomerase II inhibitor (Healy *et al.*, 1998; Hasinoff *et al.*, 1998; Hasinoff, 1998; Synold *et al.*, 1998; Elihu *et al.*, 1998). Like doxorubicin, *m*-amsacrine, etoposide, teniposide, losoxantrone, and piroxantrone are topoisomerase II inhibitors, which induce

the formation of the cleavable DNA-topoisomerase II-drug complexes, and induce changes in DNA topology. It was previously found that dexrazoxane antagonizes doxorubicin-mediated growth inhibition (Kozlowska, 1998). Thus, the combined effects of dexrazoxane with m-amsacrine, etoposide, teniposide, losoxantrone, and piroxantrone were of interest. Using the slope comparison method, it was found that dexrazoxane antagonized these drugs to a certain extent. The slopes were statistically significantly different with $P<0.05$ or smaller, and the slopes increased from more negative to less negative, or from negative to positive values. The trend in the increase of the slopes of the dose response lines of dexrazoxane by itself, and dexrazoxane with the second agent indicated that dexrazoxane antagonized m-amsacrine, etoposide, teniposide, losoxantrone, and piroxantrone. Therefore, the use of dexrazoxane as a cardioprotective agent in conjunction with other topoisomerase II inhibitors should be made with a great caution to ensure the maintenance of the potency of the second drug.

5. Synthesis of bisdioxopiperidine 1, a dexrazoxane analog

5.1. Problems with the cardioprotective drug dexrazoxane

Dexrazoxane (ICRF-187, Zinecard®, Cardioxane®) has been found to be an effective cardioprotective drug for the prevention of doxorubicin cardiotoxicity in chemotherapy (Hasinoff, 1998; Elihu *et al.*, 1998; Hasinoff *et al.*, 1998). In these studies, dexrazoxane (A) might be a prodrug of its hydrolyzed form ADR-925 (D) (Figure 5.1). Dexrazoxane is the cell membrane permeable form, and ADR-925 is presumably too polar to cross the cell membrane (Dawson, 1975). The hydrolysis of dexrazoxane to the active form ADR-925 is quite slow under physiological conditions with half times of 16.3 h for the production of the intermediates **B** and **C**, and of 23 h for the production of ADR-925 (**D**) as shown in Figure 5.1 (Hasinoff, 1990a, 1994b, a). Due to the slow hydrolysis rate of dexrazoxane, the drug has to be used at high doses, which contributes to myelosuppression side effects (Healy *et al.*, 1998). Bisdioxopiperazines, such as dexrazoxane also inhibit topoisomerase II, which is also the targeted enzyme for the co-administered anticancer drug doxorubicin (Kano *et al.*, 1992; Ishida *et al.*, 1995; Hasinoff *et al.*, 1997; Snapka *et al.*, 1996). Dexrazoxane also antagonizes with the co-administered drug, doxorubicin and other anthracyclines, since both drugs target the same enzyme topoisomerase II (Snapka *et al.*, 1996; Kozlowska, 1998). The antagonism may lower the effect of the topoisomerase II targeted anticancer agents, possibly due to the catalytic inhibition of the enzyme. Thus, this project aimed to synthesize, and characterize dexrazoxane analogs with expected shorter half times in order to generate the active hydrolyzed forms as cardioprotective agents. It would also be beneficial if the

synthesized dexrazoxane analogs would not inhibit topoisomerase II. These compounds would be more efficient cardioprotective agents if they had shorter hydrolysis half times, and if they would not inhibit topoisomerase II.
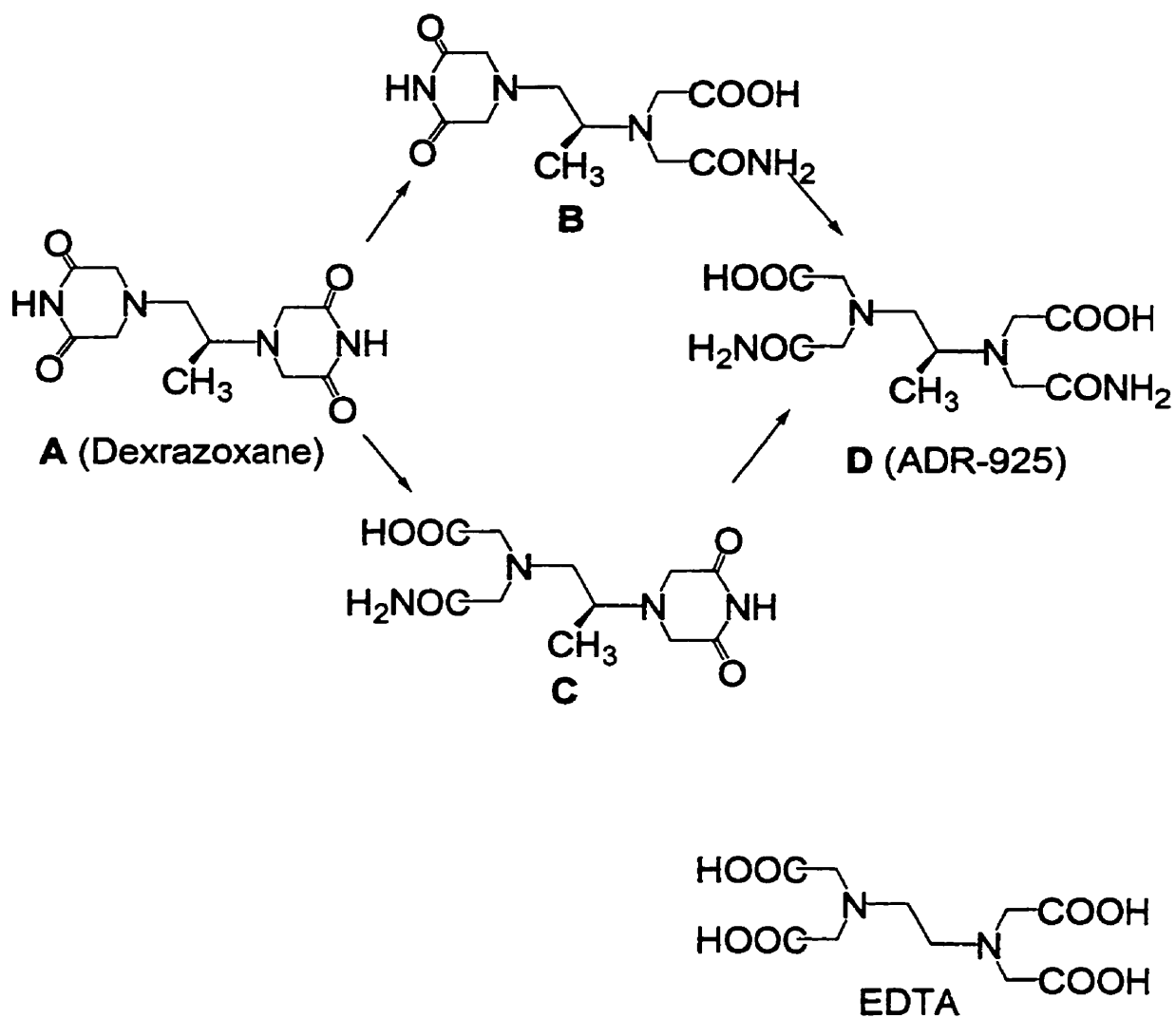
Figure 5.1. Dexrazoxane (**A**) and its hydrolyzed forms **B**, **C**, and ADR-925 (**D**).

5.2. Design of the dexrazoxane analog, bisdioxopiperidine 1

Based on a quantitative structure-activity relationship study of the hydrolysis rate

of several dexrazoxane analogs, a number of the analogs were chosen as lead compounds

for synthesis (Buss, 1998). The compound bisdioxopiperidine 1 chosen for this project is

shown below in Figure 5.2. There are several reasons why the imide 1 was targeted. It

has two bisdioxopiperidine rings instead of bisdioxopiperazine rings as in dexrazoxane.

This modification still retains the bicyclic imides as in dexrazoxane, which is probably

necessary for cell membrane permeability. There is also an ethylenediamine chain

connecting the two rings. However, the two N atoms in the imide 1 are secondary amines

instead of tertiary amines as in dexrazoxane. With the two secondary N atoms on the

main chain, the imide 1 would be protonated quite easily compared to the two tertiary N

atoms of dexrazoxane. This feature should speed up the ring opening process in the

imide 1, because the two protonated N atoms would cause a weak deactivation of the

imide rings through the inductive effect, and make the prominant carbonyl carbon

susceptible to nucleophilic attack by hydroxide, which should lead to ring opening to the

active form at a faster rate.

ICRF-154 $R_1 = R_2 = H$
ICRF-159 $R_1 = H$, $R_2 = CH_3$ (racemic)
ICRF-187 $R_1 = R_2 = CH_3$ ((S)-(+))
ICRF-186 $R_1 = R_2 = CH_3$ ((R)-(-))
ICRF-192 $R_1 = H$, $R_2 = C_2H_5$ (racemic)
ICRF-193 $R_1 = R_2 = CH_3$ (meso)
ICRF-201 $R_1 = R_2 = C_2H_5$ (meso)
ICRF-202 $R_1 = CH_3$, $R_2 = C_2H_5$ (erythro)
ICRF-215 $R_1 = CH_3$, $R_2 = C_3H_7$ (erythro)
ICRF-220 $R_1 = CH_3$, $R_2 = CH_2OCH_3$ (erythro)

Figure 5.2. Structures of dexrazoxane, its analogs, and the target compound bisdioxopiperidine 1.

5.3. Synthetic methods for the preparation of the bisdioxopiperidine 1

5.3.1. General scheme for the synthesis of bisdioxopiperazines

A general method for the synthesis of imides is from the corresponding diacids. There have been several imides prepared by this method (Hargreaves *et al.*, 1970; Creighton, 1976, 1971; Miller, 1988; Creighton, 1981). Generally, the corresponding diacid is heated at high temperature (approximately 170 °C) in formamide as shown in the following reaction scheme (Figure 5.3). Formamide serves both as the solvent and nitrogen donor for the ring closing to form the imide. Using this method, however, it is hard to control the reaction to stop at the half acid-half amide before ring closing; it was found that the reaction of tetraacid with formamide at high temperature could produce tetraamide, which could not form the subsequent imide product (Jeffery, 1987). Other reported methods are heating tetraacids in the presence of urea or ammonia gas to yield cyclic imides (Noller, 1965; Hargreaves *et al.*, 1970).

Another method for the synthesis of five- or six-membered cyclic imides is described in Figure 5.4 (Polonski, 1988b, a). The reaction is carried out by reacting the corresponding diacid with acetic anhydride or acetyl chloride to form the corresponding cyclic anhydride. This intermediate is then reacted with ammonia gas to form the half acid-half amide intermediate. The latter intermediate is then transformed to the imide using thionyl chloride. Thionyl chloride converts the acid to acid chloride, which then reacts with the amide to form the imide.
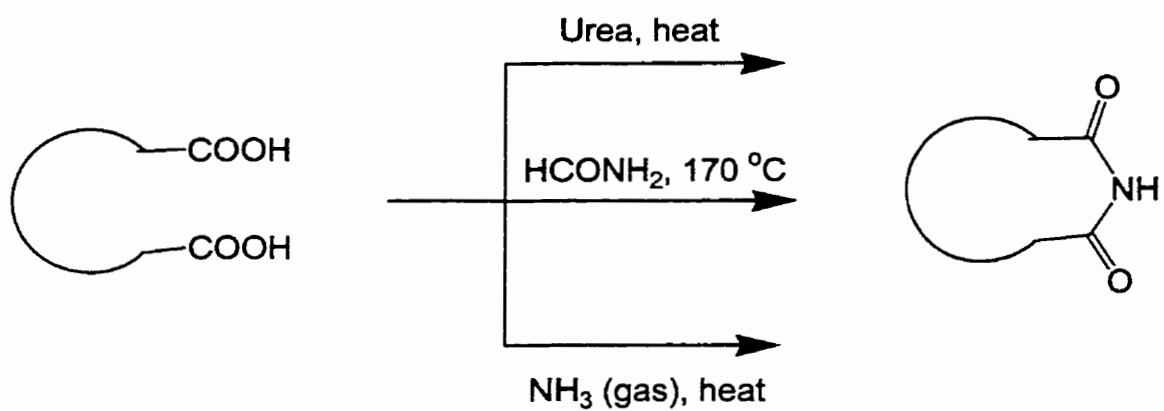
Figure 5.3. General scheme for the synthesis of five- or six-membered cyclic imides from the corresponding diacids.
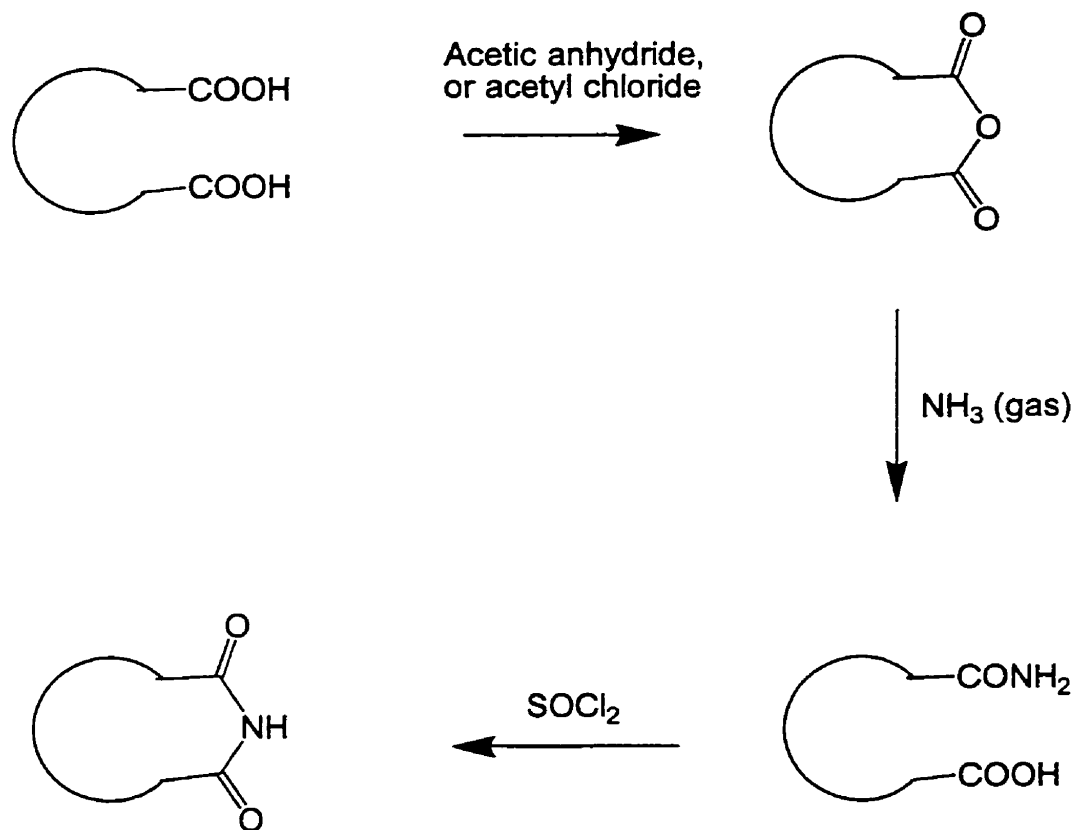
Figure 5.4. General scheme for the synthesis of five- or six-membered cyclic imides from the corresponding diacids *via* the cyclic anhydride, and the half acid-half amide intermediates.

5.3.2. Materials and methods

L-Glutamic acid was from Aldrich Chemical Company, Inc. (cat. No. 12,843-0).

Tris-HCl was from Sigma (cat. No. T-6666, St. Louis, MO). 1,2-Dibromoethane was

from Aldrich Chemical Company, Inc. (cat. No. D4, 075-2). Acetic anhydride was from

Mallinckrodt Specialties Chemicals Co. (cat. No. UN1715, Paris, Kentucky), and was

distilled before use. Ammonia gas was from Matheson Company, Inc. Silica gel was

from Aldrich Chemical Company, Inc. (cat. No. 28,862-4, 70-230 mesh, 60 Å,

Milwaukee, MI). Thin layer chromatography plates were from Analtech (cat. No. 21011,

20 x 20 cm, 250 microns, Newark, DE). Thionyl chloride was from Mallinckrodt

Specialties Chemicals Co. (cat. No. UN1836, Paris, Kentucky), and was distilled before

use. All other reagents were commercially available, and used as received without further

purification.

The products were characterized by ^{1}H-NMR, and ^{13}C-NMR on a AMX-500

MHz, Bruker AM-300-MHz, or a Gemini 200 MHz spectrometer. The melting points

were determined on a capillary melting point apparatus (Electrothermal, England), and

were uncorrected. The molecular weight of the bisdioxopiperidine 1 was confirmed by

mass spectroscopy using electrospray method with mass spectrometer LC Quatro

(Micromass, Manchester, UK).

5.3.2.1. Synthesis of the tetraacid precursor 2

This synthesis was performed using reported methods as shown in Figure 5.5

(Majer *et al.*, 1966; Byers and Douglas, 1972). L-Glutamic acid (30.0 g, 204 mmol),

NaOH (16.0 g, 400 mmol), and Na$_2$CO$_3$ (10.6 g, 100 mmol) were dissolved in distilled

water (200 mL). To this solution, 1,2-dibromoethane (38 g, 200 mmol) in 95 % ethanol (200 mL) was added dropwise. The whole mixture was refluxed at 95 °C in a water bath for 6 h. After refluxing, the solution (at pH ~ 10) was titrated down to pH 4 (using universal indicator paper) with concentrated hydrochloric acid. A white precipitate began to form at around pH 5. The whole mixture was allowed to stand at room temperature for 3 h. The precipitate was filtered off on a Buchner funnel, and washed with water and acetone. After drying in an oven at 50 °C overnight, the precipitate was identified as the tetraacid **2** (6.7 g, 20.9 mmol, 21 % yield) with melting point at 200 °C. ^{1}H-NMR, ^{1}H-COSY, ^{13}C-NMR, DEPT, and HSQC were utilized to confirm the structure of the tetraacid precursor **2**.
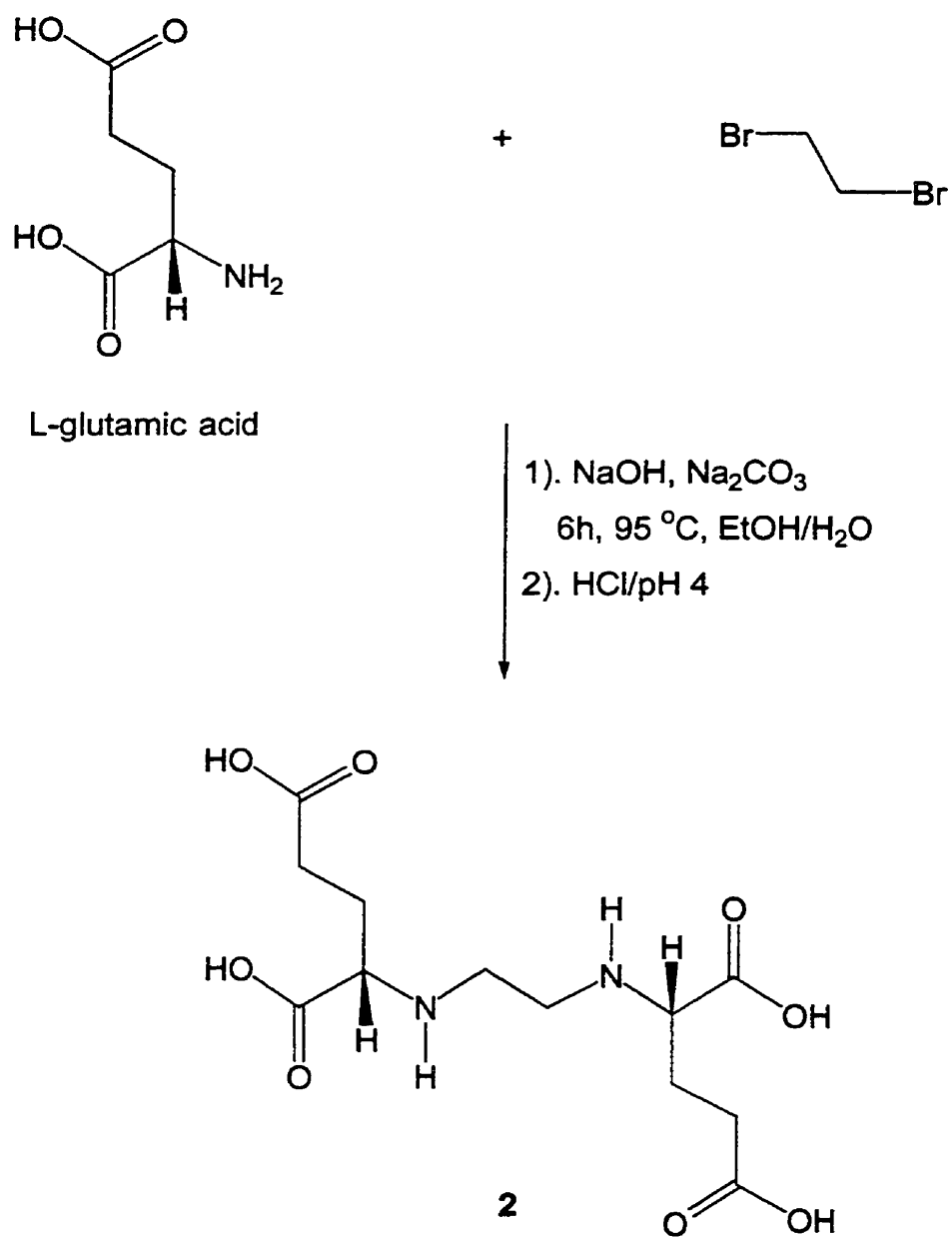
Figure 5.5. Reaction scheme for the synthesis of the tetraacid precursor 2.

5.3.2.2. Synthesis of the bisdioxopiperidine 1

The synthetic scheme employed for the synthesis of bisdioxopiperidine 1, shown in Figure 5.6, was a modification of previously reported methods (Polonski, 1988b, a). The tetraacid precursor 2 (0.74 g, 2.3 mmol) was suspended in freshly distilled acetic anhydride (7 mL), and refluxed at 130 °C for 2 h. After this period, the anhydride was evaporated under reduced pressure on a rotary evaporator at around 70 °C. The remaining viscous dark material left over, which may be the mixture of cyclic anhydride and unreacted tetraacid, was suspended in 15 mL benzene. The solution was then heated at 80 °C under a continuous flow of ammonia gas for 45 min. Benzene was removed under reduced pressure on a rotary evaporator at around 30 °C, and resulted in a dark viscous material, which partly contained the half acid-half amide intermediate. This jelly-like solid was then suspended in 1.5 mL of N,N-dimethyl formamide (DMF), and the solution was cooled to -78 °C for 1 h, and stored in a refrigerator at -10 °C. To this solution freshly distilled thionyl chloride (560 μL, 7.7 mmol) was added, and the mixture was stirred in the refrigerator at -10 °C for 18 h. The reaction was quenched by adding 30 mL of 10 % (w/v) $NaHCO_3$. The aqueous phase was extracted with chloroform (4 x 60 mL). The combined organic phase was separated from the aqueous phase with the aid of an ultrasonicator to break the emulsification. The organic phase was dried with Na_2SO_4, filtered, and evaporated under reduced pressure using a rotary evaporator to a volume of around 2 mL. This solution was loaded onto a silica gel column (150 mm long, 20 mm in diameter) which was conditioned with the mobile phase of 1:8:1 of methanol:acetone:ethyl acetate (v:v:v); and the flow rate was adjusted by an air flow to

around 12 mL/min. The eluents were collected in 10 mL fractions, evaporated, and

measured on a UV spectrophotometer (Cary 1, Varian, Mulgrave, Australia) in 50 mM

NaOH for the hydrolysis of the imide peak, which has a maximum absorbance at around

230 nm. The fractions containing the product (usually fractions 7 to 17) were combined

by dissolving in acetone in a 10 mL glass centrifuged tube. The acetone solvent was

evaporated to dryness, and around 0.5 mL chloroform was added to dissolve the residue.

Diethyl ether (6 mL) was added dropwise to this solution, during which a light brown

precipitate formed. The mixture was centrifuged at 1400 rpm for 10 min. The

supernatant was decanted, and the product was air-dried (7 mg, 0.025 mmol, 1.1 % yield).

The product gave a single spot on TLC with R_f value of 0.5 in 1:8:1

methanol:acetone:ethyl acetate (v:v:v) mobile phase. The melting point was 105 °C

(decomposition). The structure of the product was confirmed by ^{1}H- and ^{13}C-NMR. The

imide functional group of the bisdioxopiperidine 1 was characterized

spectrophotometrically on a Cary 1 spectrophotometer (Varian, Mulgrave, Australia).

The molecular weight of the bisdioxopiperidine 1 was confirmed by electrospray mass

spectroscopy with mass spectrometer LC Quatro (Micromass, Manchester, UK).
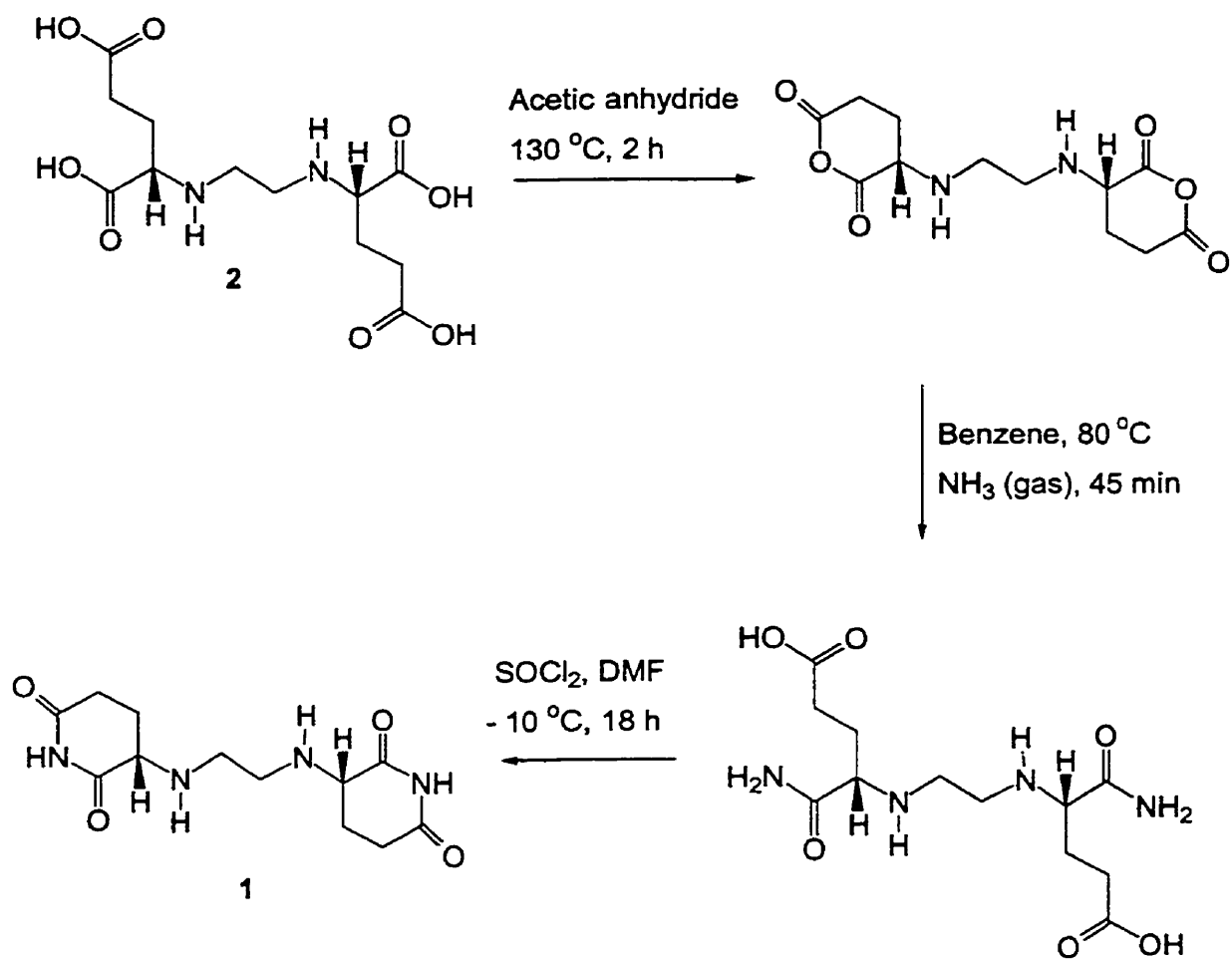
Figure 5.6. Reaction scheme for the synthesis of the bisdioxopiperidine **1**.

5.4. Characterization of the tetraacid precursor 2 and bisdioxopiperidine 1

5.4.1. The tetraacid precursor 2

The atoms of the tetraacid precursor 2 are numbered with $C_\alpha H$ as the chiral center of the molecule, CH_2 on chain as the CH_2 on the ethylenediamine main chain, $C_\beta H_2$ as the CH_2 next to the chiral center, and $C_\gamma H_2$ as the CH_2 next to the $C_\beta H_2$. The ^1H-NMR spectrum of the tetraacid precursor 2 is shown in Figure 5.7. The assignments are as follows: δ_H (D$_2$O/NaOD) 3.0 (2 H, t, J 5.5 Hz, $C_\alpha H$), 2.6 (4 H, s, CH_2 on chain), 2.2 (4 H, m, $C_\gamma H_2$), and 1.78 (4 H, m $C_\beta H_2$). Integration (the values below the NMR scale) showed that only monoalkylation at the nitrogen atom of the amino group of L-glutamic acid occurred, and resulted in the tetraacid even though 1,2-dibromoethane was used in excess.

The tetraacid precursor 2 was also analyzed in DMSO-d$_6$. Due to low solubility of the compound in DMSO-d$_6$, it was dissolved in a minimum volume of formamide. The formamide was then removed under high vacuum at around 70 °C for 1 h. The sample was dissolved in DMSO-d$_6$, and analyzed by ^1H-NMR as shown in Figure 5.8. The assignments are as follows: δ_H (DMSO-d$_6$) 4.2 (2 H, t, J 3.6 Hz, $C_\alpha H$), 3.8 (2 H, d, J 9.5 Hz, CH_a on chain), 2.9 (2 H, d, J 9.9 Hz, CH_b on chain), 2.1 (4 H, m, $C_\gamma H_2$), and 2.1-1.9 (4 H, m $C_\beta H_2$); the signals of the residual formamide also appeared at around 7-8 ppm, which are not shown in the spectrum (Figure 5.8). In this figure there are two sets of doublets with an integration of 2 protons (CH_a and CH_b) for each. These signals, assigned to the protons on the ethylenediamine main chain, appeared as a singlet at 2.6 ppm (CH_2 on chain) in the ^1H-NMR spectrum of the tetraacid 2 in D$_2$O/NaOD (Figure 5.7).

In order to confirm the coupling of the protons on the main chain, the sample was analyzed by ^{1}H-COSY NMR (^{1}H COrrelation SpectroscopY) as shown in Figure 5.9. ^{1}H-COSY NMR is a two dimensional spectrum with each proton signal appearing as a contour plot, and the proton signals appearing along the diagonal. The coupling between the protons is indicated by the peaks, which are not on the diagonals (cross-peaks), and form a square. There were several couplings observed in the spectrum. The protons on the $C_\gamma H_2$ and $C_\beta H_2$ coupled to each other to form a square from 1.85-2.15 ppm. The two geminal protons on $C_\beta H_2$ also coupled to each other due to the adjacent chiral center, and formed a very small square at around 2.2 ppm. The couplings of $C_\gamma H_2$ and $C_\beta H_2$ protons to the proton on chiral center $C_\alpha H$ were indicated by the two large squares from 4.2-1.8 ppm. Interestingly, the two geminal protons on the ethylenediamine main chain (CH_2 on chain) coupled to each other to form a square from 3.8-2.8 ppm.

The sample was also analyzed by ^{13}C-DEPT (Distortionless Enhancement by Polarization Transfer) NMR (Figure 5.10). The assignments are as follows: δ_C (DMSO-d_6) 174.7 (2 C, COOH), 173.7 (2 C, COOH), 58.5 (2 C, C_α), 37.8 (2 C, CH_2 on chain), 29.2 (2 C, $C_\beta H_2$), and 22.6 (2 C, $C_\gamma H_2$). Based on this result, only one type of carbon signal corresponded to the CH_2 on the main chain, but there were two sets of doublets coming from the four protons on the main chain, and these protons coupled to each other.

In order to confirm that the two sets of doublets at 3.8 and 2.9 ppm are the protons attached to the same type of carbon CH_2 on the ethylenediamine main chain, the sample was analyzed by HSQC NMR (Heteronuclear Single Quantum Coherence), which provides the correlation of the proton and the carbon signals. The correlation of the

proton and carbon is indicated by a contour cross peak, which is the projection from the corresponding proton and carbon signals from the two proton and carbon NMR spectra on the two axes. The HSQC NMR spectrum of the tetraacid precursor 2 is shown in (Figure 5.11). For the sake of discussion the positions of the cross peaks in the HSQC NMR spectrum are referred to the ^{1}H-NMR scale on the x-axis. The cross peak at 4.2 ppm is the correlation of the proton and carbon on the chiral center, $C_\alpha H$; the next two cross peaks are the correlations of the two geminal protons and the carbon on the CH_2 on the chain; the last three cross peaks at around 2.2 and 1.9 ppm are the correlations of the corresponding protons and carbons of the two $C_\beta H_2$ and $C_\gamma H_2$ groups. Thus, it is quite clear that the two sets of proton doublets at 3.8 and 2.9 ppm on the main chain correlated with only one type of CH_2 carbon on the chain.

The $D_2O/NaOD$ and the DMSO-d_6 solvents significantly affected the absorption profile of the protons of the tetraacid precursor 2. In $D_2O/NaOD$ the protons of the CH_2 on the chain appeared as a singlet at 3.0 ppm (Figure 5.7), while in DMSO-d_6 these protons coupled to each other, and appeared as two sets of doublets at 3.8 and 2.9 ppm separated by about 1 ppm (Figure 5.8). Close investigation of the molecular model of the tetraacid precursor 2 reveals that the molecule has a C_2 axis of symmetry. However, the symmetry operation about this axis only exchanges the whole set of protons on the right hand side with those on the left hand side of the molecule. Due to the presence of the two chiral centers, there is no symmetry operation such that the two geminal protons on the CH_2 on the chain can be exchanged with each other. These protons are defined as diastereotopic protons, which are non-interchangeable geminal protons by any symmetry

operation, and they are not chemical shift equivalent (Silverstein *et al.*, 1991; Sanders and Hunter, 1993). The observation that the protons of the CH_2 on the chain appeared as a singlet in $D_2O/NaOD$ was a coincidence. Under normal condition, these protons should couple to each other, and appear as two sets of doublets as shown in the ^{1}H-NMR spectrum of the tetraacid precursor 2 in DMSO-d_6.
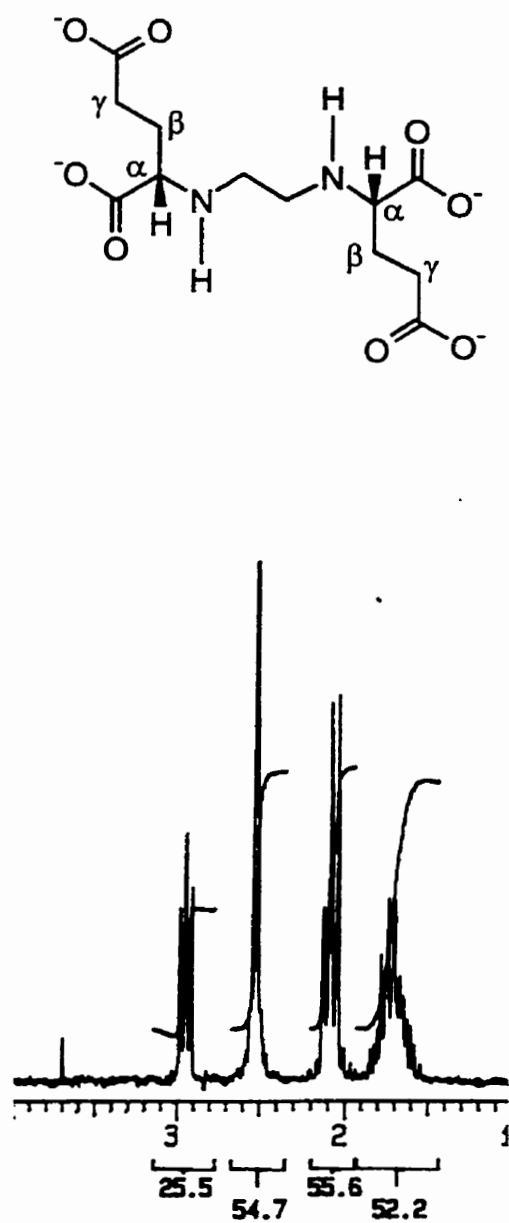
Figure 5.7. ^{1}H-NMR spectrum (recorded on Gemini 200 MHz) of the tetraacid precursor **2** in D$_2$O/NaOD.
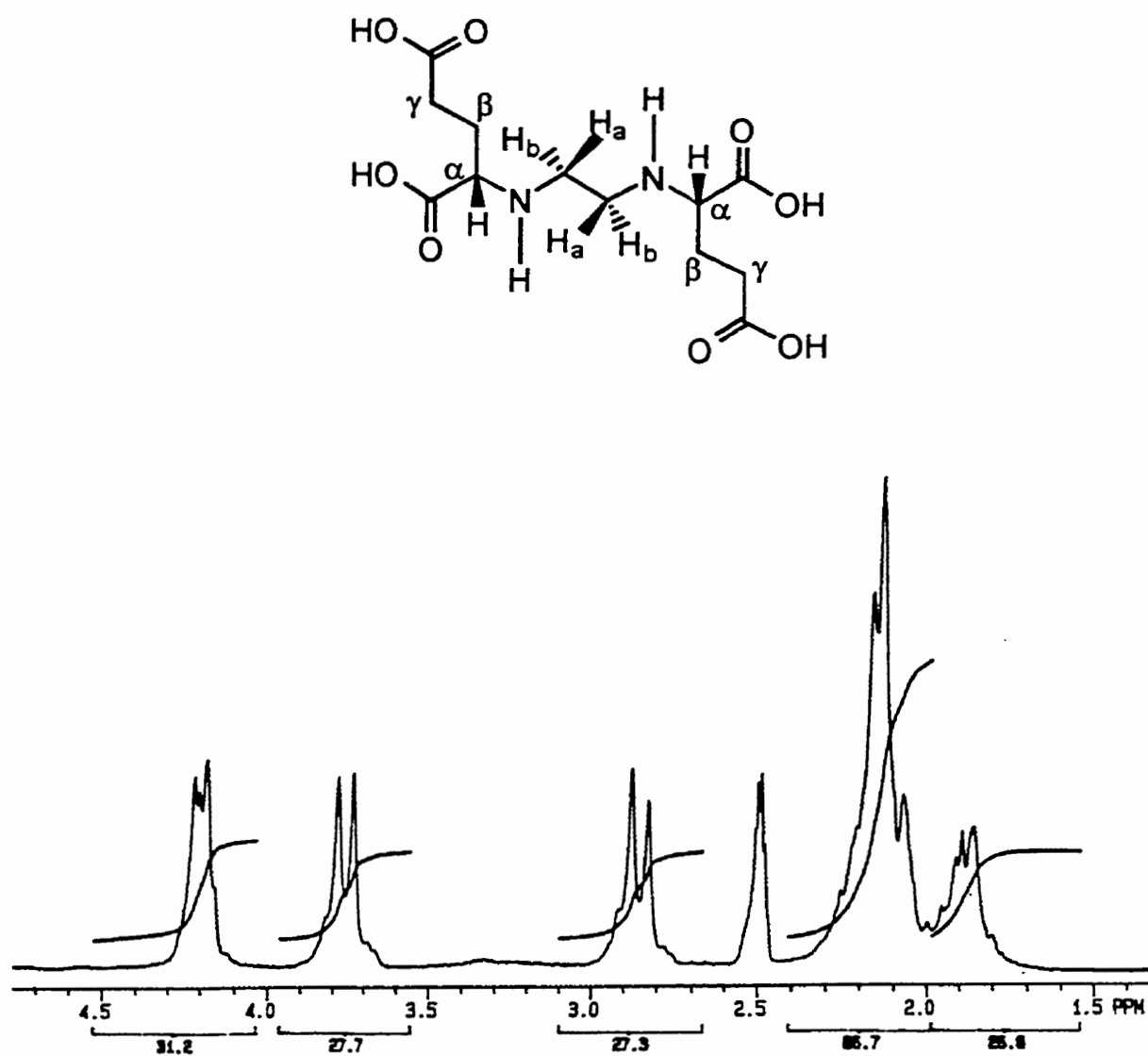
Figure 5.8. ¹H-NMR spectrum (recorded on Gemini 200 MHz) of the tetraacid precursor **2** in DMSO-d₆.
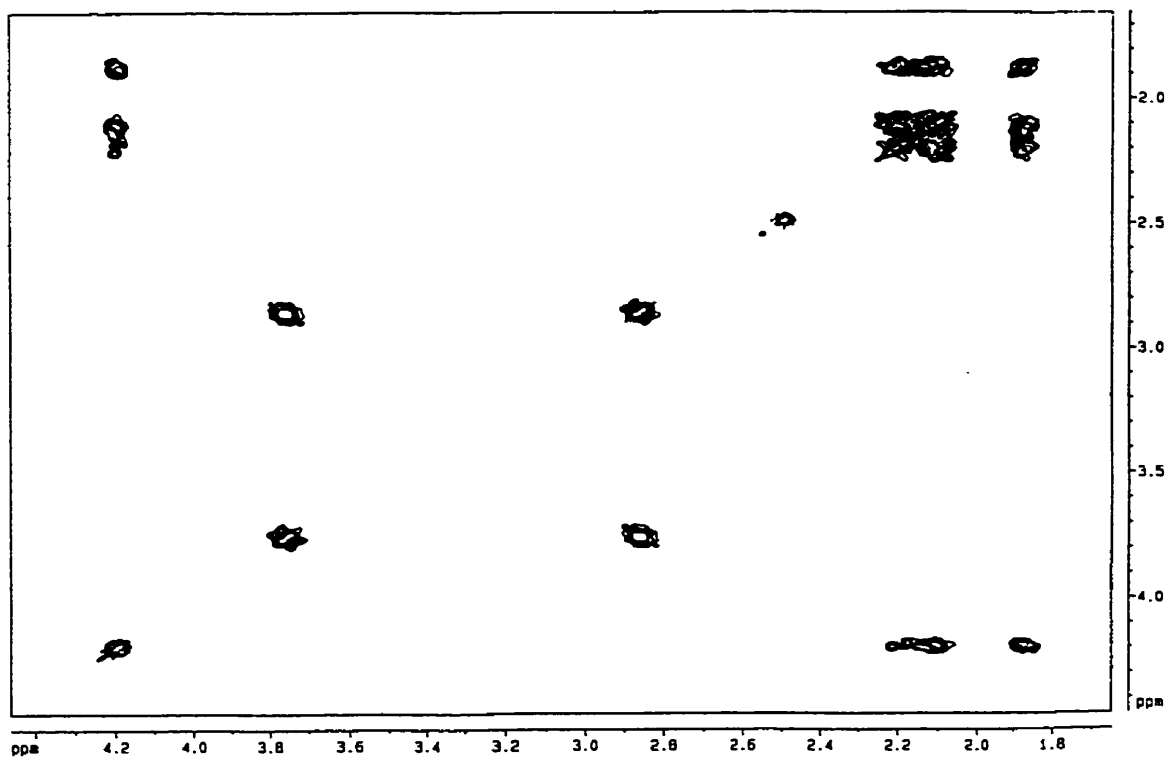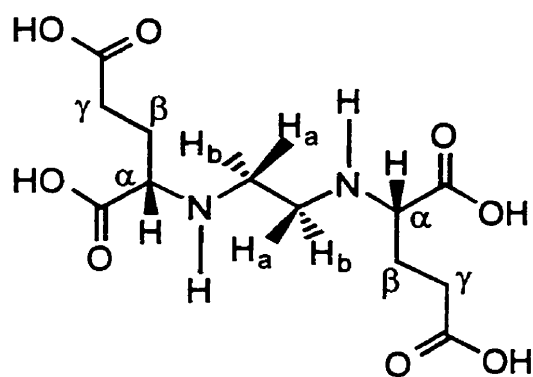
Figure 5.9. ¹H-COSY NMR spectrum (recorded on AMX-500 MHz) of the tetraacid precursor **2** in DMSO-d₆.
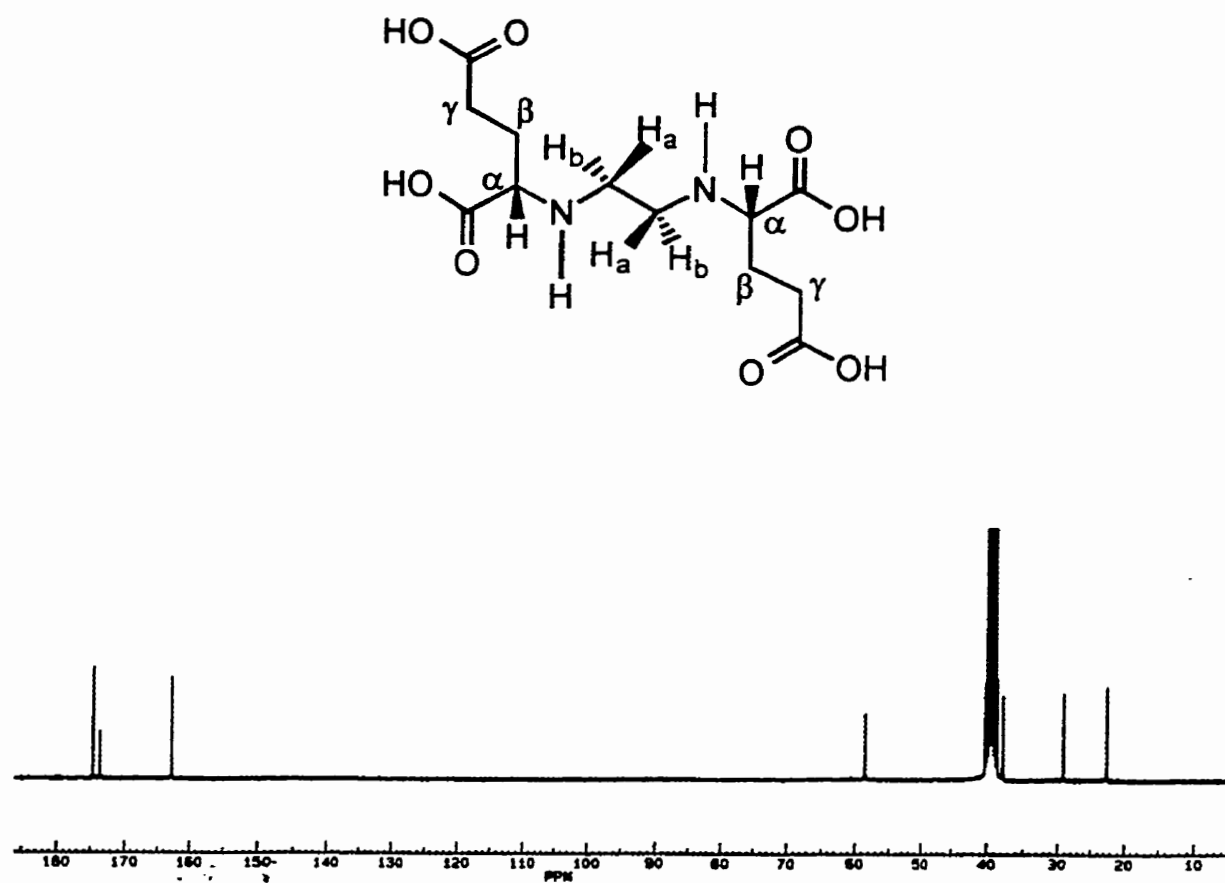
Figure 5.10. ^{13}C-DEPT NMR spectrum (recorded on Bruker AM-300 MHz) of the tetraacid precursor **2** in DMSO-d$_6$.
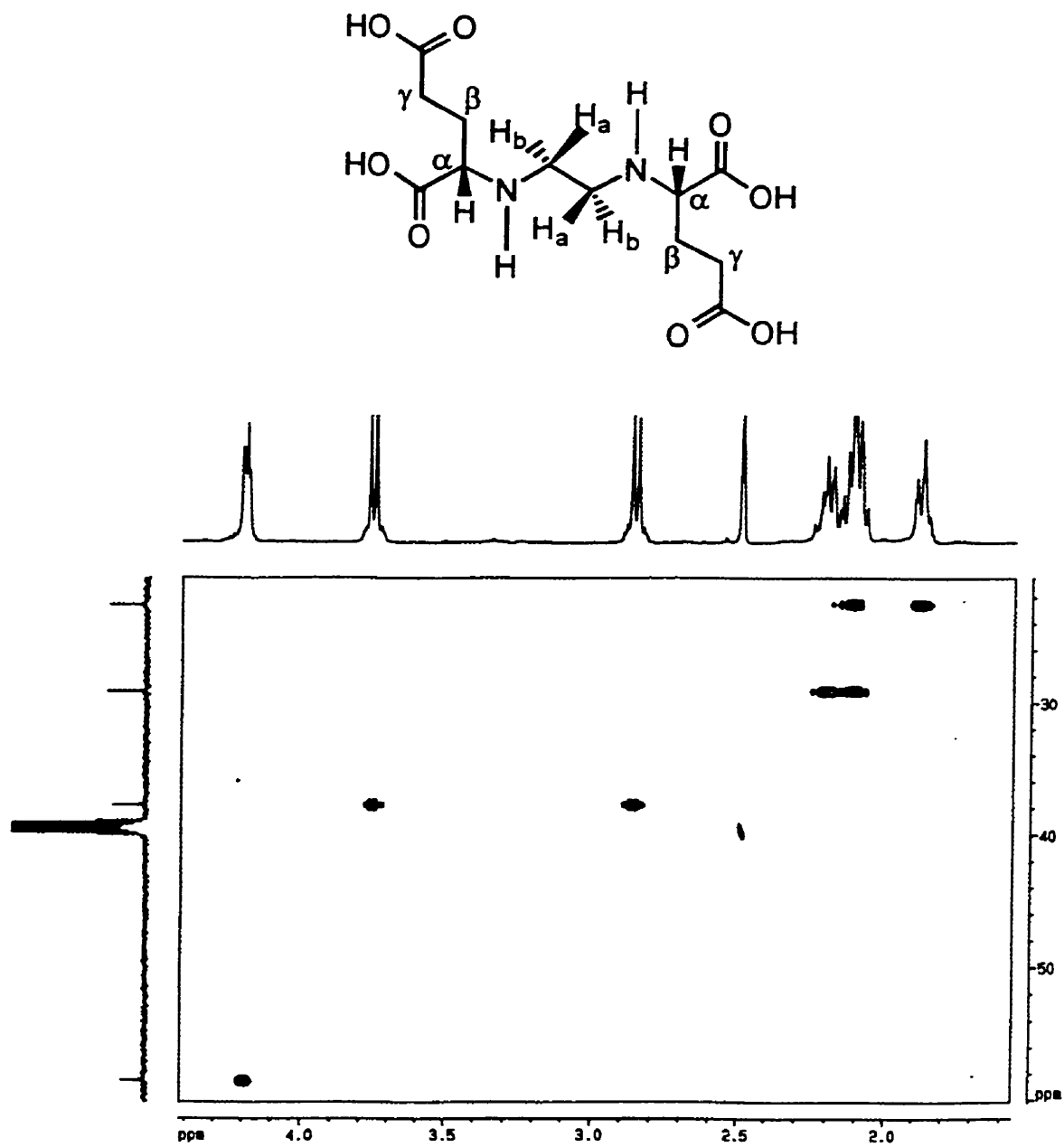
Figure 5.11. HSQC NMR spectrum (recorded on AMX-500 MHz) of the tetraacid precursor 2 in DMSO-d6.

5.4.2. The bisdioxopiperidine 1

The atoms of the bisdioxopiperidine 1 are numbered in the same way as that of

the tetraacid precursor 2. The ^{1}H-NMR spectrum of the bisdioxopiperidine 1 was shown

in Figure 5.12. The assignments are as follows: δ_H (CDCl$_3$) 7.95 (2 H, broad m, NH

imide), 5.1 (2 H, broad m, NH on the chain), 4.4-4.1 (2 H, m, C$_\alpha$H), 3.6-3.3 (4 H, m, CH$_2$

on chain), 2.8-2.4 (4 H, m, C$_\gamma$H$_2$), and 2.4-2.0 (4 H, m, C$_\beta$H$_2$). The spectrum of the imide

1 is much more complicated than that of the tetraacid precursor 2. Complex multiplets

were assigned to the protons on the chain and on the imide rings. The molecule has two

chiral centers originating from the starting material, L-glutamic acid. The presence of

two chiral centers, and the ring conformation could contribute to the complexity of the

spectrum. A similar complex ^{1}H-NMR spectrum is observed for a very closely related

compound, (S)-2-aminoglutarimide hydrobromide, whose protons appear as complex

multiplets (Polonski, 1988b).

The bisdioxopiperidine 1 was also analyzed by ^{13}C-NMR as shown in Figure

5.13. The assignments are as follows: δ_C (CDCl$_3$) 174.5 (2 C, CO), 170.5 (2 C, CO), 57.6

(2 C, C$_\alpha$), 37.3 (2 C, CH$_2$ on chain), 31.4 and 30.6 (2 C, C$_\gamma$, as two close peaks), 22.3 and

22.0 (2 C, C$_\beta$, as two close peaks). The peak assignment for this spectrum was based on

that for the tetraacid precursor 2, which was analyzed completely with ^{13}C-DEPT (Figure

5.10) and HSQC (Figure 5.11). Due to small quantity of the imide 1 obtained, only

decoupled ^{13}C-NMR analysis was performed. There are two extra carbon signals, which

are very close to each other. The molecule has several hydrogen bonding donor and

acceptor atoms, such as O and N. It is also known that the imide functional groups can

form strong hydrogen bondings with each other as seen between the base pairs in DNA. The hydrogen bonding could complicate the ^{13}C NMR spectrum. In addition, the imide functional group possibly undergo keto-enol tautomerism, and result in a complicated spectrum. This type of keto-enol tautomerism is seen clearly with acetyl acetone, of which the ^{13}C-NMR spectrum has an extra set of carbon signals (Johnson and Jankowski, 1972). The molecular weight of the imide 1 was confirmed by electrospray mass spectroscopy (Figure 5.14) with two dominant ion peaks at 305.27 m/z for $(M+Na)^+$, and at 287.28 m/z for $(M+Na-H_2O)^+$.

The bisdioxopiperidine 1 was also analyzed by UV spectrophotometry, which is discussed in the following section for the determination of the pK_a of the imide 1. It is known that the N-H imide functional group is ionized under alkaline conditions to the anion of the imide in the N^- form, which absorbs strongly with maximum absorbance at around 227 to 230 nm (Hasinoff, 1990a; Buss, 1998). This absorbance should decrease with time since under alkaline conditions, the hydroxide ion can attack the carbonyl group of the imide, and result in the cleavage of the imide bond to form the half acid-half amide, which does not absorb significantly at this wavelength. The imide 1 was dissolved in KOH solutions at different pH, and analyzed immediately by UV spectrophotometry. A series of absorption spectra were recorded as shown in Figure 5.15, which is discussed in detail in the next section. It was shown that the UV spectra of the bisdioxopiperidine 1 in solutions at different pH decreased with time at different rates, and the wavelength at the maximum absorbance shifted with the change in pH of the solutions from 230 nm at high pH to 210 nm at low pH (Figure 5.15). The absorbance at

these maximum wavelengths also decreased with time at different rates (Figure 5.17).

These UV spectral changes are similar to those seen for other imides (Hasinoff, 1990a;

Buss, 1998). Thus, with ^{1}H-NMR, ^{13}C-NMR, mass spectrometry, and UV

spectrophotometric analyses it is confident that the bisdioxopiperidine 1 was synthesized

in a pure form.
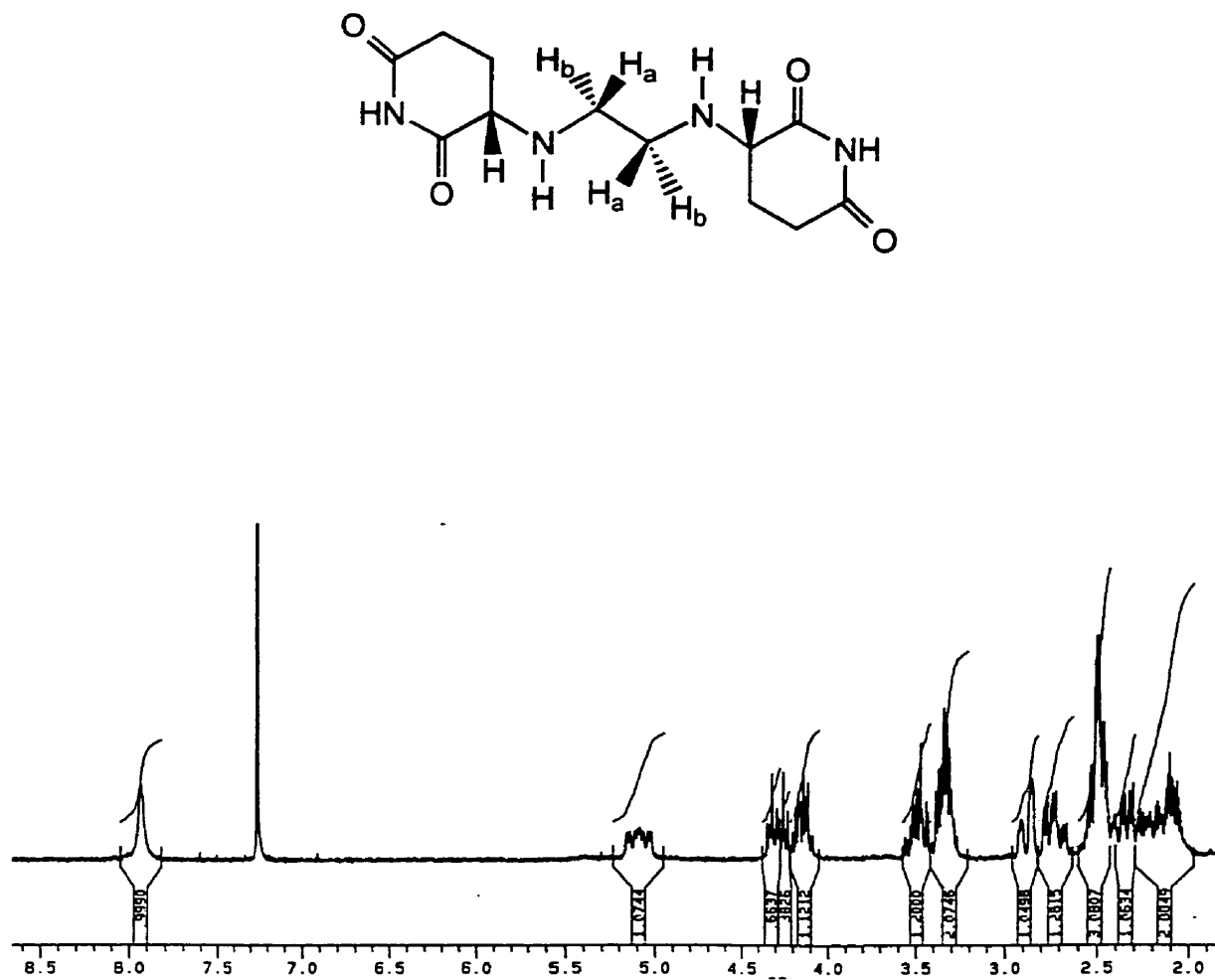
Figure 5.12. ¹H-NMR spectrum (recorded on Bruker AM-300 MHz) of the bisdioxopiperidine **1** in CDCl₃.
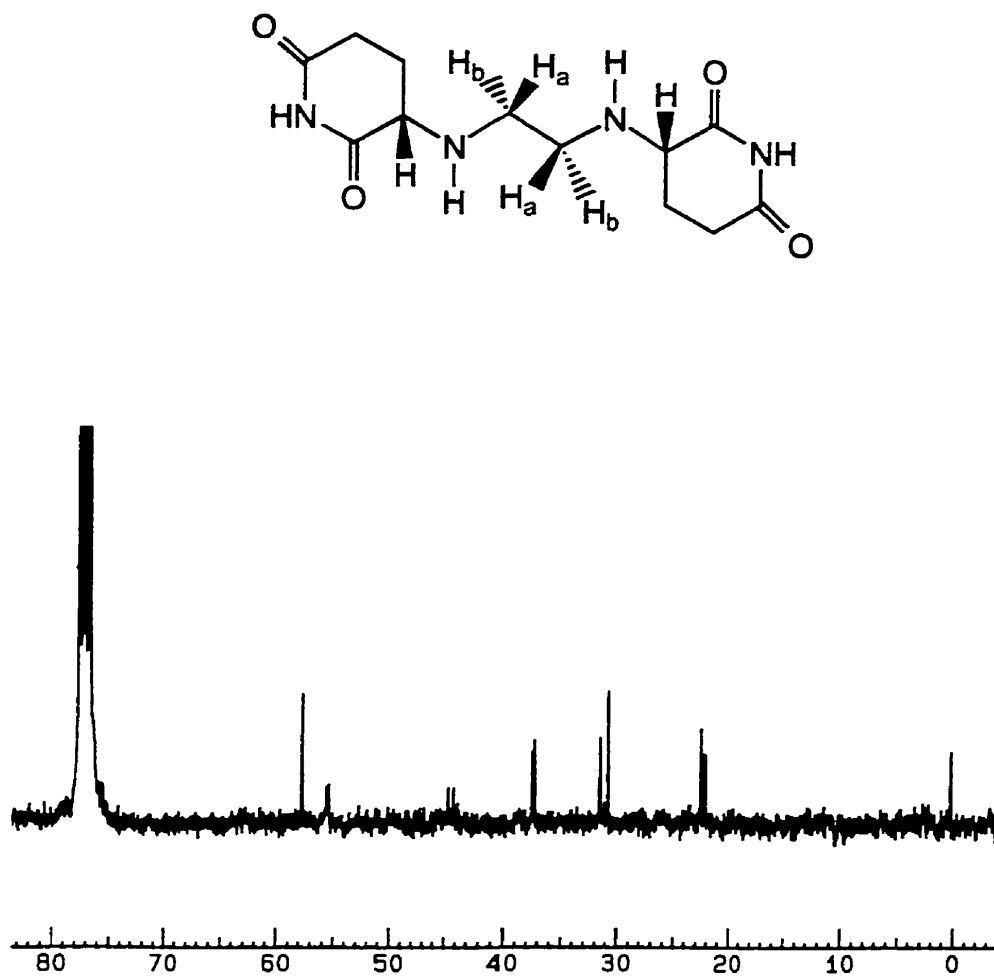
Figure 5.13. ^{13}C-NMR spectrum (recorded on Bruker AM-300 MHz) of the bisdioxopiperidine 1 in CDCl$_3$.
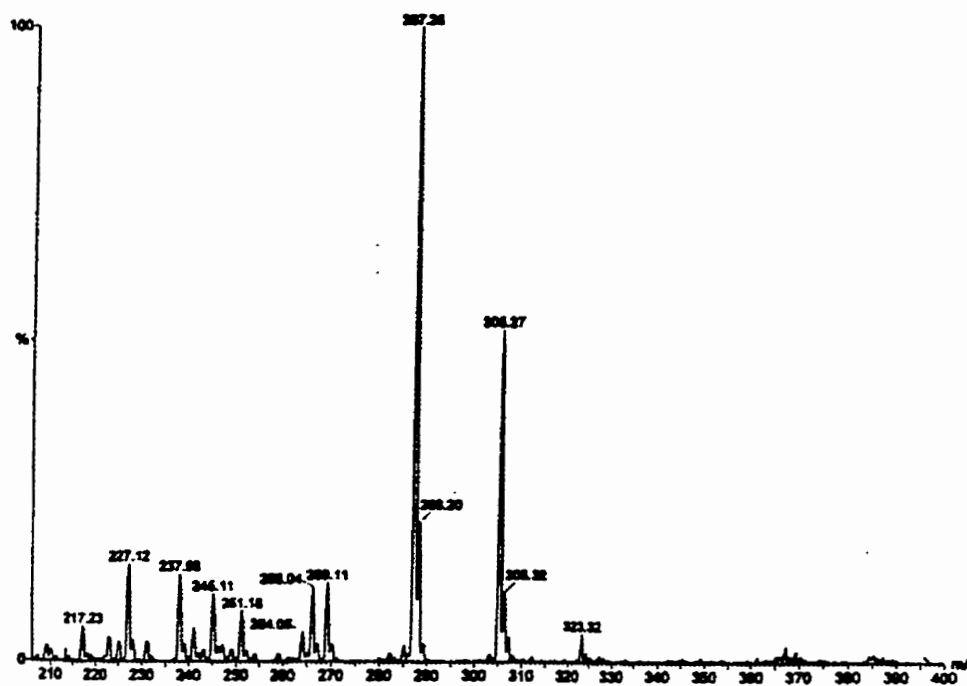
Figure 5.14. Electrospray mass spectrum of the bisdioxopiperidine **1**. There are two dominant ion peaks at 305.27 m/z for (M+Na)⁺, and at 287.28 m/z for (M+Na-H₂O)⁺. The vertical axis is expressed in relative % abundance of the ions.
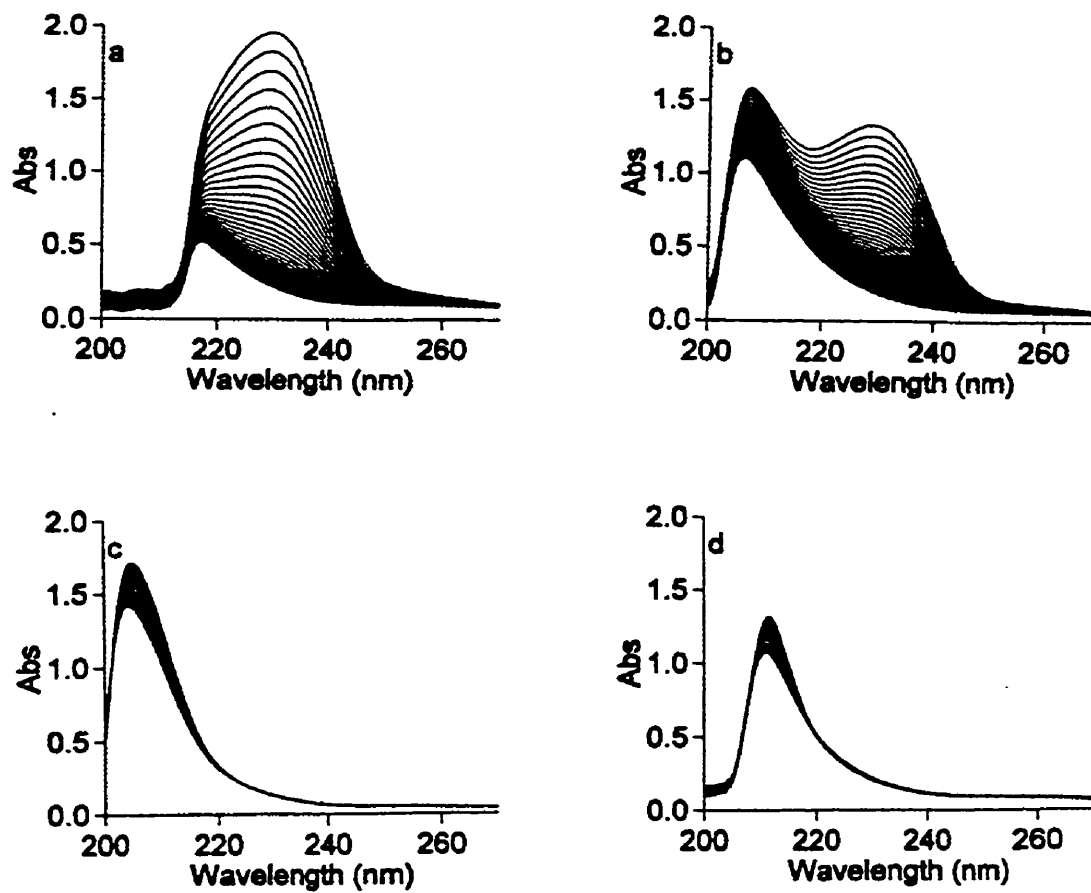
Figure 5.15. Repeat UV spectra of the bisdioxopiperidine **1** at 100 μM in solutions at pH of 13.0, 10.8, 8.5 and 7.4 for (a), (b), (c) and (d), respectively. The spectra in (a) and (b) were recorded every 1 min, and that in (c) and (d) were recorded every 60 min The spectra in (a), (b) and (c) were recorded at 25 °C, and at 37 °C for the spectra in (d). Tris/KCl (50/150 mM) was used for the solution at pH 7.4, ammonia buffer (NH₄OH/KCl) was used for the solutions at pH below 11.0, and KOH/KCl buffer was used for those at pH above 11.0. The ionic strength was maintained at 150 mM with KCl.

5.5. Determination of the pK$_a$ of the imide group of the bisdioxopiperidine 1

5.5.1. Importance of the pK$_a$ of the imides

It has been proposed that ADR-925, which is the hydrolyzed form of dexrazoxane is the active form of the drug in the prevention of the cardiocytotoxic side effects of doxorubicin and other anthracycline compounds (Hasinoff *et al.*, 1998; Elihu *et al.*, 1998). Thus, the rate of the hydrolysis of dexrazoxane to ADR-925 should be very important in determining the cardioprotective effect of the drug. It was found that dexrazoxane with the imide pK$_a$ of 10.00 at 25 °C, and 9.45 at 37 °C can hydrolyze to ADR-925 under physiological conditions with half times of around 73 h at 25 °C, and 16.3 h at 37 °C (Hasinoff, 1990a). An increase in pK$_a$ value of the imide group leads to a higher fraction of the imide in the neutral form, which is more susceptible to nucleophilic attack by OH$^-$. The anion of the imide, N$^-$ form is resistant to nucleophilic attack by OH$^-$ due to the negative charge repulsion (Hasinoff, 1990a; Buss, 1998). The general reaction scheme for the hydrolysis of several cyclic imides is described in Figure 5.16. Using UV spectrophotometric analysis, both the pK$_a$ of the acidic hydrogen of the imide, and the rates of the hydrolysis in solutions at different pH were determined based on previously reported methods (Hasinoff, 1990a; Buss, 1998). The goal of this experiment is the determination of the rates of hydrolysis in solutions at different pH, and of the pK$_a$ value of the imide group of the bisdioxopiperidine 1.
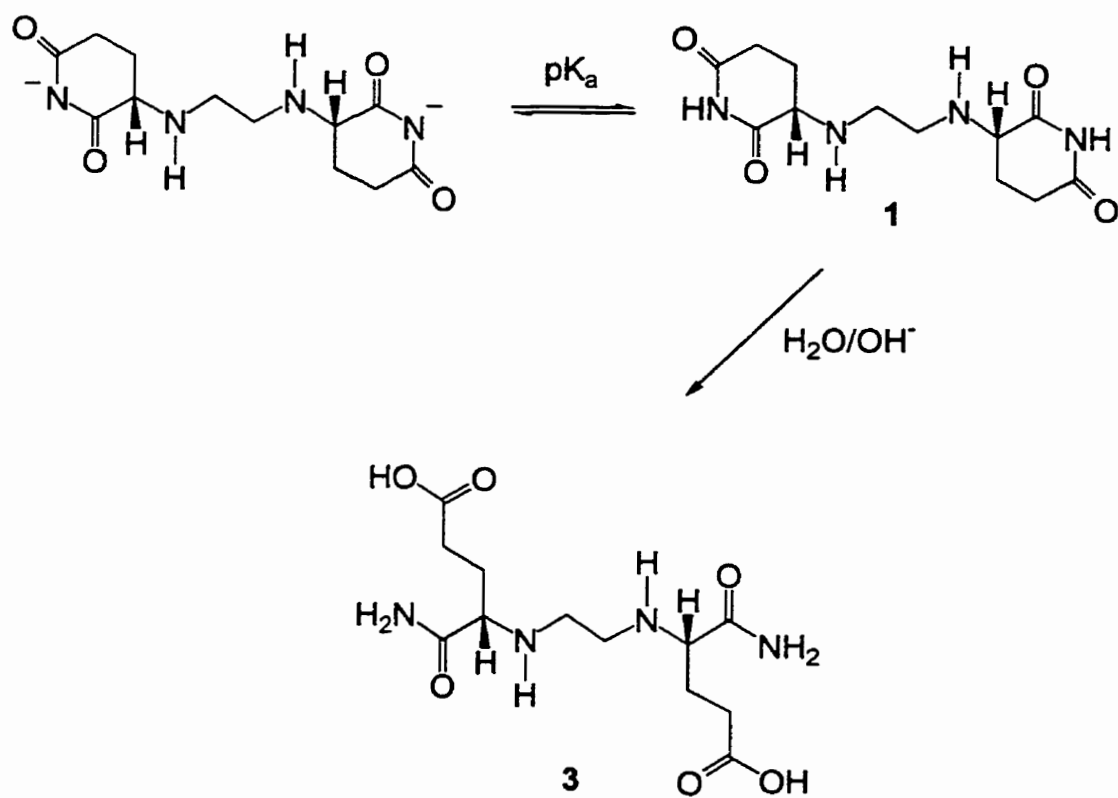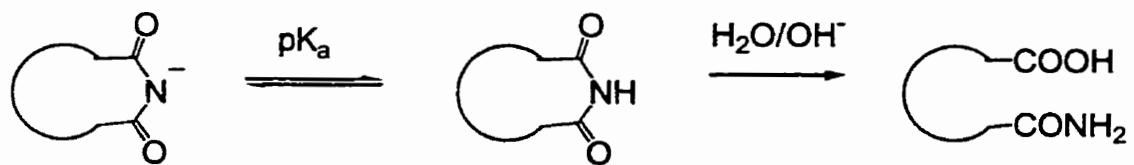
Figure 5.16. General scheme for the hydrolysis of the imide ring, and of the bisdioxopiperidine **1**.

5.5.2. Methods

The bisdioxopiperidine 1 (1.00 mg, 3.54 μmol) was dissolved in 1.0 mL of 2 mM HCl to stabilize the compound (Hasinoff, 1990a; Buss, 1998). The solution was stored in a freezer until use to prevent the hydrolysis of the imide rings. Other chemicals used in this experiment were commercially available, and were used without further purification. The hydrolysis rates of the imide 1 at 100 μM were measured spectrophotometrically in 1 cm stoppered silica cells on a Cary 1 spectrophotometer (Varian, Mulgrave, Australia) at a constant temperature of 25 °C or 37 °C as indicated. The pH of the solutions were controlled by Tris/KCl (50/150 mM) at pH 7.4, or ammonium buffer at a pH below 11.0, or potassium hydroxide at a pH over 11.0. In all of these solutions, the ionic strength was maintained at 150 mM with KCl. The pH of the solutions were measured right after the experiment. The hydrolysis reactions were started with the addition of the imide solution into the buffer. The first-order decrease in absorbance was followed at the maximum absorbance at 230 nm or 210 nm as indicated. Some absorbance-time traces were shown in Figure 5.17. Several repeat spectra of the imide 1 in solutions at different pH were shown in Figure 5.15.
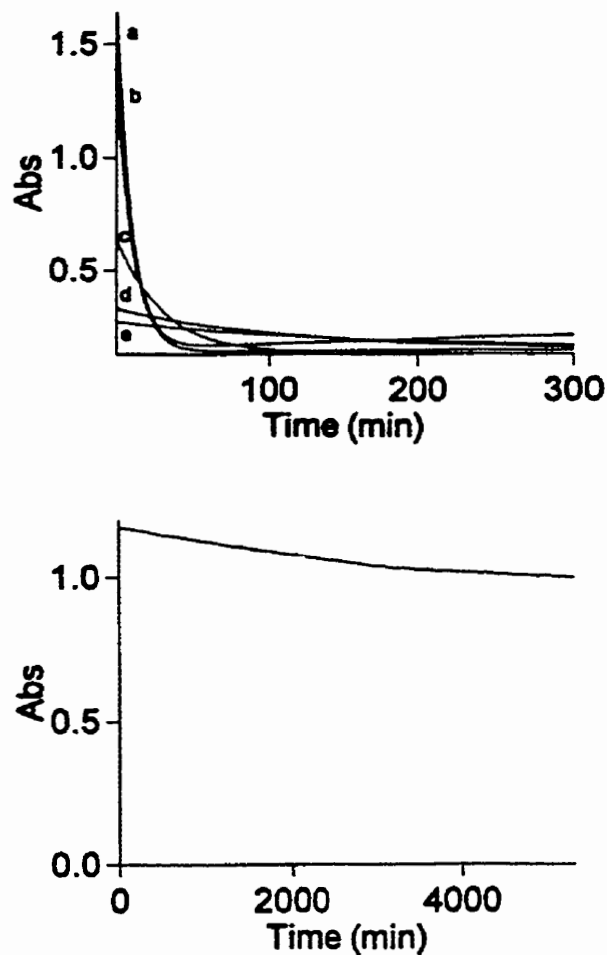
Figure 5.17. Absorbance-time traces for the hydrolysis of the bisdioxopiperidine 1.
(Top) At 100 µM in solutions at 25 °C, and at pH of 12.9, 11.2, 10.39, 9.71 and 9.50 for
(a), (b), (c), (d) and (e), respectively. Ammonia buffer (NH₄OH/KCl) was used for the
solutions at pH below 11.0, and KOH/KCl buffer was used for those at pH above 11.0.
The ionic strength was maintained at 150 mM with KCl. The absorbance was monitored
at 230 nm for all traces.
(Bottom) At 100 µM in Tris/KCl (50/150 mM) buffer solution at 37 °C and pH 7.4. The
absorbance was monitored at 210 nm.

5.5.3. Determination of pK$_a$ of the bisdioxopiperidine 1

The absorbance-time traces of the bisdioxopiperidine 1 at different pH values were fit to the following equation using the Cary kinetics software (Varian, Mulgrave, Australia) (Hasinoff, 1990a; Buss, 1998).

$$A = (Amp) \cdot e^{-k_{obs} \cdot t} + A_\infty \qquad (3.1)$$

in which A and A_∞ are the absorbances at time t and infinity, respectively, and k_{obs} is the pseudo-first-order rate constant, and Amp is the amplitude of the absorbance change. This reaction is true with the assumption that the compound has a single pK$_a$ value, and both imide rings hydrolyze independently, and at the same rate. The k_{obs} values were plotted against the pH values of the solutions as shown in Figure 5.18. The data points were then fit by a three-parameter nonlinear least square analysis to Equation 5.1, which was applied for the hydrolysis of dexrazoxane (Hasinoff, 1990a). The pH value at the inflection point is a good estimation of the pK$_a$ value of the imide 1.

$$k_{obs} = (k_w + k_{OH}[OH])/(1 + K_a/[H^+]) \qquad (5.1)$$

in which k_{OH} is a second order rate constant for the reaction of OH⁻, k_w is a first order rate constant for a pH-independent unimolecular decomposition (or reaction with water), and K_a is the acid dissociation constant of the imide. The $[OH]$ is equivalent to $K_w/[H^+]$, and K_w is the equilibrium constant for the reaction of the imide 1 with water.

Since the three parameter fit to Equation 5.1 gave the value of k_w very close to zero, the equation was simplified by setting k_w equal to zero, and a two parameter fit to Equation 5.2 was utilized.

$$k_{obs} = (k_{OH}[OH])/(1 + K_a/[H^+]) \qquad (5.2)$$

The pK_a value of the imide 1 was determined as 10.69 ± 0.02, which is very close to that of dexrazoxane as 10.00 ● 0.02 at 25 °C (Hasinoff, 1990a) . The second order rate constant for the reaction of the imide 1 with OH⁻, k_{OH} was determined to be 216.6 ± 10.8 $M^{-1} \cdot min^{-1}$, which is about four times smaller than that of dexrazoxane at 820 ± 50 $M^{-1} \cdot min^{-1}$ (Hasinoff, 1990a).

At high pH value the concentration of H^+ is very small, and $K_a/[H^+] \gg 1$. This leads to a new expression of the k_{obs} as shown in Equation 5.3

$$k_{obs} = (k_{OH} [OH^-][H^+])/K_a = (k_{OH}K_w)/K_a \qquad (5.3)$$

Equation 5.3 predicts that in strong alkaline aqueous solutions, the observed rate of the hydrolysis of the imide 1 is independent of the OH⁻ concentration. According to the two parameter fit to Equation 5.2, the imide 1 has a k_{OH} value four times smaller than that of dexrazoxane. The imide 1 in alkaline solution at pH 12 has a half time of around 8 min.

At low pH values the concentration of H^+ is high, and $K_a/[H^+] \ll 1$. This leads to a new expression of the k_{obs} as shown in Equation 5.4

$$k_{obs} = (k_{OH} [OH^-][H^+])/1 = k_{OH} [OH^-] \qquad (5.4)$$

Equation 5.4 predicts that in neutral or slightly acidic aqueous solutions, the observed rate of the hydrolysis of the imide 1 varies linearly with the OH⁻ concentration. According to the two parameter fit to Equation 5.2, the imide 1 hydrolyzed with a k_{OH} value four times smaller than that of dexrazoxane. With an increase in k_{OH} the imide 1 should hydrolyze slower than dexrazoxane in neutral or slightly acidic solutions. Indeed, the imide 1 was found to hydrolyze with half time of 38.5 h under physiological condition at pH 7.4, 37 °C in Tris/KCl buffer as shown in Figures 5.14 (d) and 5.17 (bottom). This rate is slower

than that for dexrazoxane with half time of 16.3 h (Hasinoff, 1990a) as shown in Table

5.1. k_{obs} value at 3.0 x 10^{-4} min^{-1} under physiological condition was obtained by a non-

linear fit of the absorbance-time trace in Figure 5.17 (bottom) to Equation 3.1 with the

assumption that the absorbance, A_∞ decreases to zero at time infinity. Using Equation 5.4

and under physiological conditions (at pH 7.4 and 37 °C), the predicted k_{obs} was also

calculated at 3.4 x 10^{-5} min^{-1}. Within the error in the determination of k_{obs}, this value is

quite close to the measured k_{obs} at 3.0 x 10^{-4} min^{-1} under the same conditions. The slow

hydrolysis of the imide 1 is probably due to a more complex reaction mechanism.

Indeed, a much more complicated expression for the hydrolysis of dexrazoxane is derived

from a detailed study of the hydrolysis of dexrazoxane reported in literature (Sisco,

1989). The main goal of the project, however, is not a mechanistic study of the

hydrolysis of the imide 1. It is rather the development of dexrazoxane analogs with faster

rates of hydrolysis to the active forms, which can act as a good metal ion chelators to

prevent the cardiotoxicity induced by anthracycline antitumor drugs. Thus, the reaction

mechanism was not examined further.

Table 5.1. Rate constants, and half times for the hydrolyses at 37 °C, pH 7.4 in Tris/KCl (50/150 mM), and the pK_a values of the bisdioxopiperidine 1 and dexrazoxane.

Compound	pK_a	$t_{1/2}$ (h)	k_{OH} ($M^{-1} \cdot min^{-1}$)	k_{obs} (min^{-1})
Bisdioxopiperidine 1	10.69 ± 0.02	38.5	216.6 ± 10.8	3.0 x 10^{-4}
Dexrazoxane*	9.45 ± 0.05	16.3	820 ± 50	7.1 x 10^{-4}

*The parameters for the hydrolysis of dexrazoxane were taken from Hasinoff, 1990a.
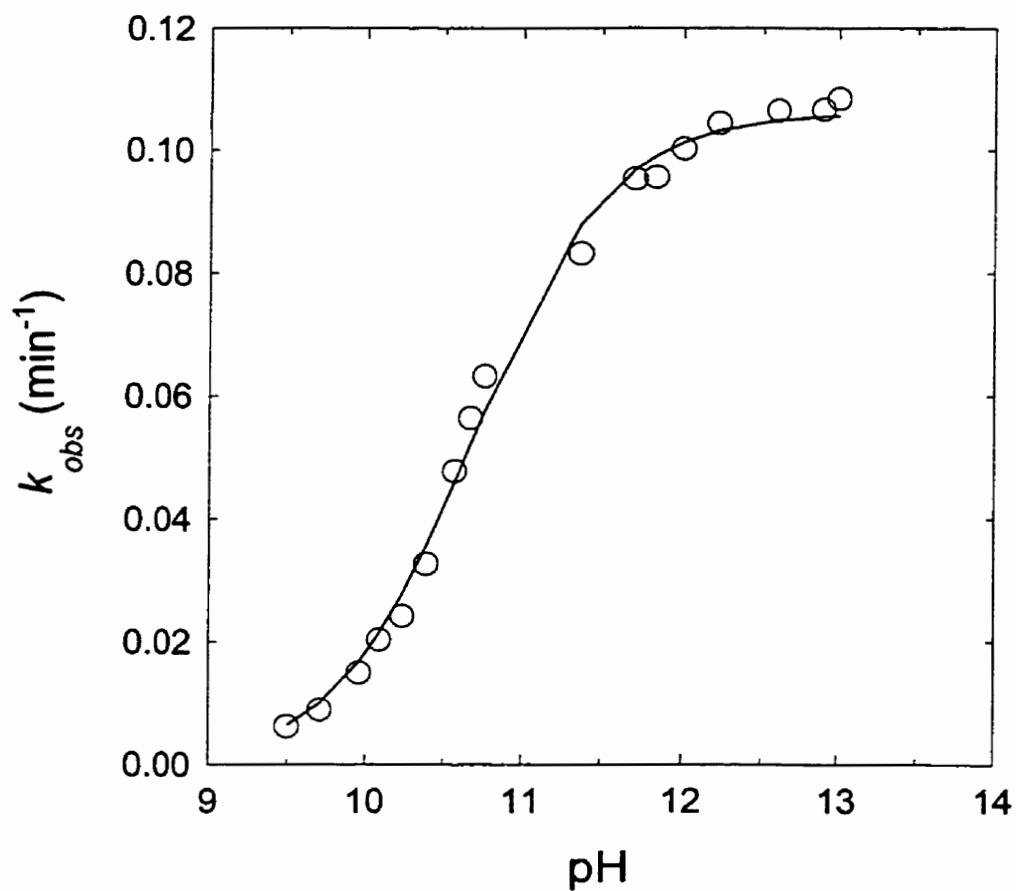
Figure 5.18. Variation of k_{obs} with pH for the hydrolysis of the bisdioxopiperidine **1**. The pH dependence of the hydrolysis of the bisdioxopiperidine **1** at 25 °C were performed in ammonia buffer for pH below 11 and KOH solutions for pH above 11. The values of k_{obs}, were measured at 230 nm for all experiments.

5.6. Chelation ability of the hydrolyzed form of the bisdioxopiperidine 1

The cardioprotective effect of the bisdioxopiperidine 1 may be associated with the ability of its hydrolyzed form to competitively dissociate the Fe^{3+}-anthracycline complex to prevent the cardiotoxic side effects as seen with ADR-925, the hydrolyzed form of dexrazoxane (Hasinoff, 1989a; Hasinoff *et al.*, 1998; Herman *et al.*, 1998; Hasinoff, 1998; Synold *et al.*, 1998; Hasinoff, 1989a; Sobol *et al.*, 1992). The hydrolyzed form of the imide 1 (Figure 5.19), which is structurally similar to ADR-925 was predicted to be a strong metal ion chelator, and could displace Fe^{3+} from the Fe^{3+}-drug complex *via* the chelation to the Fe^{3+}. In this experiment, the hydrolyzed form of the imide 1 as compound 3 was tested with Fe^{3+}-daunorubicin complex to evaluate the chelation effect of the compound. Ethylenediaminetetraacetic acid (EDTA), and the tetraacid precursor 2 were also used to compare the chelation effects. The Fe^{3+}-daunorubicin complex was utilized in this testing model because this complex was found to be more stable, and not to undergo self reduction (Malisza and Hasinoff, 1995a).
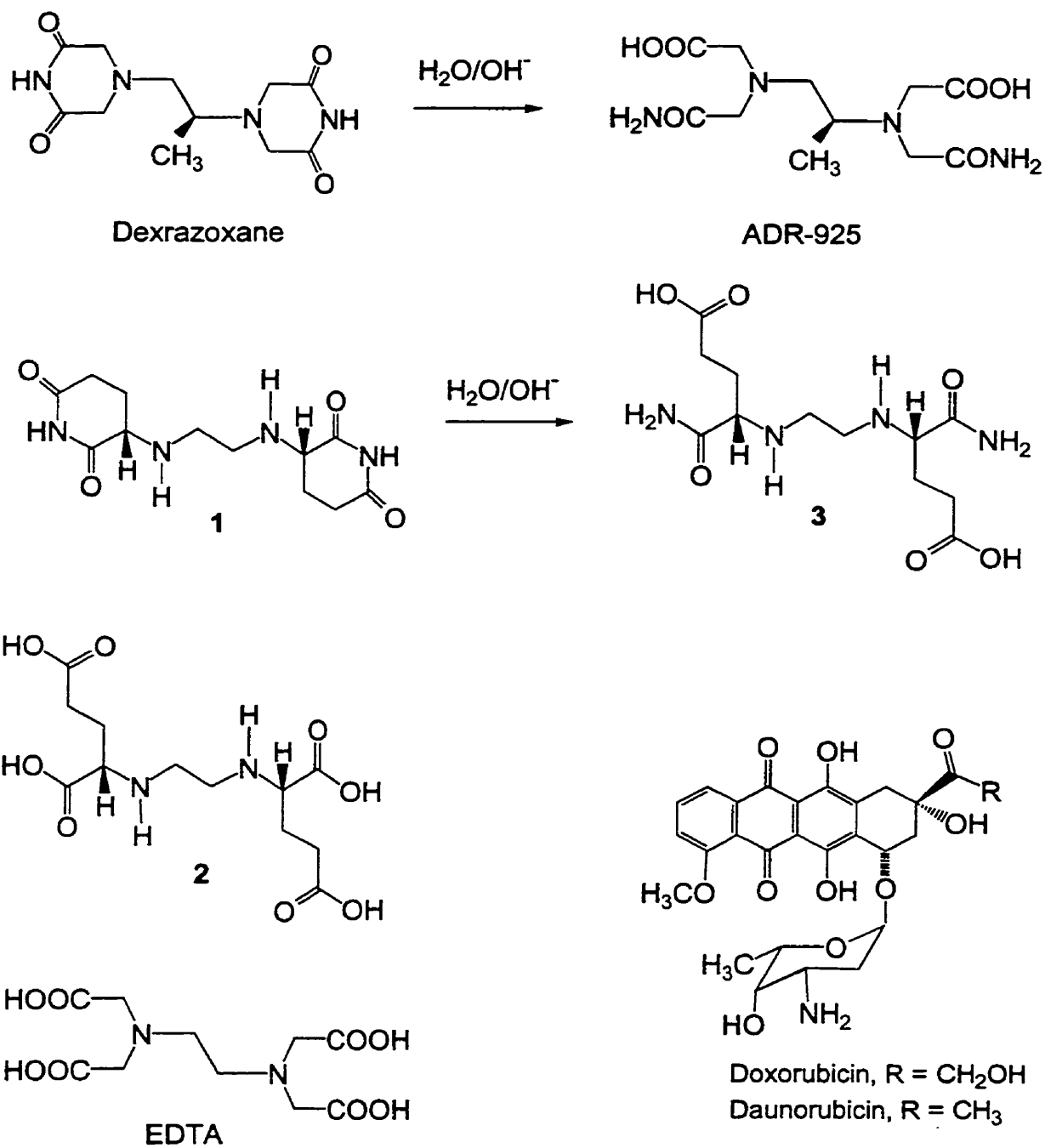
Figure 5.19. Structures of EDTA, daunorubicin, doxorubicin, the tetraacid precursor **2**, the bisdioxopiperidine **1**, and its hydrolyzed form **3**.

5.6.1. Methods

The procedure for this experiment is the same as that described in detail in Section 3.2. The Fe^{3+}(daunorubicin)$_2$ complex was prepared at fixed concentrations of Fe^{3+} at 135 μM, and of daunorubicin at 68 μM under slightly acidic conditions to prevent the formation of insoluble ferric hydroxides. $FeCl_3 \cdot 6H_2O$ (10 mM) dissolved in 1 mM HCl was added to the drug (4 mM) in a 1:2 mole ratio. The solution turned dark reddish-brown upon mixing, indicating the complex formation. A small amount of the pre-formed Fe^{3+}-daunorubicin complex was added to a thermostatted (25 °C) 1 cm plastic cell containing Tris/KCl (50 mM/150 mM, pH 7.4) buffer in a Cary 1 spectrophotometer (Varian, Mulgrave, Australia), and the solution was allowed to equilibrate for about 1 min for the absorbance to stabilize. The absorbance of the Fe^{3+}-drug complex solution was measured over time at 600 nm, at which wavelength daunorubicin does not absorb significantly. This wavelength was chosen based on previously reported experiments for the determination of the Fe^{3+}-daunorubicin complex formation, and dissociation in the presence of metal ion chelators (Buss, 1998). After starting the absorbance-time traces for 1 min, various concentrations of the chelators, such as EDTA, tetraacid precursor 2, and the hydrolyzed form 3 were added. The hydrolyzed form 3 of the imide 1 was prepared by a 2 h incubation of the imide 1 in KOH solution at pH 12.0 and 25 °C. The rate constants at which the Fe^{3+}-drug complex dissociated was obtained by first-order kinetic fit as described in Sections 3.2 and 3.3 if any complex dissociation occurred.

5.6.2. Displacement of Fe^{3+} from its complex with daunorubicin by metal ion chelators

The absorbance-time traces of the Fe^{3+}-daunorubicin complex in the absence of chelator, and in the presence of the chelators, such as EDTA, tetraacid precursor 2, and the hydrolyzed form 3 are shown in Figure 5.20. The dissociation of the Fe^{3+}-daunorubicin complex was measured by the decrease in the absorbance at 600 nm. At this wavelength daunorubicin itself has an absorbance very close to zero (Buss, 1998). The results showed that the Fe^{3+}-daunorubicin complex can be dissociated quickly and completely by EDTA. The Fe^{3+}-drug complex was also dissociated by the tetraacid precursor 2. However, the Fe^{3+} removal by the tetraacid precursor 2 was not as complete at 100 µM as with EDTA at the same concentration. The hydrolyzed form 3 was not effective, even at a concentration of 500 µM, in displacing Fe^{3+} from the Fe^{3+}-daunorubicin complex. The relative percentage of Fe^{3+} removal is tabulated in Table 5.2. The percentage of Fe^{3+} removal was obtained from Figure 5.20, and 100 % Fe^{3+} removal was assigned when the absorbance at 600 nm and at 500 min dropped to zero, and 0 % Fe^{3+} removal was assigned for the control trace without the addition of chelator.

The logarithm of Fe^{3+} formation constants are 22.0 for the tetraacid 2, and 25.1 for EDTA at 20 °C (Majer et al., 1966). This shows that the tetraacid 2 and EDTA have similar stability constants for Fe^{3+}. The hydrolyzed form 3, however, lost most of its ability to chelate to Fe^{3+} as shown in Figure 5.20. This result was unexpected at the beginning of the synthetic project of the imide 1, which was postulated to be an effective chelator. A second process might occur since the absorbance increased slightly as the

reaction proceeded for a longer time as shown in Figure 5.20 (c). This second process could be the result of the cyclization of the hydrolyzed form **3**, and convert it to a derivative of pyroglutamic acid **4**, which does not possess a high affinity for the metal ion (Figure 5.21). This cyclization is observed both with L-glutamine in alkaline solution and/or at elevated temperature as shown in Figure 5.21 (Gilbert *et al.*, 1949). The imide **1** upon being attacked by hydroxide nucleophile could produce two types of half acid-half amide intermediates **3** and **3'** as shown in Figure 5.21. The intermediate **3'**, which is structurally similar to L-glutamine could cyclize, and produce the pyroglutamic acid derivative **4**. This cyclized species may not possess any chelation ability to metal ion. Thus, the removal of Fe^{3+} from its complex with daunorubicin was not observed. The drop in the absorbance of trace (b) in Figure 5.20 is simply due to the instability of the instrument after operating for 1800 min. For comparison, the percentage of Fe^{3+} removal is tabulated in Table 5.2 based on the change in the absorbance at 600 nm and at 1000 min reaction time. The Fe^{3+} removal was assigned with 100 % Fe^{3+} removal when the absorbance (at 600 nm and at 1000 min) dropped to zero, and 0 % Fe^{3+} removal for the control without chelator.

Table 5.2. Fe^{3+}-daunorubicin complex dissociation upon the addition of various chelators.

Percentage of Fe^{3+} removal was obtained from Figure 5.20, and 100 % Fe^{3+} removal was assigned when the absorbance (at 600 nm and at 1000 min) dropped to zero, and 0 % Fe^{3+} removal was assigned for the control trace (a).

Chelator	Concentration, μM	% dissociation
control	0	0
EDTA	100	95.9
tetraacid **2**	100	70.3
tetraacid **2**	500	90.5
hydrolyzed form **3**	100	0
hydrolyzed form **3**	500	0
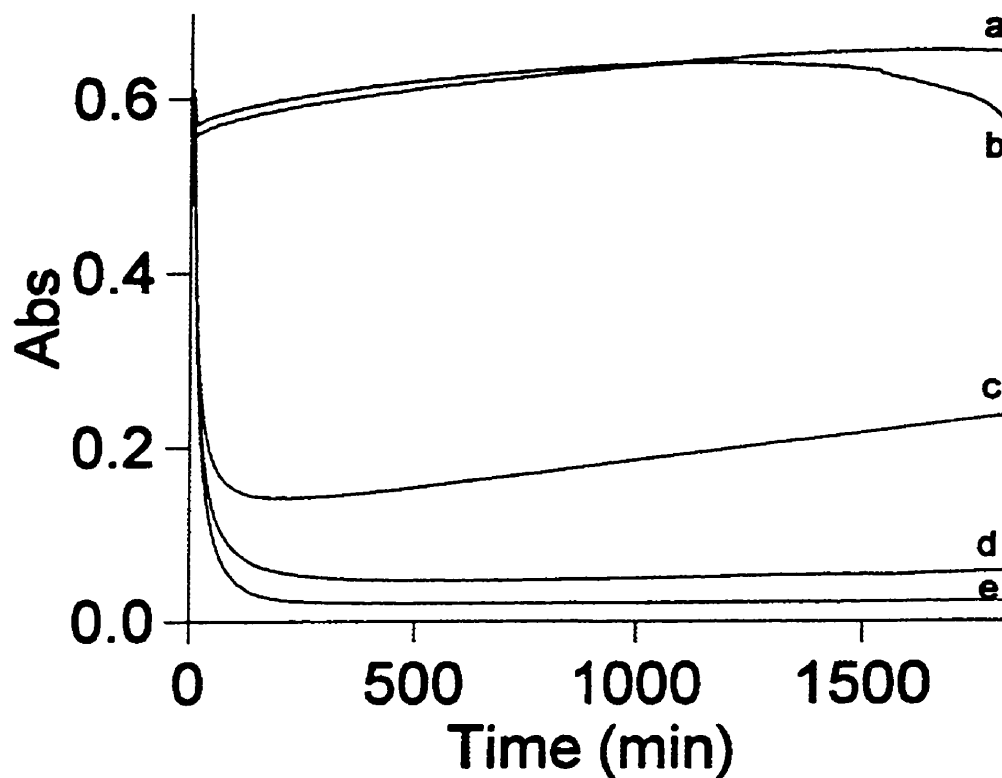
Figure 5.20. Absorbance-time traces at 600 nm of the Fe^{3+}-daunorubicin complex in the presence of different chelators under physiological conditions (Tris/KCl buffer, pH 7.4, 25 °C). The Fe^{3+}-daunorubicin complex was pre-formed at 68 μM Fe^{3+}, 135 μM daunorubicin. The chelators at zero concentration (a), at 500 μM of the hydrolyzed form **3** (b), 100 μM (c) and 500 μM (d) of the tetraacid precursor **2**, and 500 μM EDTA (e) were added 1 min after starting the recording of the absorbance.
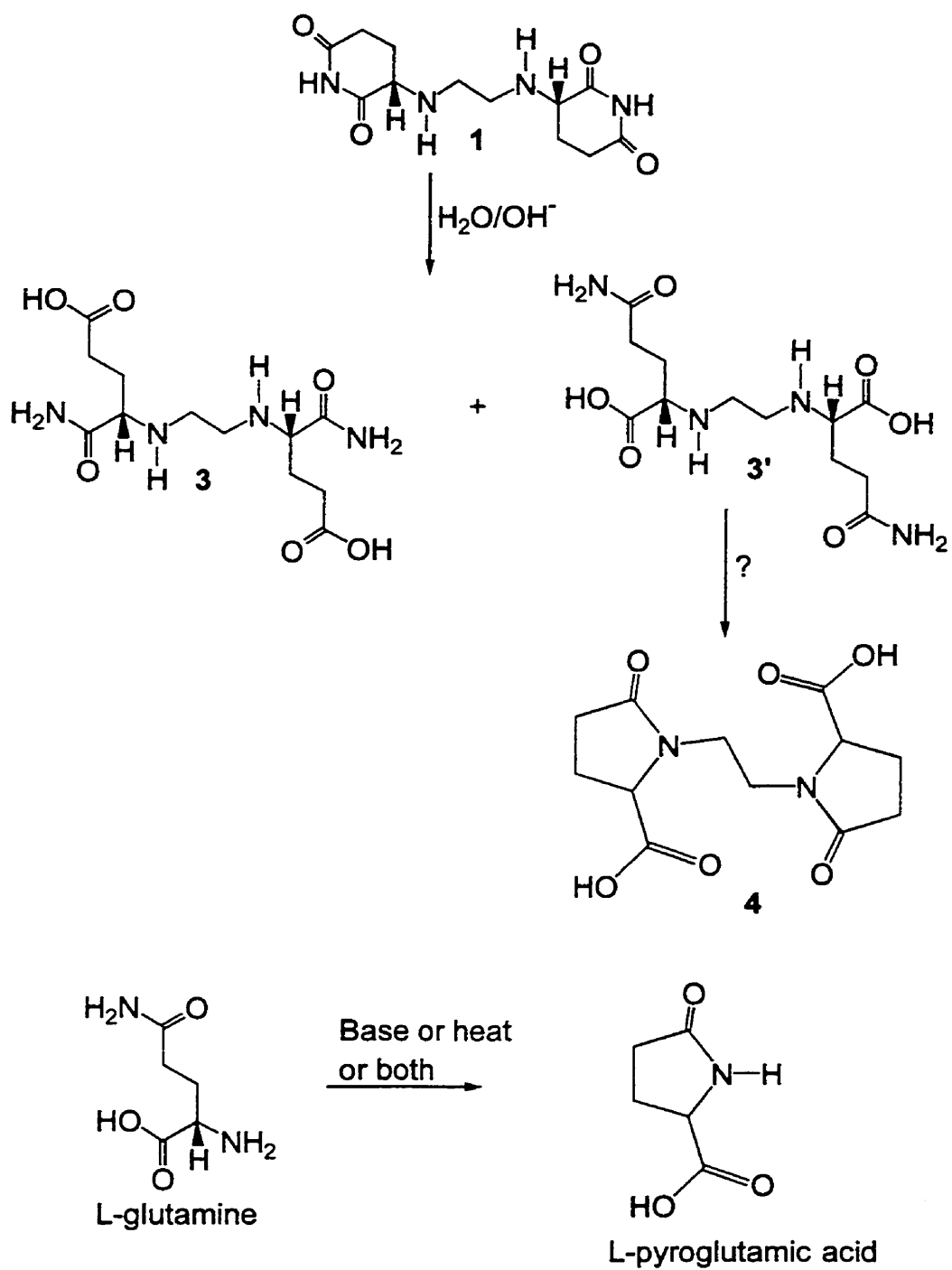
Figure 5.21. Proposed cyclization of L-glutamine, and the hydrolyzed form **3**.

5.7. Testing the cytotoxicity of the bisdioxopiperidine 1 on Chinese hamster ovary cells

It has been shown that dexrazoxane inhibits topoisomerase II, and that the drug inhibits the activity of the enzyme by preventing its binding to DNA (Snapka *et al.*, 1996; Hasinoff *et al.*, 1997, 1998). The bisdioxopiperidine **1** is structurally similar to dexrazoxane. In this experiment, the enzyme inhibition was studied indirectly by testing the cytotoxic effect of the imide **1** on Chinese hamster ovary cell growth inhibition. The experimental detail was described in Section 4.2. Briefly, the imide **1** was dissolved in DMSO, and added to Chinese hamster ovary cells after their having grown for 24 h. The whole mixture was then incubated for a further 72 h. The cytotoxic effect was measured spectrophotometrically at 490 nm by the MTT assay. The growth inhibition of the cells by the imide **1** is shown in Figure 5.22. The result showed that the imide **1** did not have any cytotoxic effect on Chinese hamster ovary cells even at the highest concentration of 500 μM.
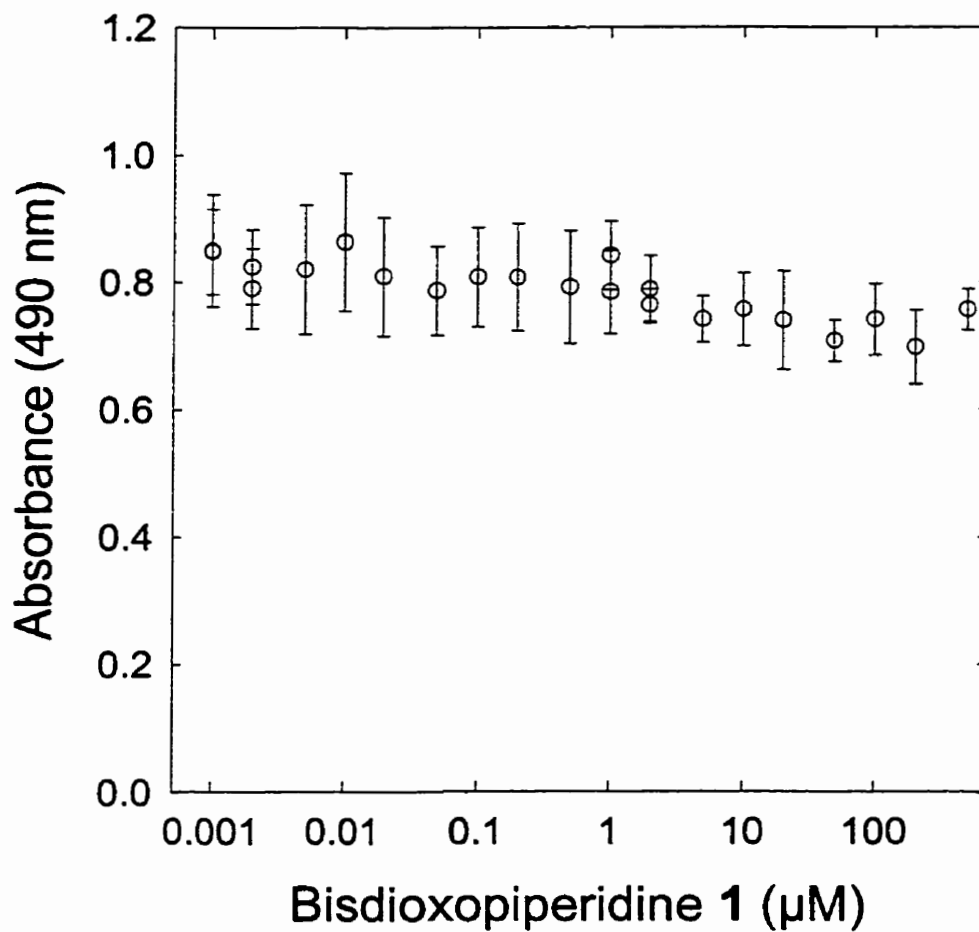
Figure 5.22. Growth inhibition of Chinese hamster ovary cells by the bisdioxopiperidine **1**. The cells were incubated with the drug for 72 h, and then assayed with MTT. Each data point is the average of six replicates with the errors shown as standard deviations. The lowest data point is the control without drug and without DMSO, and the next data point is a control with 0.5 % (v/v) DMSO only.

5.8. Evaluation of the importance of the bisdioxopiperidine 1

The hydrolysis study of the bisdioxopiperidine 1 showed that this compound did not hydrolyze as quickly as dexrazoxane under physiological conditions. The pK_a value of the imide 1 was found to be slightly higher than that of dexrazoxane. This property of the compound 1 should speed up the hydrolysis rate since the higher the pK_a, the larger the fraction which would be in the neutral imide form, and the faster the hydrolysis. However, it was found that the imide 1 hydrolyzed faster at high pH, and slower at low pH. Also, the Fe^{3+} removal from the Fe^{3+}-daunorubicin complex by the hydrolyzed form 3 was shown not to be effective. The hydrolyzed form 3 was not a strong enough Fe^{3+} chelator to competitively dissociate the Fe^{3+}-daunorubicin complex. The cytotoxic effect of the imide 1 was found to be very small, indicating that it is a poor topoisomerase II inhibitor. The imide 1 has two secondary amines on the main chain, and would be protonated at pH 7.4; this feature of the compound may make it become non cell membrane permeable, and thus, not cytotoxic. In order to test this hypothesis, a direct topoisomerase II inhibition experiment could be performed. Therefore, it is predicted that the bisdioxopiperidine 1 is not a better cardioprotective agent than dexrazoxane.

6. References

Alberts B, Bray D, Lewis J, Raff M, Roberts K and Watson JD (1994) *Molecular Biology of the Cell.* Garland Publishing Inc., New York and London.

Arslan P, DiVirgilio F, Beltrame M, Tsien RY and Pozzan T (1985) Cytosolic Ca^{2+} homeostasis in Ehrlich and Yoshida carcinomas: a new membrane-permeant chelator of heavy metals reveals that these ascites tumor cell lines have normal cytosolic free Ca^{2+}. *J Biol Chem* **260**:2719-2727.

Bachur NR, Gordon SL, Gee MV and Kon H (1979) NADPH cytochrome P-450 reductase activation of quinone anticancer agents to free radicals. *Proc Natl Acad Sci USA* **76**:954-957.

Berger JM, Gamblin SJ, Harrison SC and Wang JC (1996) Structure and mechanism of DNA topoisomerase II. *Nature* **379**:225-232.

Buss JL (1998): Mechanism of Hydrolysis-Activation of the Cardioprotective Antioxidant Dexrazoxane and Identification of More Effective Analogs. Ph.D. Dissertation, The University of Manitoba, Winnipeg, Manitoba. 275 p.

Buss JL and Hasinoff BB (1995) Ferrous ion strongly promotes the ring opening of the hydrolysis intermediates of the antioxidant doxorubicin cardioprotective agent ICRF-187 (dexrazoxane). *Arch Biochem Biophys* **317**:121-127.

Byers W and Douglas BE (1972) Circular dichroism of a cobalt(III) complex of ethylenediamine-N,N'-diacetic-N,N'-di-3-propionic acid. *Inorg Chem* **11**:1470-1473.

Chen AY and Liu LF (1994) DNA topoisomerases: essential enzymes and lethal targets. *Ann Rev Pharmacol Toxicol* **34**:191-218.

Corbett AH and Osheroff N (1993) When good enzymes go bad: conversion of topoisomerase II to a cellular toxin by antineoplastic drugs. *Chem Res Toxicol* **6**:585-597.

Creighton AM (1971): Piperazine derivatives. U. K. Patent 1,234,935.

Creighton AM (1976): Bis diketopiperazines. U. S. Patent 3,941,790, issued 2 Mar 1976.

Creighton AM (1981): Pharmaceutical compositions. United States Patent 4,275,063, issued 23 Jun 1981.

Dawson KM (1975) Studies on the stability and cellular distribution of dioxopiperazines in cultured BHK-21S cells. *Biochem Pharmacol* **24**:2249-2253.

Demant EJF and Jensen PK (1983) Destruction of phospholipids and respiratory-chain activity in pig-heart submitochondrial particles induced by an adriamycin-iron complex. *Eur J Biochem* **132**:551-556.

Elihu N, Anandasbapathy S and Frishman WH (1998) Chelation therapy in cardiovascular disease: ethylenediaminetetraacetic acid, deferoxamine, and dexrazoxane. *Clin Pharmacol Ther* **38**:101-105.

Foster BJ, Newell DR, Graham MA, Gumbrell LA, Jenns KE, Kaye SB and Calvert AH (1992) Phase I trial of the anthrapyrazole CI-941: prospective evaluation of a pharmacokinetically guided does-escalation. *Eur J Cancer* **28**:463-469.

Frank P and Novak RF (1986) Effects of anthrapyrazole antineoplastic agents on lipid peroxidation. *Biochem Biophys Res Comm* **140**:797-807.

Froelich-Ammon SJ and Osheroff N (1995) Topoisomerase poisons: harnessing the dark side of enzyme mechanism. *J Biol Chem* **270**:21429-21432.

Fukuda Y, Herman EH and Ferrans VJ (1992) Effect of ICRF-187 on the pulmonary damage induced by hyperoxia in the rat. *Toxicol* **74**:185-202.

Gelvan D and Samuni A (1988) Reappraisal of the association between adriamycin and iron. *Cancer Res* **48**:5645-5649.

Gianni L, Corden BJ and Myers CE (1983) The biochemical basis of anthracycline toxicity and anti-tumor activity. *Rev Biochem Toxicol* **5**:1-82.

Gianni L, Zweier JL, Levy A and Myers CE (1985) Characterization of the cycle of iron-mediated electron transfer from adriamycin to molecular oxygen. *J Biol Chem* **260**:6820-6826.

Gilbert JB, Price VE and Greenstein JP (1949) Effect of anions on the non-enzymatic desamidation of glutamine. *J Biol Chem* **180**:209-218.

Graham MA, Newell DR, Foster BJ and Calvert AH (1989) The pharmacokinetics and toxicity of the anthrapyrazole anti-cancer drug CI-941 in the mouse: a guide for rational dose escalation in patients. *Cancer Chemother Pharmacol* **23**:8-14.

Gutteridge JMC (1984) Lipid peroxidation and possible hydroxyl radical formation stimulated by the self-reduction of a doxorubicin-iron(III) complex. *Biochem Pharmacol* **33**:1725-1728.

Hargreaves MK, Pritchard JG and Dave HR (1970) Cyclic carboxylic monoimides. *Chem Rev* **70**:439-468.

Harris WE and Kratochvil B (1969) *Chemical Analysis.* Barnes and Noble, New York.

Hasinoff BB (1989a) The interaction of the cardioprotective agent ICRF-187 ((+)-1,2-bis(3,5-dioxopiperazinyl-1-yl)propane), its hydrolysis product ICRF-198, and other chelating agents with the Fe(III) and Cu(II) complexes of adriamycin. *Agents Actions* **26**:378-385.

Hasinoff BB (1989b) Self-reduction of the iron(III)-doxorubicin complex. *Free Radic Biol Med* **7**:583-593.

Hasinoff BB (1990a) The hydrolysis-activation of the doxorubicin cardioprotective agent ICRF-187 ((+)-1,2-bis(3,5-dioxopiperazinyl-1-yl)propane). *Drug Metab Dispos* **18**:344-349.

Hasinoff BB (1990b) The iron(III) and copper(II) complexes of adriamycin promote the hydrolysis of the cardioprotective agent ICRF-187 ((+)-1,2-bis(3,5-dioxopiperazinyl-1-yl)propane). *Agents Actions* **29**:374-381.

Hasinoff BB (1990c) Oxyradical production results from the Fe^{3+}-doxorubicin complex undergoing self-reduction by its a-ketol group. *Biochem Cell Biol* **68**:1331-1336.

Hasinoff BB (1994a) An HPLC and spectrophotometric study of the hydrolysis of ICRF-187 (dexrazoxane, (+)-1,2-bis(3,5-dioxopiperazinyl-1-yl)propane) and its one-ring opened intermediates. *Int J Pharm* **107**:67-76.

Hasinoff BB (1994b) Pharmacodynamics of the hydrolysis-activation of the cardioprotective agent (+)-1,2-bis(3,5-dioxopiperazinyl-1-yl)propane. *J Pharm Sci* **83**:64-67.

Hasinoff BB (1995) NADPH-cytochrome-P450 reductase promotes hydroxyl radical production by the iron complex of ADR-925, the hydrolysis product of ICRF-187 (dexrazoxane). *Free Radic Res* **22**:319-325.

Hasinoff BB (1998) Chemistry of dexrazoxane and analogues. *Semin Oncol* **25**:3-9.

Hasinoff BB, Kuschak TI, Creighton AM, Fattman CL, Allan WP, Thampatty P and Yalowich JC (1997) Characterization of a Chinese hamster ovary cell line with acquired resistance to the bisdioxopiperazine dexrazoxane (ICRF-187) catalytic inhibitor of topoisomerase II. *Biochem Pharmacol* **53**:1843-1853.

Hasinoff BB, Hellmann K, Herman EH and Ferrans VJ (1998) Chemical, biological and clinical aspects of dexrazoxane and other bisdioxopiperazines. *Curr Med Chem* **5**:1-28.

Healy T, Fevang L and Gillis CM (1998) *Compendium of Pharmaceuticals and Specialties.* Bruce, L. D., Toronto.

Herman EH, Zhang J, Hasinoff BB, Clark JRJ and Ferrans VJ (1997) Comparison of the structural changes induced by doxorubicin and mitoxantrone in the heart, kidney and intestine and characterization of the Fe(III)-mitoxantrone complex. *J Mol Cell Cardiol* **29**:2415-2430.

Herman EH, Zhang J, Hasinoff BB, Tran KT, Chadwick DP, Clark JRJ and Ferrans VJ (1998) Comparison of the chronic toxicity of piroxantrone, losoxantrone and doxorubicin in spontaneously hypertensive rats. *Toxicol* **128**:35-52.

Hsiang Y-H, Lihou MG and Liu LF (1989) Arrest of replication forks by drug stabilized topoisomerase I-DNA cleavable complexes as a mechanism of cell killing by camptothecin. *Cancer Res* **49**:5077-5082.

Ingle JN, Kuross SA, Mailliard JA, Loprinzi CL, Jung SH, Nelimark RA, Krook JE and Long HJ (1994) Evaluation of piroxantrone in women with metastatic breast cancer and failure on nonanthracycline chemotherapy. *Cancer* **74**:1733-1738.

Ishida R, Hamatake M, Wasserman RA, Nitiss JL, Wang JC and Andoh T (1995) DNA topoisomerase II is the molecular target of bisdioxopiperazine derivatives ICRF-159 and ICRF-193 in *Saccharomyces cerevisiae*. *Cancer Res* **55**:2299-2303.

Jeffery WA (1987): Bisdioxopiperazines and related prodrugs: Physico-chemical and antitumour properties. Ph.D. Dissertation, Council for National Academic Awards, London.

Johnson LF and Jankowski WC (1972) *Carbon-13 NMR Spectra. A Collection of Assigned, Coded, and Indexed Spectra*. John Wiley & Sons, New York.

Judson IR (1991) Anthrapyrazoles: true successors to the anthracyclines? *Anticancer Drugs* **2**:223-231.

Kano Y, Narita T, Suzuki K, Akutsu M, Suda K, Sakamoto S and Miura Y (1992) The effects of ICRF-154 in combination with other anticancer agents in vitro. *Br J Cancer* **66**:281-286.

Kozlowska H (1998): Interaction of Dexrazoxane with Anticancer Drugs. M. Sc. Thesis, The University of Manitoba, Winnipeg, Manitoba. 203 p.

Lehninger AL, Nelson DL and Cox ML (1993) *Principles of Biochemistry*. Worth Publishers, New York.

Leteurtre F, Kohlhagen G, Paull KD and Pommier Y (1994) Topoisomerase II inhibition and cytotoxicity of the anthrapyrazoles DuP 937 and DuP 941 (Losoxantrone) in the National Cancer Institute preclinical antitumor drug discovery screen. *J Natl Cancer Inst* **86**:1239-1244.

Macpherson JS, Cummings J, Meikle I, Miller EP and Smyth JF (1997) Cell cycle effects of the novel topoisomerase I inhibitor NU?ICRF 505 in a panel of Chinese hamster ovary cell lines. *Eur J Cancer* 33:280-283.

Madden KR, Stewart L and Champoux JJ (1995) Preferential binding of human topoisomerase I to superhelical DNA. *EMBO J* 14:5399-5409.

Majer J, Springer V and Kopeska B (1966) Nove komplexany (VIII) kyselina etylendiamin-N,N'-dijantarova a spektrofotometricke studiium jej komplexov s fazkymi kovmi. *Chemicke Zvesti* 20:414-422.

Malisza KL and Hasinoff BB (1995a) Doxorubicin reduces the iron(III) complexes of the hydrolysis products of the antioxidant cardioprotective agent dexrazoxane (ICRF-187) and produces hydroxyl radicals. *Arch Biochem Biophys* 316:680-688.

Malisza KL and Hasinoff BB (1995b) Production of hydroxyl radical by iron(III)-anthraquinone complexes through self-reduction and through reductive activation by the xanthine oxidase/hypoxanthine system. *Arch Biochem Biophys* 321:51-60.

Malisza KL and Hasinoff BB (1996a) Hydroxyl radical production by the iron complex of the hydrolysis product of the antioxidant cardioprotective agent ICRF-187 (dexrazoxane). *Redox Rep* 2:69-73.

Malisza KL and Hasinoff BB (1996b) Inhibition of anthracycline semiquinone formation by ICRF-187 (dexrazoxane) in cells. *Free Radic Biol Med* 20:905-914.

May PM, Williams GK and Williams DR (1980) Speciation studies of adriamycin, quelamycin, and their metal ion complexes. *Inorg Chim Acta* 46:221-228.

Miller WD (1988): Process for preparing (S)(+)-4,4'(methyl-1,2-ethanediyl)-bis(2,6-piperazinedione). United States Patent 4,764,614, issued 16 Aug 1988.

Muggia FM and Green MD (1991) New anthracycline antitumor antibiotics. *Crit Rev Oncol Hematol* 11:43-64.

Myers CE, Gianni L, Simone CB, Klecker R and Greene R (1982) Oxidative destruction of erythrocyte ghost membranes catalyzed by the doxorubicin-iron complex. *Biochemistry* 21:1707-1713.

Nitiss JL (1994a) Roles of DNA topoisomerases in chromosomal replication and segregation. *Adv Pharmacol* 29A:103-134.

Nitiss JL (1994b) Yeast as a genetic model system for studying topoisomerase inhibitors. *Adv Pharmacol* 29B:201-226.

Nogrady (1988) *Medicinal Chemistry. A Biochemical Approach.* Oxford University Press, New York.

Noller (1965) Derivatives of carbonic acid and of thocarbonic acid, in *Chemistry of Organic Compounds* (Noller ed) pp 331, Saunders, New York.

Ogawa M and Ariyoshi Y (1993) New anthracyclines. *Gan To Kagaku Ryoho* **20**:27-33.

Osheroff N (1989) Biochemical basis for the interaction of type I and type II topoisomerases with DNA. *Pharmacol Ther* **41**:223-241.

Polonski T (1988a) Chiroptical properties and molecular geometry of substituted succinic anhydrides and imides. *J Chem Soc Perkin Trans I* **00**:629-637.

Polonski T (1988b) Circular dichroism spectra and molecular geometry of six-membered ring anhydrides and imides. *J Chem Soc Perkin Trans I* **00**:639-648.

Pommier Y (1993) Review: DNA topoisomerase I and II in cancer chemotherapy: update and perspectives. *Cancer Chemother Pharmacol* **32**:103-108.

Pommier Y, Kohn KW, Capranico G and Jaxel C (1993) Base sequence selectivity of topoisomerase inhibitors suggests a common model for drug action, in *Molecular Biology of DNA Topoisomerases* (Andoh T, Ikeda H and Oguro M eds) pp 215-227, CRC Press, Inc., U.S.A.

Pommier Y, Leteurtre F, Fesen MR, Fujimori A, Bertrand R, Solary E, Kohlhagen G and Kohn KW (1994) Cellular determinants of sensitivity and resistance to DNA topoisomerase inhibitors. *Cancer Invest* **12**:530-542.

Rajagopalan S, Politi PM, Sinha BK and Myers CE (1988) Adriamycin-induced free radical formation in the perfused rat heart: implications for cardiotoxicity. *Cancer Res* **48**:4766-4769.

Redinbo MR, Stewart L, Kuhn P, Champoux JJ and Hol WGJ (1998) Crytal structures of human topoisomerase I in covalent and noncovalent complexes with DNA. *Science* **279**:1504-1513.

Sanders JKM and Hunter BK (1993) *Modern NMR Spectroscopy. A Guide for Chemists.* Oxford University Press, United States.

Sengupta SK (1995) Topoisomerase II inhibitors, inhibitors of DNA topoisomerases, in *Cancer Chemotherapeutic Agents* (Foye WO ed) pp 205-260, ACS Professional Reference Book Massachusetts College of Pharmacy and Allied Health Sciences, Washington, DC.

Silverstein RM, Bassler GC and Morrill TC (1991) *Spectrometric Identification of Organic Compounds*. John Wiley & Sons, Inc., New York.

Sisco JM (1989): The physicochemical, analytical and pharmacokinetic properties of the antineoplastic agent, ICRF-187. Ph.D. Dissertation, University of Kansas, Lawrence, Kansas. 254 p.

Snapka RM, Woo SH, Blokhin AV and Witiak DT (1996) Inhibition of topoisomerase II by ICRF-193, the meso isomer of 2,3-bis(2,6-dioxopiperazin-4-yl)butane. Critical dependence on 2,3-butanediyl linker absolute configuration. *Biochem Pharmacol* 52:543-549.

Sobol MM, Amiet RG and Green MD (1992) In vitro evidence for direct complexation of ADR-529/ICRF-187 [(+)-1,2-bis-(3,5-dioxo-piperazin-1-yl)propane] onto an existing ferric-anthracycline complex. *Mol Pharmacol* 41:8-17.

Sosman JA, Flaherty LE, Liu PY, Fletcher W, Thompson JA, Hantel A and Sondak V (1995) A phase II trial of piroxantrone in disseminated malignant melanoma. A Southwest Oncology Group study. *Invest New Drugs* 13:83-87.

Stewart L, Redinbo MR, Qiu X, Hol WGJ and Champoux JJ (1998) A model for the mechanism of human topoisomerase I. *Science* 279:1534-1541.

Synold T, Tetef ML and Doroshow JH (1998) Antineoplastic activity of continuous exposure to dexrazoxane: potential new role as a novel topoisomerase II inhibitor. *Semin Oncol* 25:93-99.

Talbot DC, Smith IE, Mansi JL, Judson I, Calvert AH and Ashley SE (1991) Anthrapyrazole CI941: a highly active new agent in the treatment of advanced breast cancer. *J Clin Oncol* 9:2141-2147.

van-Reyk DM, Sarel S and Hunt NH (1992) In vitro effects of three iron chelators on mitogen-activated lymphocytes: identification of differences in their mechanisms of action. *Int J Immunopharmacol* 14:925-932.

Verweij J (1995) Topoisomerase I inhibitors and other new cytotoxic drugs. *Eur J Cancer* 31A:828-830.

Walsh SM, Walley VM, Chandra L, Huan SD, Veinot JP and Higginson LA (1995) Potential cardiotoxicity with the use of DuP-941: a case report. *Can J Cardiol* 11:419-422.

Wang HK, Morris-Natschke SL and Lee KH (1997) Recent advances in the discovery and development of topoisomerase inhibitors as antitumor agents. *Medicinal Research Reviews* 17:367-425.

Wang JC (1985) DNA topoisomerases. *Ann Rev Biochem* 54:665-697.

Weiss RB (1992) The anthracyclines: will we ever find a better doxorubicin? *Semin Oncol* **19**:670-686.

Zweier JL, Gianni L, Muindi J and Meyers CE (1986) Differences in O_2 reduction by the iron complexes of adriamycin and daunomycin: the importance of the sidechain hydroxyl group. *Biochim Biophys Acta* **884**:326-336.